Structural geology and controls of gold mineralization in the Siguiri Mine, Guinea, West Africa

By

Juan Greisch Steyn

Thesis presented in partial fulfilment of the requirements for the degree Master of Science in Geology, at the University of Stellenbosch

Supervisor: Prof. Alex Kisters

Faculty of Science
Department of Earth Sciences

March 2012

Declaration

By submitting this thesis electronically, I declare that the entirety of the work contained therein is my own, original work, that I am the sole author thereof, that reproduction and publication thereof by Stellenbosch University will not infringe any third party rights and that I have not previously in its entirety or in part submitted it for obtaining any qualification.

Abstract

This study presents results of a detailed geological mapping and structural analysis of auriferous quartz-vein sets of the nine current open-pit operations, of the Siguiri Mining Complex in the northeastern parts of Guinea. The Siguiri Mining Complex is hosted by a low-grade metamorphic, turbiditic succession within the larger Siguiri Basin, which forms part of the Palaeoproterozoic Birimian Supergroup of the Boualé-Mossi domain on the West African Craton.

The Siguiri Mining Complex is located in a deeply weathered saprolite profile developed over the monotonous succession of interlayered metapelites and -psammites. In fresh bedrock and core samples, the host succession is mainly made up of quartz-muscovite schists, muscovite-chlorite schists and metagreywackes, with isolated occurrences of intraformational breccias.

The main deformation to have affected the metasedimentary succession of the Siguiri Mining Complex can be assigned to a D_2 deformational event. D_2 structures comprise of north-south trending strike-slip and reverse faults anastomosing around and enveloping open- to tightly folded domains exposed over an area of 12 by 3 km. The geometry, orientation and kinematics of faults and folds suggest that D_2 structures formed during progressive deformation in an overall dextral transpressive brittle-ductile shear zone. Structures within the D_2 corridor record east-northeast subhorizontal shortening and north-northwest subhorizontal extension.

An omnipresent carbonate alteration in form of carbonate-alteration spots testifies to the pervasive, syn-D_2 hydrothermal fluid-flow within the sediments. A structurally- and fracture-controlled fluid-flow is evidenced by the abundance of auriferous quartz veins throughout the Siguiri Mining Complex. These quartz veins host the bulk of the gold mineralization. One main and, at least, three minor sets of auriferous quartz veins can be distinguished. The main quartz-vein set shows very consistent easterly to northeasterly trends and steep southerly dips throughout the Siguiri Mining Complex. This orientation is consistent with the dextral transpressive kinematics and strain within the D_2 host structure and illustrates the significance of D_2 strains for the mineralization. The volumetrically minor vein sets can be shown to be related to different stages of F_2 folding and fold amplification.

Zones of economic-grade mineralization occur in areas where competent, psammitic units are developed in structural sites of increased dilatancy. Areas of dilatancy are represented by either dilational jog geometries within the overall transpressive structure or zones of pronounced shear-zone subparallel stretch. Jog geometries could be identified in the larger Bidini-Toubani-Sanu Tinti Complex having formed as a result of the anastomosing geometry of the bounding D_2 shear zones. In the large Kami Complex, F_2 axial culminations and depressions correspond to zones of increased stretch within the D_2 transpression zone, delineated by closer vein spacing and the formation of D_2 normal faults parallel to the main vein set and normal to F_2 fold hinges.

The size and extent of the Siguiri Mining Complex suggests that the host D_2 transpressive corridor must be assumed to have a significantly larger along-strike continuation, being part of a larger shear zone system related to the accretionary history of Palaeoproterozoic basins and arcs onto the Archaean Man Shield in West Africa.

Opsomming

Hierdie studie lewer die resultate voor van ‘n gedetailleerde geologiese kartering en strukturele analise van die gouddraende kwarts-aar stelle in die huidige nege oop-groef operasies van die Siguiri Myn Kompleks, in die noordoostelike deel van Guinea. Die Siguiri Myn Kompleks is geherberg deur ‘n lae metamorfiese graad turbidiet suksessie in die groter Siguiri Kom, wat deel form van die Paleo-Proterosoïkum Birimian Supergroep van die Bouálé-Mossi streek op die Wes Afrika Kraton.

Die Siguiri Myn Kompleks is geleë in die diep veweerde saproliet profiel, wat onwikkel het oor die eentonige suksessie van metapeliete en -psammiete. In vars bodemrots en kern monsters is die herberg-gesteente opgemaak uit kwarts-muskoviet skiste, muskoviet-chloriet skiste en metagrouwakte, as ook afgesonderde voorvalle van intraformasie breksies.

Die hoof deformasie fase wat die metasedimentêre suksessie van die Siguiri Myn Kompleks geaffekteer het, kan toegeken word aan ‘n D_2 deformasie gebeurtenis. D_2 strukture bestaan uit noord-suid neigende strekkingwaartse verskuiwings en opskuiwings, wat anastomoserend oop- en steil geplooide gebiede omsluit en is oor ‘n area van 12 by 3 km ontbloot. Die geometrie, oriëntasie en kinematika van verskuiwings en plooie stel voor dat D_2 strukture gevorm het tydens progressiewe deformasie in ‘n algemene regse transpressie skuifskeursone, onder brosheid-duktiliteit toestande. Strukture in die D_2 gang wys ‘n oos-noordoos subhorisontale verkorting en ‘n noord-noordwes subhorisontale verlenging.

Die alomteenwoordigheid van karbonaat alterasie, in die vorm van karbonaat-alterasie spikkels, getuig van die deurdringende, sin-D_2 hidrotermiese vloeistof vloei in die sedimente. Die strukturele- en breuk-beheerde vloeistof vloei is ook duidelik, as gevolg van die oorvloed van gouddraende kwarts-are reg deur die Siguiri Myn Kompleks. Die kwarts-are bevat die grootmaat van die goud mineralisasie. Een hoof, en te minste drie minder belangrike stele van gouddraende kwarts-aar stelle kan uitgeken word. Die hoof kwarts-aar stel wys konstante oostelike to noordoostelike neigings en steil suidelike hellings, reg deur die Siguiri Myn Kompleks. Die oriëntasie is konstant met regse transpressie kinematika en vervorming in die D_2 strukture en illustreer die belangrikheid van D_2 vervorming vir mineralisasie. Die minder-

belangrike aar stelle is verwant aan die verskillende staduims van F_2 plooiing en plooi amplifikasie.

Sones van ekonomiese graad mineralisasie kom voor in areas waar bevoegde eenhede van psammiete ontwikkel het in strukturele terreine van verhoogde dilatasie. Areas van dilatasie word verteenwoordig deur dilatasie uitwykings in die transpressie strukture of sones van skuifskeur subparalelle verlenging. Uitwykings geometrië kan geidentifiseer word in die groter Bidini-Toubani-Sanu Tinti Kompleks, waar dit gevorm het asgevolg van die anastomoserende geometrie van die D_2 skuifskeur sones. In die groter Kami Kompleks kom F_2 aksiale kulminerings en depressies voor in sones van verhoogde strekking binne-in die D_2 transpressie sone en word uitgebeeld deur nader aar-spasiëring en die formasie van D_2 afskuiwings, parallel aan die hoof kwarts-aar stel en normaal met betrekking tot die F_2 plooi-skarniere.

Die groote en omvang van die Siguiri Myn Kompleks stel voor dat die D_2 transpressiewe gang nog n groter voorsetting het, en vorm deel van ‘n groter skuifskeur sisteem en is verwant aan die anngroeings geskiedenis van die Paleo-Proterosoïese komme en boë aan die Argeïese Man Skild in Wes Afrika.

Acknowledgements

This thesis would not have been possible without the guidance and the help of several individuals who in one way or another contributed and extended their valuable assistance in the completion of this study.

First and foremost I would like to acknowledge the debt I owe to my supervisor, Prof. Alex Kisters for all the assistance provided in order to have been able to finish this thesis. Your aid and support were priceless and this thesis would not have been possible without you.

It is also a pleasure to thank the rest of those who made this thesis possible. The people at the Siguiri mine, especially Peter Winkler for organising the project. A thanks also goes out to Mark Watts and Shawn Kitt for all the lifts to and from the pits, as well as a thanks to George and Eddie for all the laughs.

I would also like to show my gratitude to the staff at the Department of Earth Sciences, at Stellenbosch University. A special thanks goes out to Tannie Loxie for the chit chats during breaks.

Megan and Peter, thank you for taking the time to review my thesis.

Last but not least a special thanks goes to all those who supported me through this year and a half, my friends and family, especially my mom, dad and sister, for always being there through the difficult times. Your encouragement will not be forgotten.

This thesis and its content are dedicated to the memory of my late grandfather, Karel Johan Dumas.

Table of Contents

List of Figures

Chapter 1 Introduction

1.1 Lode-gold deposits and structurally controlled fluid-flow

Mesothermal or orogenic gold deposits are a distinctive class of gold deposit and form an integral part of the tectonometamorphic evolution of their host terrain (Goldfarb et al., 2001, 2005; Groves et al., 1998). These gold deposits are characterized by a number of unifying features. Orogenic gold deposits are almost exclusively associated with auriferous quartz ± carbonate veins that indicate veining in the presence of supralithostatic fluid pressures (Groves et al., 1998, 2000; Ridley and Diamond, 2000). Quartz veining testifies to the structurally- (fracture-) controlled fluid infiltration over a broad range of upper- to mid-crustal pressures and temperatures, between about 200 - 650°C and 1-5 kbar (Goldfarb et al., 2001; Groves et al., 1998). This also emphasizes the significance of deformation for veining, most commonly in the form of shear zones and folds. These structures control fracture-controlled fluid-flow and quartz-vein formation, focussing the large volumes of hydrothermal fluids required for an economic-grade mineralization (Groves et al., 1998; Ridley, 1993; Sibson and Scott., 1998).

The key to understanding lode-gold deposits involves defining the structural and regional tectonic conditions that allow the accumulation and containment of fluids overpressured to near-lithostatic values and their intermittent release through fault-valve action (Ridley, 1992; Sibson et al., 1988; Sibson and Scott, 1998). The deformation of rocks creates regional and/or localized hydraulic gradients that may trigger fluid migration. Fluid movement in the largely impermeable wall-rocks is largely determined by fracture permeabilities, i.e. veins. Veining is recorded over a wide range of metamorphic conditions, but is favoured under brittle-ductile and commonly greenschist-facies conditions (Goldfarb et al., 2005; Groves, 1993; Groves et al., 2000; Ridely and Diamond, 2000). The relationship between deformation in brittle-ductile terrains and fluid flow explains the close spatial association between auriferous vein systems and shear zones or folds in volcano-sedimentary terrains (e.g. Ferry, 1994; Hodgson, 1987; Ridley, 1992; Robert and Poulsen, 2001). Fluid flow, and thus mineralization are commonly localized around second- and higher-order shear or fault zones adjacent to first-order structures (Goldfarb et al., 2005; Groves et al., 1998). These structures have commonly developed late in the overall

tectonometamorphic evolution of the host terrain and commonly involve a compressional or transpressional component. High-angle reverse faults are regarded as particularly important targets (e.g. Groves et al., 1998; Sibson and Scott, 1998), favouring the development of temporarily supralithostatic fluid pressures that lead to fracturing and associated destabilization of gold complexes from the hydrothermal fluid. The kinematics along the shear zones, together with the geometry and intersection of adjoining host lithologies or structures largely determine the orientation of quartz veins and vein sets and, as such, the geometry of the ore bodies (Hodgson, 1987; Ridley and Diamond, 2000). Hence, an understanding of the controls of mineralized vein systems and delineation of ore body geometries requires, amongst other factors, a comprehensive integration of structural and lithological data, describing fluid-flow during the time of mineralization.

1.2 Background and rationale

The Siguiri Mine Complex is a world-class gold deposit in the northeastern parts of Guinea, situated near the town of Siguiri (coordinates: latitude - 11°25'16.80"N; longitude - 9°10'7.28"W), some 830 km to the east-northeast of Conakry, the capital of Guinea (Fig. 1.1) The Siguiri Mining Complex is located in the northeastern parts of the Siguiri Basin in the rocks that form part of the Palaeoproterozoic Birimian Supergroup of West Africa (Feybesse and Milési, 1994)(Fig. 1.2). The host rocks have previously been described as a succession of low-grade metamorphic metaturbidites with minor intercalated volcanic units (Egal et al., 2002). The current mining focuses on a number of kilometre-scale open-pit operations distributed over an area of 12 km (north-south) by 3 km (east-west). Annual gold production was 316,000 oz in 2009, with a lower production for 2010, but plans to increase production to up to 700.000 oz in the future. Mining focuses on the bulk mining of *in situ* auriferous quartz veins through mainly excavators. This mining method is possible, since the quartz veins occur in an up to 80 m thick, deeply weathered saprolite profile developed in Proterozoic metasedimentary rocks of the Siguiri Basin (Fig. 1.2). In many of the open pits, mining has reached bedrock. This requires a much better understanding of the bedrock geology and actual controls of quartz veining. However, to date there has been no detailed structural mapping of the geology of the Siguiri Mining Complex and its quartz-vein inventory.

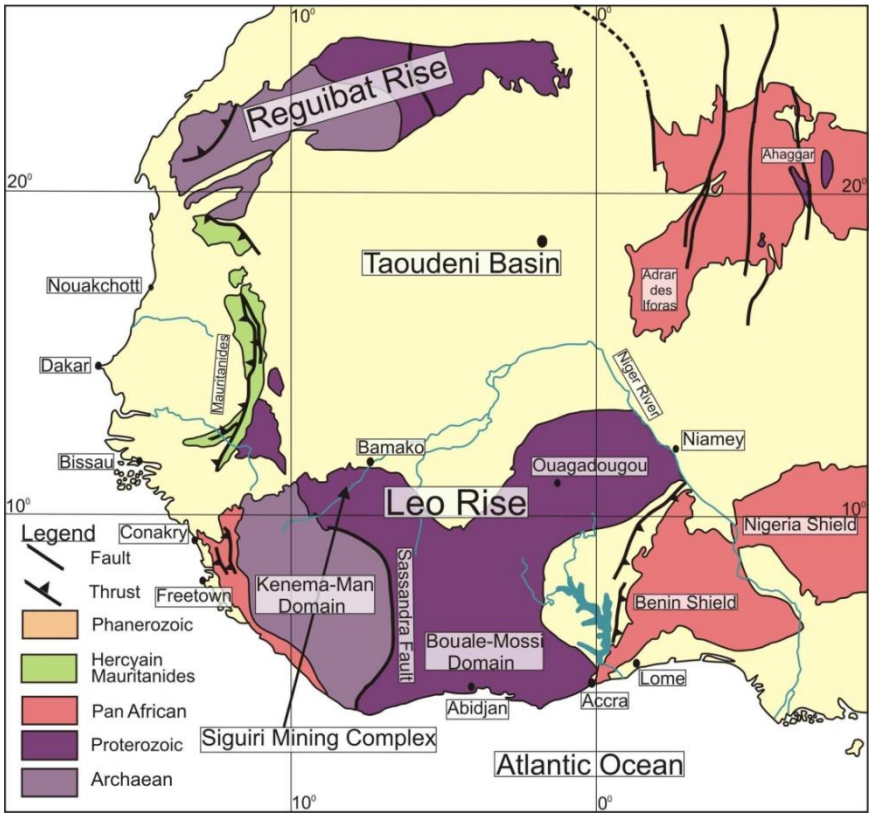

Figure 1.1: Geological sketch map of the West African Craton. The map shows Archaean kernels, surrounded by progressively younger orogenic belts. The boundaries between these are commonly delineated by major thrust or transpressional shear zones (*Edited from: Lahondère et al., 2002*).

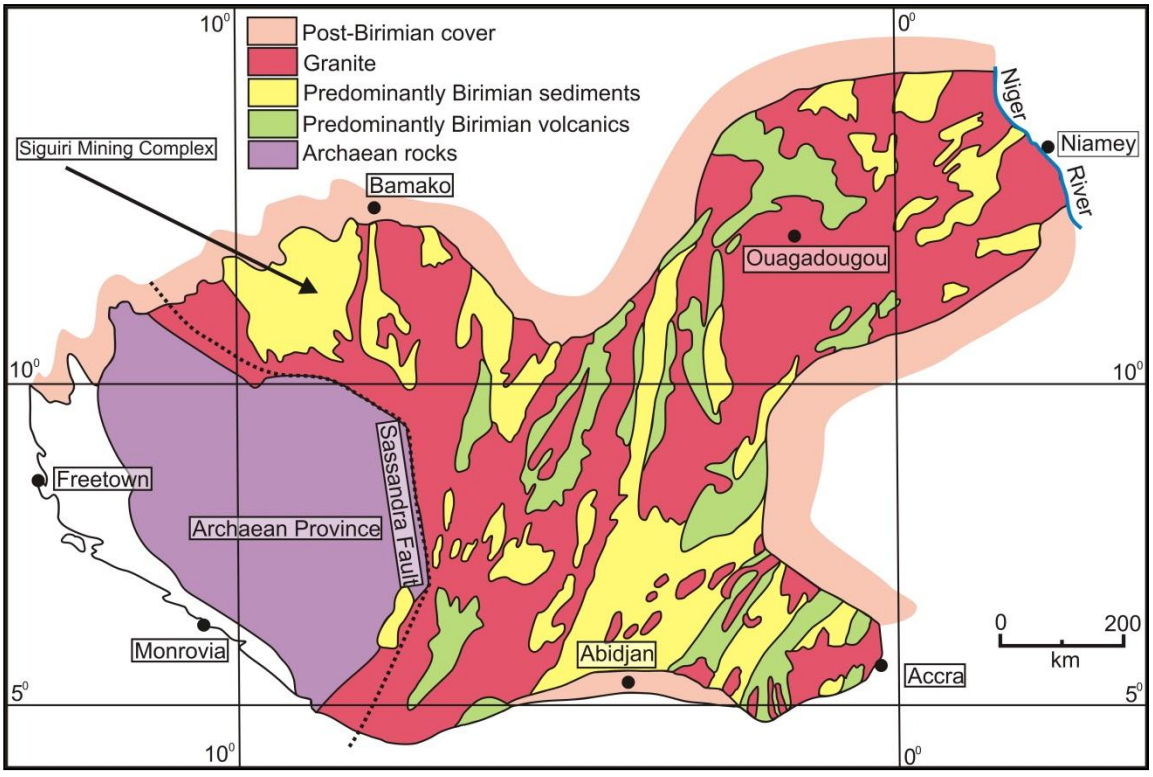

Figure 1.2: Geological sketch map of the Archaean-Paleoproterozoic Man-Leo Shield showing Archaean basement gneisses and linear to arcuate volcano-sedimentary belts intruded by voluminous granitoids (*Edited from: Feybesse and Milési, 1994).*

1.3 Aims of the study

The aims of the study can be summarized as follows:

a) Documentation of the mine-scale geology, based on the mapping of existing open pits. This includes mapping of the structural inventory, including folds, shear zones and late-stage faults as well as the identification and mapping of lithological packages in the deeply weathered profile and their possible correlation throughout the mine complex.
b) Integration of structural and lithological data into 2D sections, aimed at developing a better understanding of the structural architecture and geology of the Siguiri Mining Complex.
c) Documentation of quartz veins, their orientation, occurrence, abundances and relative timing of different quartz-vein generations and cross-cutting relationships, also with respect to controlling structures.
d) Integration of the geological (lithological and structural data) and quartz-vein data into an overall kinematic-mineralization model for the mine.

1.4 Methodology

The field work was done over a three month field season between May and August 2010. The initial two week reconnaissance-style mapping was followed by detailed mapping of individual open pits between June and August. The field work was chosen to coincide with the rainy season in Guinea, during which the sidewalls of the open pits were cleaned from dust generated during the mining operations.

Mapping in the nine accessible pits was approached on foot and covered all benches and ramps of the respective open pits. The field work focused on the collection of structural, lithological and quartz-vein data. Satellite images of the mine area served, together with a GPS, as the base for the structural mapping. Sampling of diamond drill core for petrographic studies was also done during the main field season.

Structural readings and quartz-vein data were recorded using a *Clar-type* structural compass. A *Garmin Gecko* GPS was used to mark locations where measurements and observations were made. Readings of planar elements are given as dip direction and dip, whereas linear elements are given as plunge direction and plunge. All readings are given with respect to true north, corrected for a westerly declination of 6

degrees. All orientation diagrams are equal area stereographic projections into the lower hemisphere. Cross-sections were drawn using CorelDRAW® 12 (version 12.0.0.458). Maps were drawn up using ESRI ArcMap™ (version 9.2). Thin sections were prepared for a petrographic analysis of the main rock types, mainly taken from fresh core or bedrock samples from within the pits.

Chapter 2 Regional geology and background

2.1 Historical background

The northeastern region of Guinea and the central-northern region of Mali are situated in the centre of an ancient gold-mining district that is believed to have been a major gold producer since the 3rd century, at the time of the Mandingo Empire. The first records of modern mining activity in Guinea date back to 1903, whereas the first mechanized mining operation is recorded in 1909, when a stretch of the Tinkisso River was dredged for alluvial gold. Throughout the 20th century various exploration and mining operations were undertaken by Australian, French and Russian companies in close proximity to the present Siguiri Mining Complex (Paranhos, 2008). The modern mine named Société Ashanti Goldfields de Guinée or SAG has been operated by AngloGold Ashanti since 2004 when the mine was acquired from Ashanti Gold Fields Ltd.

2.2 Regional Geology

Our current knowledge of the geological inventory and evolution of West Africa mainly relies on a few publications and regional maps that were compiled by workers of the Bureau de Recherches Geologiques et Minieres (BRGM) during their regional mapping campaigns in the 1970's to 1990's (e.g. Ledru et al., 1991; Milési et al., 1992; Feybesse and Milési, 1994), as well as papers by other research groups (e.g. Taylor et al., 1992; Hirdes et al., 1992, 1996). More recent papers have added some crucial geochronological data that may help to correlate units and geological events across West Africa (Lahondère et al., 2002; Egal et al., 2002; Hirdes and Davis, 2002; Feybesse et al., 2006; Lompo, 2010), but our knowledge of the geology of West Africa and Guinea, in particular, remains very patchy.

The Archaean to Palaeoproterozoic West African Craton underlies a large portion of Western Africa (Fig. 1.1). The craton can be subdivided into two main parts, namely: 1) The Reguibat Rise in the north; and 2) the Leo Rise or Man-Leo Shield in the south. The latter comprises the Archaean Kenema-Man domain and the Palaeoproterozoic (Birimian) Boualé-Mossi domain (Fig. 1.2) (Lompo, 2010). The Archaean domain, constituting the southwestern part of the Man-Leo shield, was formed during the Leonian (3.0 – 2.9 Ga) and the Liberian (2.8 - 2.7 Ga) orogenic

cycles (Hirdes et al., 1996; Egal et al., 2002). The domain consists of high-grade metamorphic mafic to felsic gneisses and migmatites, structurally overlying the infolded greenstone belts and intruded by granitic rocks (Feybesse and Milési., 1994). The Archaean craton is surrounded by supracrustal rocks and granitoids of the Palaeoproterozoic Birimian (Boualé-Mossi) domain. The Birimian domain forms the central- and eastern parts of the Man-Leo Shield and is composed of granite batholiths, volcanic arc sequences and metasedimentary belts (e.g. Hirdes et al, 1992; Taylor et al., 1992)

The Birimian Supergroup unconformably overlies or is in structural contact with the Archaean basement. The sediments and volcanic rocks were deposited and shortly thereafter deformed and intruded by granitoids during the Eburnean Orogeny (2.27 - 2.05 Ga) recording a major episode of juvenile continental crust formation (Ledru et al., 1991; Taylor et al., 1992; Hirdes et al., 1992, 1996; Hirdes and Davis, 2002). The weakly metamorphosed volcano-sedimentary sequences of the Birimian Supergroup are mostly preserved as linear- to arcuate volcanic belts and intervening sedimentary basins. The sedimentary basins ascribed to the Lower Birimian (B1) essentially consist, from the base up, of (1) basic volcanic rocks and plutons of tholeiitic affinity, (2) turbiditic, flyschoid sedimentary sequences with volcanic intercalations, and (3) carbonate formations (Ledru et al., 1991; Milési et al., 1992; Feybesse and Milési, 1994, Hirdes et al., 1996). The volcanic belts are generally assigned to the Upper Birimian (B2) showing bimodal (tholeiitic and calc-alkaline) volcanism, polyphase intrusive magmatic complexes and fluvio-deltaic sedimentary successions (Milési et al., 1992; Feybesse and Milési, 1994). Extrusive and related intrusive events took place between ca. 2.25 – 2.10 Ga, while sediment deposition took place ca. 2.18–2.05 Ga (Lompo, 2010). Overall, the succession of arcuate volcanic belts and intervening sedimentary basins is interpreted as representing island-arc complexes and associated back- and/or fore-arc basins accreted to the Archaean craton during the Eburnean Orogeny (e.g. Ledru et al., 1994).

The northerly-trending Sassandra Fault system in the southern part of the West African craton is traditionally regarded as the main structural boundary between the Archaean and Palaeoproterozoic domains. This fault system also outlines the southern boundary of the Siguiri Basin in the northeastern part of Guinea (Egal et al., 2002). The fault system is developed as an up to ca. 100 km wide (the maximum

width of the plutonic belt between the Siguiri basin and the Kenema-Man domain; see below) and ca. 1000 km long zone of anastomosing, mylonitic, transcurrent or reverse faults (Kouamelan et al., 1997). Most workers interpret the Sassandra Fault as a composite and possibly repeatedly reactivated thrust zone along which the Birimian rocks in the east were accreted onto the older Man-Leo Shield in the west (Cohen and Gibbs, 1988). The fault system also experienced later left-lateral displacement, with dominantly sinistral strike-slip faults (Cohen and Gibbs, 1998; Kouamelan et al., 1997).

The polycyclic character of the Birimian orogenic belt was established from more detailed work by the BRGM in Ghana, which is commonly taken as a possible template for the evolution of, and correlations with other areas in West Africa (Milési et al., 1992). Palaeoproterozoic Birimian continental crust was created during a succession of tectonic events:

1. The initial deposition of the mainly sedimentary Lower Birimian (B1) is suggested to have occurred into an intracratonic, possibly continental back-arc basin, with basic tholeiitic rocks preserved locally at the base, and tholeiitic volcano-sedimentary intercalations at the top. Lahondère et al. (2002) located a suite of volcanic rocks in the northeastern part of the Siguiri Basin. Radiometric ages of 2212 ± 6 Ma for the volcanics constrain the age of early Birimian volcanic activity in northeastern Guinea. The intermediate- to acidic, calc-alkaline magmas with high-Al/low-Yb concentrations are indicative of subduction magmatism (Lahondère et al., 2002).

2. Accretionary tectonics around the Archaean nucleus is attributed to convergence and collision tectonics during the first tectonic phase (D_1). D_1 thrusting started in the south between 2165 and 2100 Ma, creating a composite tectonostratigraphic pile consisting of pre- to syn- D_1 Proterozoic terrains, Archaean rocks, and some of the earliest B1 deposits. During this time, B1 sedimentation continued to the east of the main suture zone, including that of the Siguiri Basin, and sediments were derived, at least in part, by erosion of the domain undergoing crustal thickening to the west (Feybesse and Milési, 1994). As D_1 deformation progressed, the flyschoid deposits in the hinterland were affected by shortening, resulting in fold-and-thrust tectonics and crustal thickening until ca. 2095 Ma.

According to Hirdes et al., (1992, 1996) and Feybesse and Milési (1994), the timing of D_1 was diachronous across the Man-Leo Shield, progressing from southeast to northwest. The timing for D_1 across the western region of the Kenema-Man domain, and the northwestern region of the Boualé-Mossi domain (east of the Siguiri Basin), is suggested to be after ca. 2095 Ma, whereas D_1 affected the rest of the Kenema-Man domain between 2165 and 2095 Ma.

The protracted nature of the D_1 deformation, together with the overlap of sedimentation and deformation, reworking of sediments and volcanism/plutonism, are all indicative of the accretion of B1 sediments, and more generally of Palaeoproterozoic terrains, onto the Archaean Kenema-Man domain during crustal convergence. This implies the progressive burial of accreted terranes and is consistent with the observed metamorphic evolution reflecting two main stages: (a) a period of prograde metamorphism of rock units and clockwise P-T paths during accretion and crustal thickening, followed by (b) a period of uplift, erosion and associated retrograde metamorphism. The transition from the accretionary stage to subsequent uplift and erosion coincided with the regional-scale, late-D_1 deformation and thermal evolution (Feybesse and Milési, 1994).

3. D_1 thrusting and folding was succeeded by a period dominated by B2 volcanic activity, voluminous granite plutonism and transcurrent tectonism marking the onset of a second tectonic event (D_2). Sheeted dykes, submarine lava flows and pyroclastic rocks were emplaced before D_2 transcurrent tectonics and upon deformed and metamorphosed B1 terranes. This suggests that a rapid period of uplift and erosion must have separated the end of D_1 from the deposition of the B2 sequence. The geochemical signature of B2 volcanism suggests a variety of geodynamic settings for the respective area, including continental and oceanic island arc magmatic activity (Feybesse and Milési, 1994). Local areas of calc-alkaline volcanism and intercalated fluvio-deltaic sedimentation bounded by transcurrent faults are interpreted to represent volcanism in continental, transtensive basins (Feybesse and Milési, 1994).

B2 volcanism and sedimentation was followed by major strike-slip and/or transpressive tectonics, corresponding to a final accretionary phase that dominated the late stages of the Eburnean Orogeny. The D_2 deformation phase is marked by N- to NNE-trending sinistral strike-slip fault zones along the eastern

margin of the Archaean Kenema-Man domain, that are locally associated with SE-verging thrust zones. This phase is associated with shortening from the southeast. This includes the first-order, transcontinental Sassandra fault system. The coeval fluvio-deltaic deposits in the West African and Guyana Cratons filled rapidly subsiding basins and are associated with major D_2 sinistral faults. The deposits show coarse-grained, molasse-type sediments derived from areas of high relief, most likely the mountain belt built during the D_1 tectonic phase (Feybesse and Milési, 1994).

The timing of D_2 coincides with major plutonic activity at the south to southwestern limit of the Siguiri Basin, i.e. northeastern boundary of the Kenema-Man domain and is characterized by major WNW- to NW-trending sinistral strike-slip faults. These intense sinistral deformation trends, under ductile conditions is absent in the rest of the Siguiri basin, relating to lower degrees of deformation towards the north, away from the Kenema-Man boundary. The magmatic and structural evolution of the D_2 plutonism occurred over a short time span between 2090-2070 Ma and constrains the timing of the D_2 deformation event at the southwestern margin of the Siguiri Basin (Egal et al., 2002). This corresponds to a phase of Late Eburnean ENE-WSW shortening and postdates major north-south sinistral displacement described elsewhere across the Man-Leo Shield (Lahondère et al., 2002).

4. The D_3 deformation is characterized by northeast-southwest dextral strike-slip faults. The D_2 and D_3 deformation phases most probably form part of a progressive deformation. The bulk of the deformation coincided with the waning stages of the B2 volcanic period and both D_2 and D_3 deformations are marked by granite emplacement (Milési et al., 1992; Feybesse and Milési, 1994). In the Siguiri Basin the occurrence of intense hydrothermal alteration along NNE- and NE-trending dextral faults is associated with the injection of monzogranites. Petrographically, these monzogranites are similar to the monzogranites dated at 2074 ± 5 Ma (Lahondère et al., 2002).

In summary, the Palaeoproterozoic geological evolution of the West African Craton involves a D_1 collisional phase, recording the accretion of volcanic arcs and intervening basins onto the Archaean Kenema-Man domain. Accretionary tectonics (D_1) was accompanied by high-grade metamorphism with, in places, migmatization of

rocks in the west and syn-tectonic intrusions. The post-collisional evolution involved the uplift of the accreted tectonic pile, accompanied by further accretion of terranes from the east associated with major sinistral transpressional shear zones (D_2) and widespread granite emplacement. The subsequent isostatic uplift of the accreted terranes was followed by the collapse and fragmentation of the orogen (D_3) (Feybesse and Milési, 1994).

2.3. Geology and geological context of the Siguiri Basin

The Siguiri Basin, which hosts the Siguiri Mining Complex, occupies an extensive area of ca. 200 000 km^2, in northeastern Guinea extending northeastward towards Mali. To the north, rocks of the Siguiri basin are covered by Neoproterozoic sediments of the Taoudéni Basin. Elsewhere, the basin is bounded by intrusive granitic rocks.

The typical turbiditic sequence of the Siguiri Basin is essentially composed of weakly metamorphosed sedimentary rocks (argillite, greywacke, conglomerates and psammites), and, to a lesser degree, volcanic rocks (mafic lava and intermediate- to felsic pyroclastics) intercalated with the sediments as well as subvolcanic dykes (Egal et al., 2002).

2.4 Previous studies of the Siguiri Mining Complex

Previous work on the Siguiri Mining Complex and associated mineralization is, for the most part, summarized in only two company reports (Holcombe, 2007; Paranhos Jr, 2008).

Holcombe (2007) suggested the Siguiri Mining Complex to be hosted by a west-verging fold-and-thrust stack. The mineralization was interpreted to form part of the mine-scale structural pattern. Holcombe (2007) based his conclusion on the westerly vergence of, at the time, some of the better exposed fold structures in the Siguiri Mining Complex and purported low-angle thrusts. Folds and thrusts were supposed to be part of a larger imbricate stack made up of at least four emerging and/or blind thrusts. A slightly different view was expressed by Paranhos Jr, (2008) who suggested mineralization to be controlled by brittle-ductile, N-S and WNW-trending shear zones. The northerly-trending faults recorded supposedly sinistral strike-slip displacement, whereas high-angle shear zones recorded a top-to-the-southwest

thrust sense of displacement. The pattern of strike-slip- and thrust faults were interpreted to have developed in response to northwest-southeast shortening. Hence, Paranhos Jr. (2008) model for the mineralization involved an overall transpression model.

Chapter 3 Introduction to the Siguiri Mine

3.1 Introduction

The Siguiri Mining Complex currently consists of nine recently excavated open pits, four of which were being mined at the end of the field period. Older pits include a number of shallow excavations that only mined the lateritic cover (Kossise East), but also deeper pit operations (The Toubani- and Sintroko Old Pits). The latter reached the underlying saprolite zone. All of these older operations were deeply weathered and partly flooded or overgrown, making data collection unfeasible.

The main operating pits are located in an area of 12 km (north-south) by 3 km (east-west. From north to south, the main open pits of the Siguiri Mining Complex are Eureka North, Sanu Tinti, Bidini, Toubani, Kozan, Kami North, Kami South, Kossise and Sintroko (Fig. 3.1). The presently (October/2010) mined open pits are, from north to south, Toubani, Kami North, Kami South and Sintroko. These pits reveal new data on a daily basis as new parts of the pits are exposed.

3.2 Overview of open pits at Siguiri Mining Complex

This chapter provides a brief overview of the location of the open-pit operations that were investigated in this study (Fig. 3.3). Detailed descriptions of the lithological packages, geology and quartz-vein inventories of individual pits are given in Chapters 4 to 6.

3.2.1 Eureka North

Eureka North is currently the northernmost pit of the Siguiri Mining Complex. The main pit is elongated in a northwest-southeast orientation and consists of two open pits located in the northwest and southeast respectively. A NW-trending embayment of around 200 m in length and 70 m width has also been mined in the southeast. The dimensions of the combined two pits are 670 m along strike and 240 m at the widest point in the northwest.

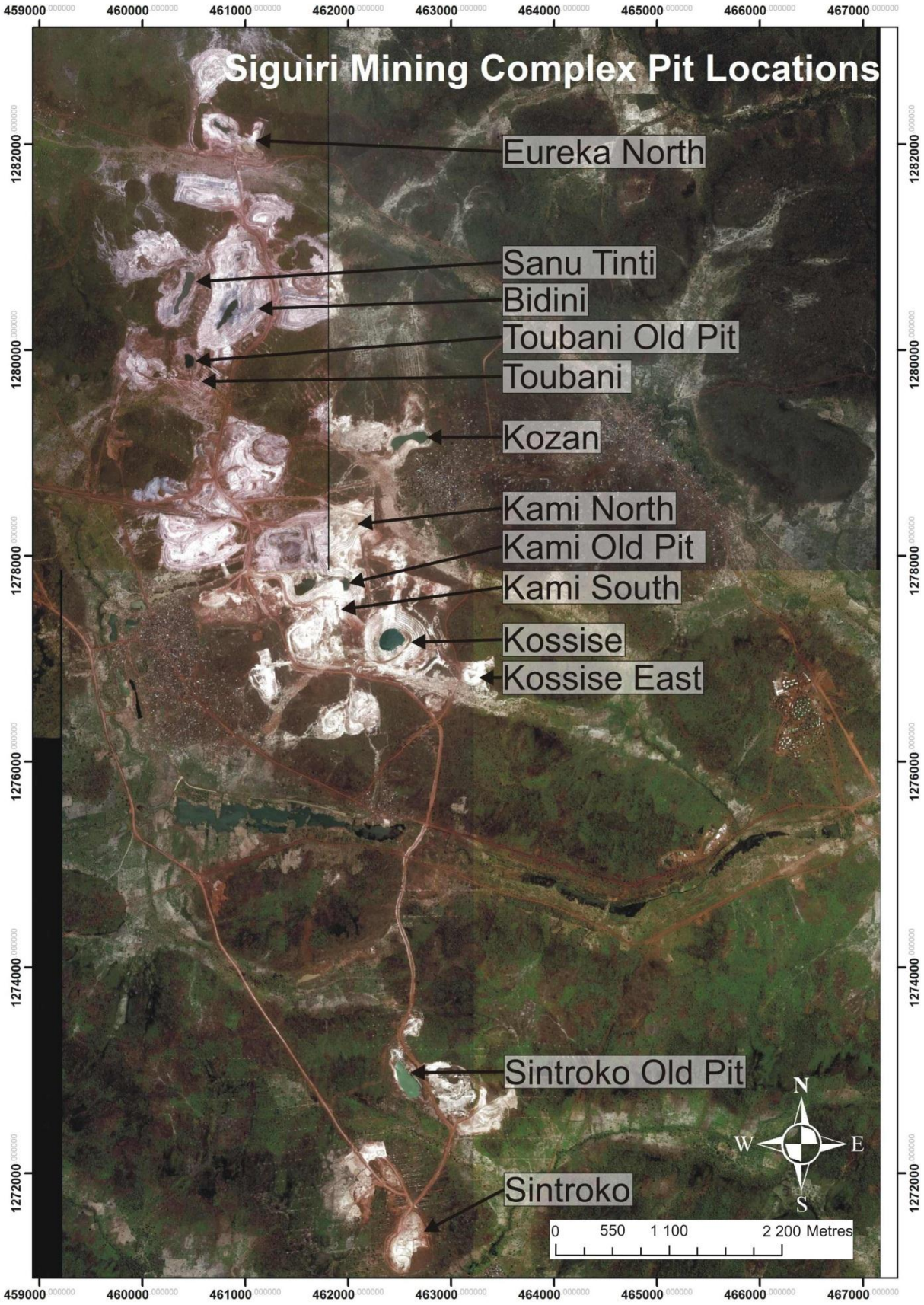

Figure 3.1: Satellite image showing the location of the main pit operations and some older pits of the Siguiri Mining Complex.

3.2.2 Sanu Tinti

The Sanu Tinti pit is one of the older and deeply weathered open pits. It is oval shaped and elongated in a NNE-SSW direction. The pit has a total length of 580 m and a maximum width of 360 m.

3.2.3 Bidini

Bidini, together with Sanu Tinti and Toubani, forms part of a larger and structurally complex mineralized area. The Bidini operation consists of a northern and a southern pit that combine to form an elongated, NNE-trending open pit with a combined length of 1050 m and a maximum width of 650 m.

3.2.4 Toubani

The Toubani pit consists of an older northern pit (Toubani Old Pit) with a circular outline, whereas more recent mining operations extend toward the south. Overall, the current dimensions of the entire Toubani operation measures about 600 m in length (northwest-southeast extent) and about 500 m in width (northeast-southwest extent).

3.2.5 Kozan

Kozan is the easternmost pit of the Siguiri Mining Complex. The main pit is elongated in an east-west direction and consists of two smaller pits in the east and the west. The main pit has three cut-backs (75 m long) towards the north. The pit has a length of 450 m and is 200 m at the widest.

3.2.6 Kami North

Kami North forms the northern part of the larger Kami complex. The main pit of Kami North is elongated in an east-northeast direction, but with a southerly-trending embayment in the far west. The pit has a dimension of 1100 by 700 m.

3.2.7 Kami South

Kami South forms the southern extent of the Kami complex. The main pit consists of a larger southern pit and with a smaller pit (Kami Old Pit) in the northeast. The main pit is 800 m long and has a maximum width of 400 m.

3.2.8 Kossise

The Kossise pit has a round outline, in plan view, with a small (150 m in length, 60 m wide) embayment towards the north. The overall diameter of the pit is ca. 550-600 m.

3.2.9 Sintroko

Sintroko is the southernmost pit in the Siguiri Mining Complex. The pit has an oval geometry and dimensions of 630 m in length along its north-northeast extent and 450 m in width.

3.3 Introduction to weathering profile

The Siguiri Mining Complex is underlain by rocks that have undergone extensive and deep chemical weathering. The resulting thick lateritic regoliths are widespread in inter-tropical regions of the world, where they form under humid and warm tropical to subtropical conditions characterized by a wet rainy season, followed by a dry, dry season. The intense weathering, including leaching and oxidation of the original bedrock, produce similar, deep-reaching weathering profiles in all lateritic regions of the world (e.g. Butt et al., 2000). This weathering profile is represented by the following horizons, from top to bottom (Fig. 3.2.A):

1) **Mottled and ferruginous zone** – The mottled and ferruginous (laterite) zone at the Siguiri Mining Complex shows a vesicular texture and has an average thickness of between 4 m to 10 m. This zone is mostly rusty-red in colour, due to the high amount of Fe-oxides, -hydroxides and Al-hydroxides. Most of the original mineral constituents, except for quartz, are commonly completely weathered in this horizon (Fig. 3.2.B). This zone is characterised by the domination of Si, Al and Fe resident in kaolinite, quartz, hematite, goethite and gibbsite. Primary geological features such as bedding are only very rarely preserved in the mottled zone (Butt et al., 2000).

2) **Saprolite zone** – The underlying and very thick saprolite zone of the Siguiri Mining Complex is typically white- to beige and grey- to red in colour,

dominated by fine-grained clays and, as a result, a rather soft and soapy appearance (Ollier et al., 1990). The saprolite zone reaches an average thickness of between 30 m and 90 m. The saprolite zone can be further divided into the lower-, middle-, and upper saprolite. These zones differ from each other by the amount of altered primary- and secondary minerals present in the profile. Only weathering-resistant primary minerals are present in the upper saprolite zone, whereas the lower saprolite zone is characterized by the weathering of only the less stable minerals such as feldspars and most ferromagnesian silicates. Original geological features of the bedrock can be discerned and include bedding as well as foliations and/or linear fabrics.

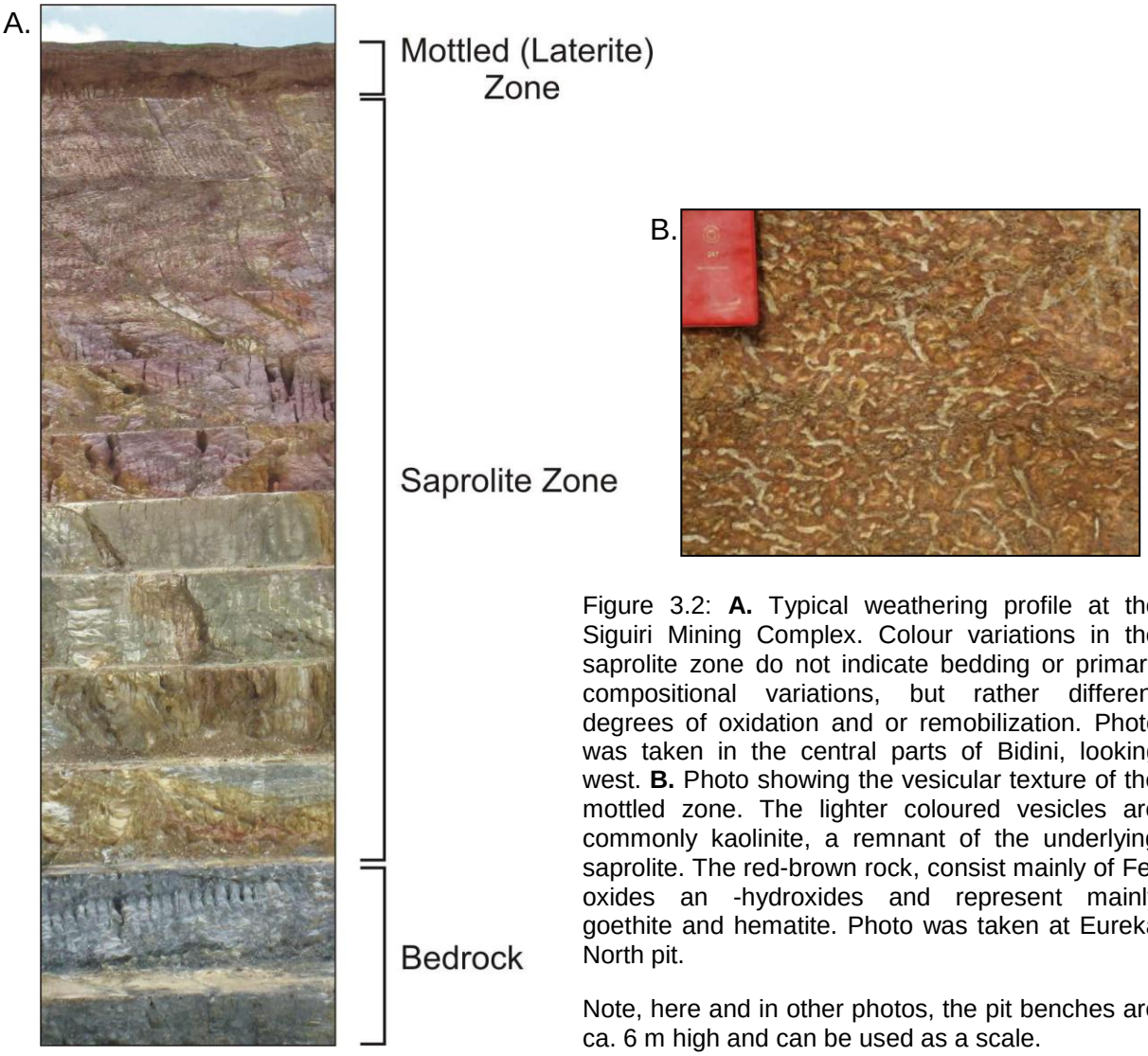

Figure 3.2: **A.** Typical weathering profile at the Siguiri Mining Complex. Colour variations in the saprolite zone do not indicate bedding or primary compositional variations, but rather different degrees of oxidation and or remobilization. Photo was taken in the central parts of Bidini, looking west. **B.** Photo showing the vesicular texture of the mottled zone. The lighter coloured vesicles are commonly kaolinite, a remnant of the underlying saprolite. The red-brown rock, consist mainly of Fe-oxides an -hydroxides and represent mainly goethite and hematite. Photo was taken at Eureka North pit.

Note, here and in other photos, the pit benches are ca. 6 m high and can be used as a scale.

3) **Bedrock** – The deep weathering profile is underlain by the original bedrock. The top part (weathering front and saprock) of the substratum underwent alteration of only the most unstable minerals, sulphides, but remains unaltered further down. The bedrock contains all primary sedimentary features as well as tectonic fabrics, most of which are absent from the upper horizons of the weathering profile. In the Siguiri Mining Complex, the transition between the saprolite zone and bedrock can be very sharp, as mapped in Bidini (Fig 3.2.A).

Mining in the Siguiri Mining Complex presently focuses on the oxidized, clay-dominated rocks of the saprolitic zone. The relatively soft rocks not only facilitate mining through excavators with only little need for blasting, but the current setup of the metallurgical plant also does not allow for the processing of sulphide ores of the bedrock. Consequently, the detailed knowledge of the depth and extent of the weathering profile is of paramount importance.

The depth of chemical weathering in the Siguiri Mining Complex varies between open pits. Local variations may be as much as several tens of metres. These variations commonly occur around more prominent shear zones, in Sintroko. Graphitic schists, in particular, seem to be preserving primary features very well and the reducing nature of the schists prevents oxidation of even sulphides in the weathering profile. Most of the weathering fronts cannot be seen due to the flooding of the bottom parts of most open pits. Fresh bedrock was encountered at the bottom of the Kami North and Bidini pits.

Chapter 4 Lithostratigraphy

4.1 Introduction

The Siguiri Mining Complex forms part of the Palaeoproterozoic Siguiri Basin for which only a very broad lithological inventory, but no detailed or even regional lithostratigraphy has been established. As a consequence, a correlation of lithological units and the lithostratigraphy of the Siguiri Mining Complex with the rest of the basin is not possible. As will be outlined in Chapter 5, lithological variations exert an important control on the distribution of auriferous quartz veins in the Siguiri Mining Complex. For this reason, and wherever possible, lithological packages were distinguished and integrated into the structural maps. A detailed sedimentological characterization of the rocks of the Siguiri Mining Complex is beyond the scope of this thesis. The intense saprolitization has also obscured many primary sedimentary structures. Primary features such as graded bedding, rip-up clasts, or ball-and-pillow and soft-sediment deformation structures that are easily observed in core remain largely unnoticeable in the saprolite profile. This, together with the complete obliteration of original mineralogical composition renders a detailed characterization of the rocks almost impossible. The aim of the lithological mapping and subdivision followed in this study was rather to distinguish lithological packages that could be traced through individual pits and possibly between pits in order to aid exploration and mining.

The Siguiri Mining Complex is underlain by a clastic sedimentary succession of pelites, siltstones and psammitic sandstones or greywackes. This broad subdivision was adopted for a general distinction of rock types, without going into any more petrographic detail. For example, many “sandstone” units, when fresh, show lithic fragments and a significant clay component, rather pointing to a greywacke-like composition. Sedimentary breccia units are distinct, but volumetrically subordinate, although some of the characteristically oligomict breccias can reach several tens of metres in thickness (Sanu Tinti). Volcanic horizons (or intrusive sills/dykes) were only observed with certainty at Eureka North, forming thin (<30 cm thick) layers, with a characteristic columnar weathering pattern. A strongly graphitic schist unit was mapped at Sintroko, forming an up to 15 m wide lens that can intermittently be followed along strike for ca. 250 - 300 m.

4.2 Field characteristics and petrography

4.2.1 Pelitic unit

Description

Pelitic or shaly units are easily recognized in the field having a soft and soapy touch, with colours varying from light-brown, yellow- to light-green, depending on the depth of the unit in the saprolite profile. Individual beds are mostly well defined. Fine-scale laminations are locally observed, but the beds appear largely homogeneous. Graded bedding of pelites into siltstone- and greywacke units is common in some of the pits, such as Bidini (Fig 4.1 and 4.2), but is otherwise only sporadically observed. Pencil weathering in some less weathered pelitic beds indicates the presence of secondary fabrics.

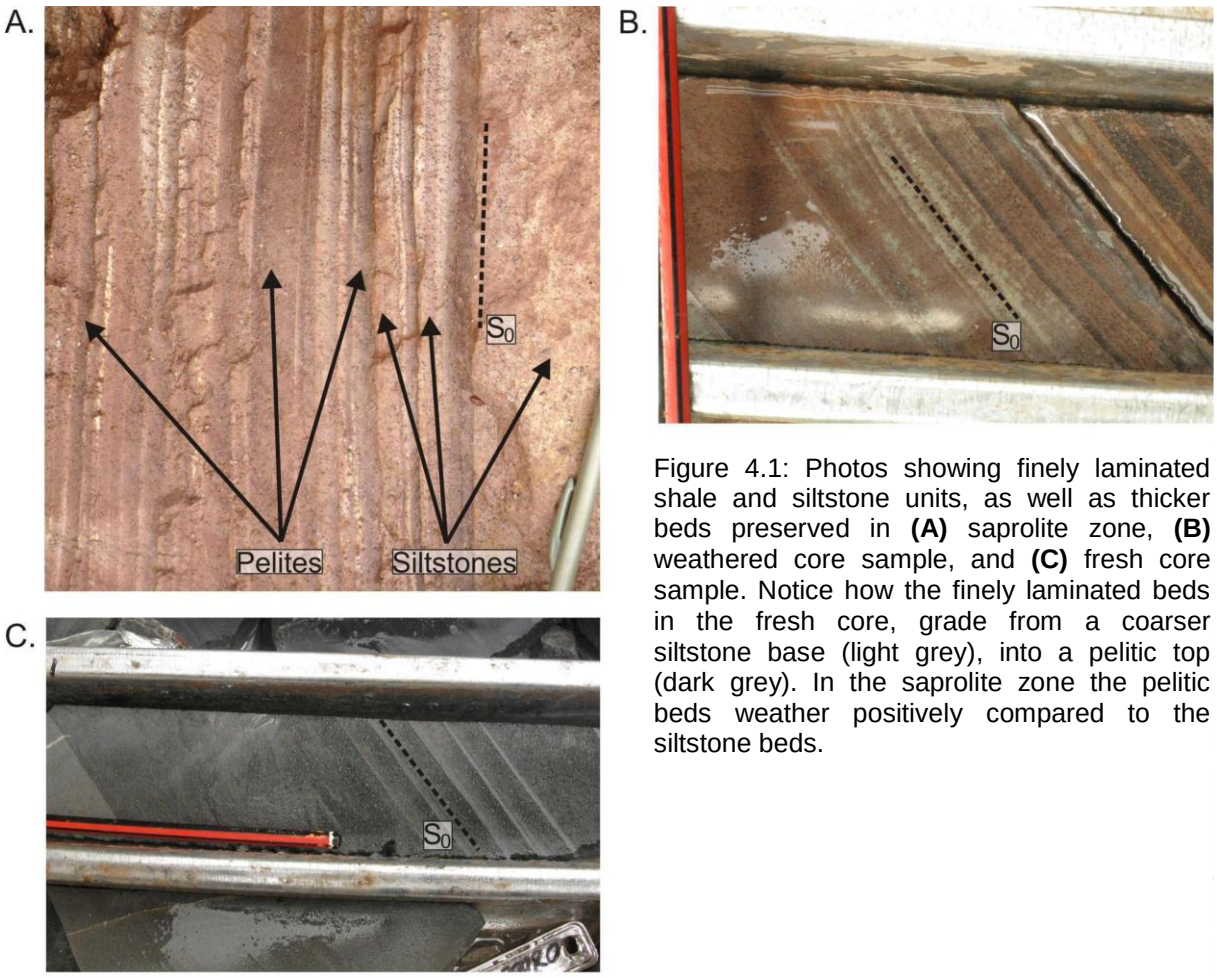

Figure 4.1: Photos showing finely laminated shale and siltstone units, as well as thicker beds preserved in **(A)** saprolite zone, **(B)** weathered core sample, and **(C)** fresh core sample. Notice how the finely laminated beds in the fresh core, grade from a coarser siltstone base (light grey), into a pelitic top (dark grey). In the saprolite zone the pelitic beds weather positively compared to the siltstone beds.

In core samples the shale beds are commonly rich in sulphides. Sulphides include mainly pyrite and less commonly arsenopyrite that may form up to 5 mm large, euhedral grains. The pelitic units found in core samples differ significantly from those in the saprolite zone in colour, texture and hardness. Unaltered core samples and fresh rocks show the pelites to be dark-grey, almost black, to grey, homogeneous or finely laminated units. Cross-bedding was rarely observed in the finely laminated pelitic beds in the saprolite zone.

Distribution

Pelitic units are found in all the pits, commonly interlayered with siltstone (as shown in Fig. 4.1). Gradational contacts between the two are common, but contacts between pelites and siltstones may also be sharp. The interlayered pelite/siltstone units typically form up to ca. 4 m thick packages. These packages are distinct by being less susceptible to quartz veining (see Chapter 6). Good examples of pelitic units can be found in the open pits of the Kossise and Kami complex.

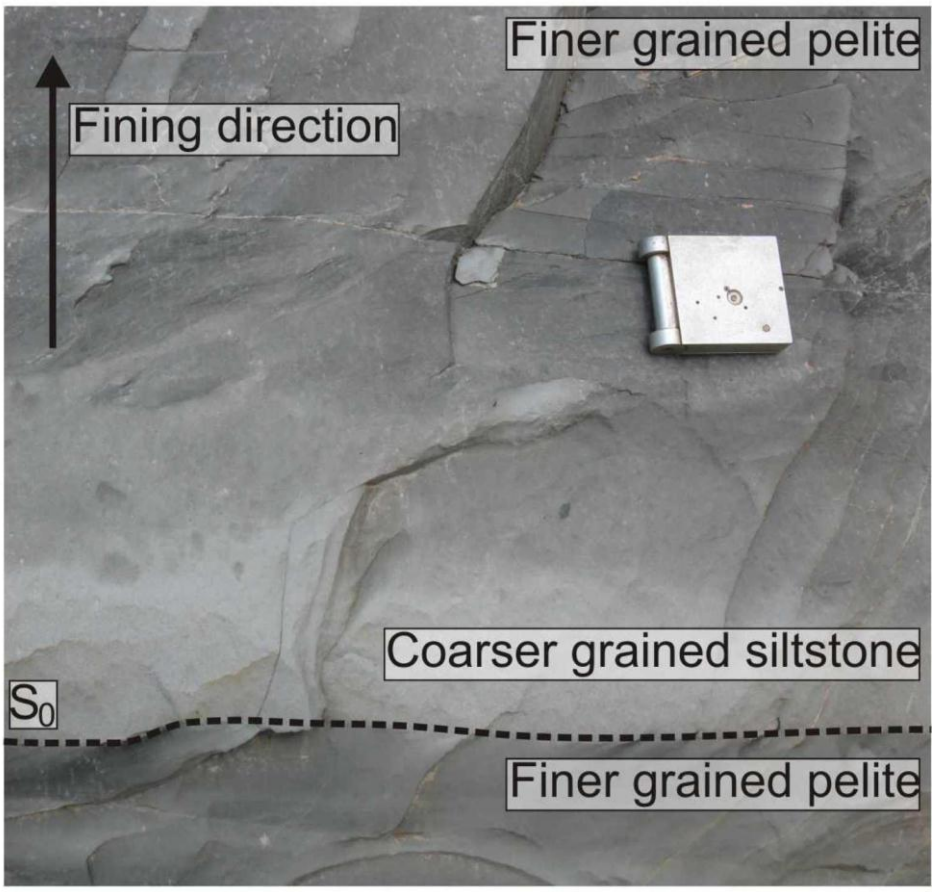

Figure 4.2: Photo showing normal grading in a siltstone bed. This siltstone bed grades from coarser-grained siltstone at the base (medium grey), into a finer-grained siltstones and pelite at the top (darker grey). Photo was taken in the folded central domain of Bidini pit, view to the west.

Petrography

Fine-grained pelitic units consist dominantly of quartz, plagioclase and muscovite/ sericite (Fig. 4.3). Very fine-grained (< 0.05 mm) quartz and plagioclase are present in equal quantities and individual minerals are difficult to make out in the optical microscope even under 50x magnification. Coarser-grained quartz and feldspar grains are only sporadically developed and contribute less than 5% of the total mineral assemblage. Muscovite/sericite is developed as very fine-grained, platy-grains defining a foliation in the rock. From the mineralogical report by Theron and Coetzee (2010) the feldspar is classified to predominantly develop as albite. Shale units commonly contain sulphides (Fig. 4.3). The sulphides occur as euhedral to subhedral grains (< 1 mm), most commonly of pyrite and arsenopyrite and are sparsely distributed throughout the lithotype.

Figure 4.3: A thin section photo taken of a pelite in the Siguiri Mining Complex, using cross-polarized light. Here the rock shows a very fine-grained texture, with a few larger albite and quartz minerals in the matrix. Platy muscovite/sericite is abundant and the grain-shape preferred orientation of minerals defines the foliation. Sulphides, commonly pyrite, are sparsely developed in the pelite units.

4.2.2 Siltstone unit

Description

Siltstone units are coarser-grained than pelites. Siltstones are well bedded and show both sharp as well as gradational contacts with pelitic units. Laminar bedding is well developed in thinner siltstone beds (Fig 4.1), with normal graded bedding observed in

the thicker siltstone beds (Fig. 4.2). The colour of siltstones in the saprolite zone varies with depth in the weathering profile from brown- to light-yellow. The siltstone units also tend to preserve secondary fabrics particularly well. In places, fresh siltstone samples show evidence of alteration preserved in the form of rounded- to angular alteration spots (Fig. 4.4). The alteration spots are classified as siderite and commonly develop an Fe-rich chlorite rim, around the siderite core (Fig. 4.6.B) (Theron and Coetzee, 2010). Some of the alteration spots appear flattened and also show a preferred orientation, parallel to the foliation defined by the white mica. In core samples, the siltstone beds appear light-grey in colour, but the rocks are too fine-grained to identify individual minerals with the naked eye. Rip-up clasts of dark shaly material at the base of siltstone units (Fig 4.5) are readily observed in fresh bedrock or in core, but these features remain unnoticed in the saprolite zone.

Distribution

Siltstone units are common in all of the nine pits of the Siguiri Mining Complex. The thickness of individual beds ranges from thin, mm- to cm-scale laminations to beds of up to a few metres in thickness. Siltstone beds are commonly interlayered with thinner pelite beds.

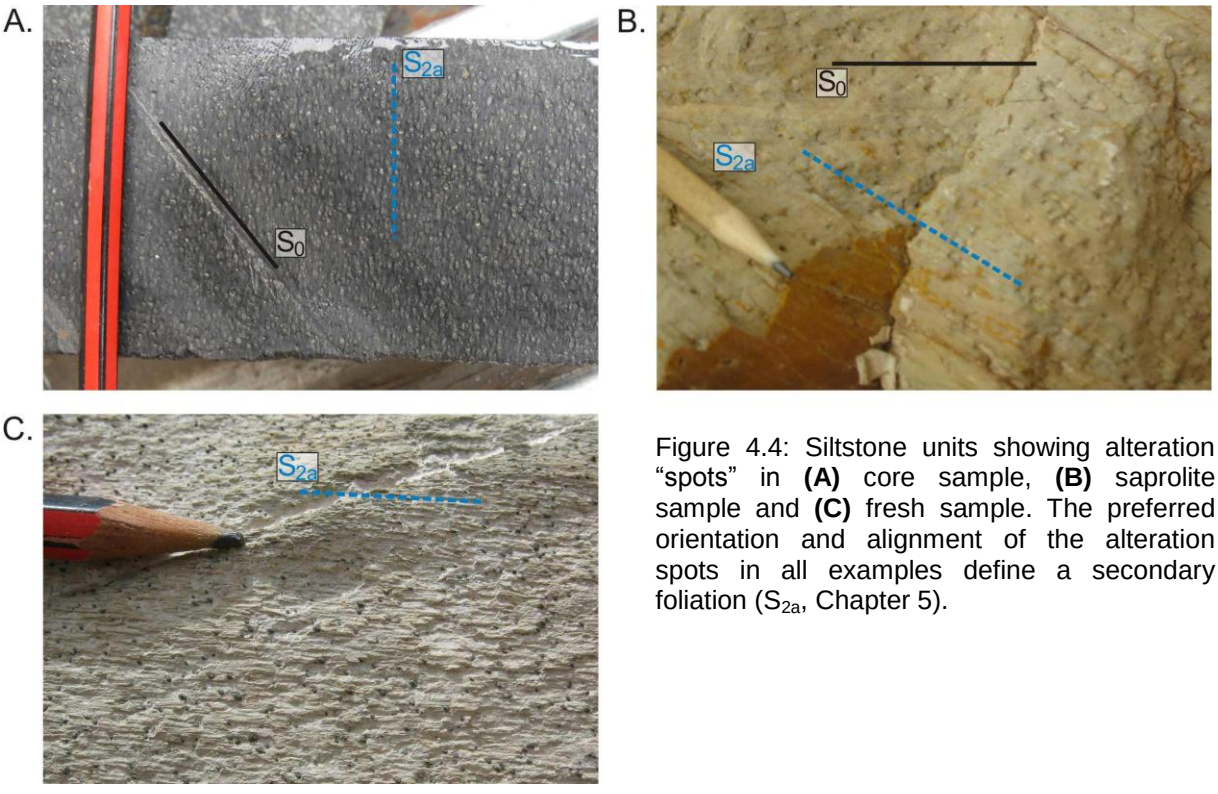

Figure 4.4: Siltstone units showing alteration "spots" in **(A)** core sample, **(B)** saprolite sample and **(C)** fresh sample. The preferred orientation and alignment of the alteration spots in all examples define a secondary foliation (S_{2a}, Chapter 5).

Petrography

Siltstone units are slightly coarser grained than the pelitic units. Here angular to rounded, quartz and albite grains (< 0.3 mm) occur at almost equal amounts and make up the bulk of the mineral composition (Fig. 4.6.A). Pervasive carbonate "spots" are commonly developed in siltstone units, making up to 10% of the bulk composition of the rocks. Geochemical analysis of the carbonate nodules indicate that the grains (< 2 mm) commonly consist of a siderite core, surrounded by an Fe-rich chlorite rim (Fig. 4.6.B)(Theron and Coetzee, 2010). Very fine-grained white mica is also present in the matrix anastomosing and wrapping around the carbonate nodules, accentuating the secondary fabric. Pressure shadows at either end of the siderite nodules are elongated in the plane of the foliation. Larger (1-2 mm), euhedral pyrite and arsenopyrite grains are commonly developed in the siltstones.

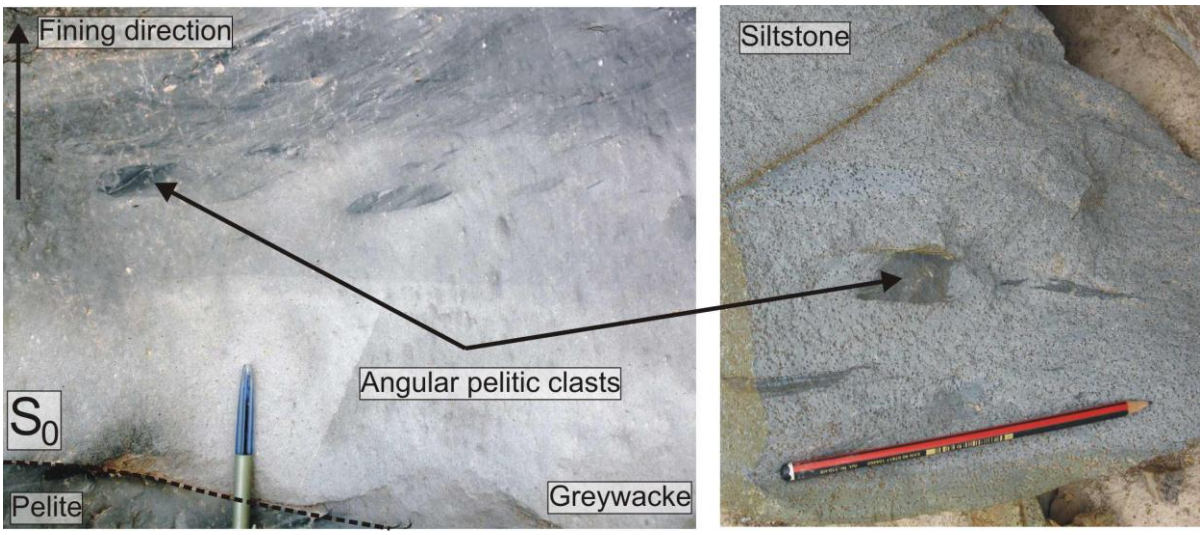

Figure 4.5: Outcrop photos of shale rip-up clasts at the base of siltstone and greywacke units. Photos were taken in Bidini and Kami North pits.

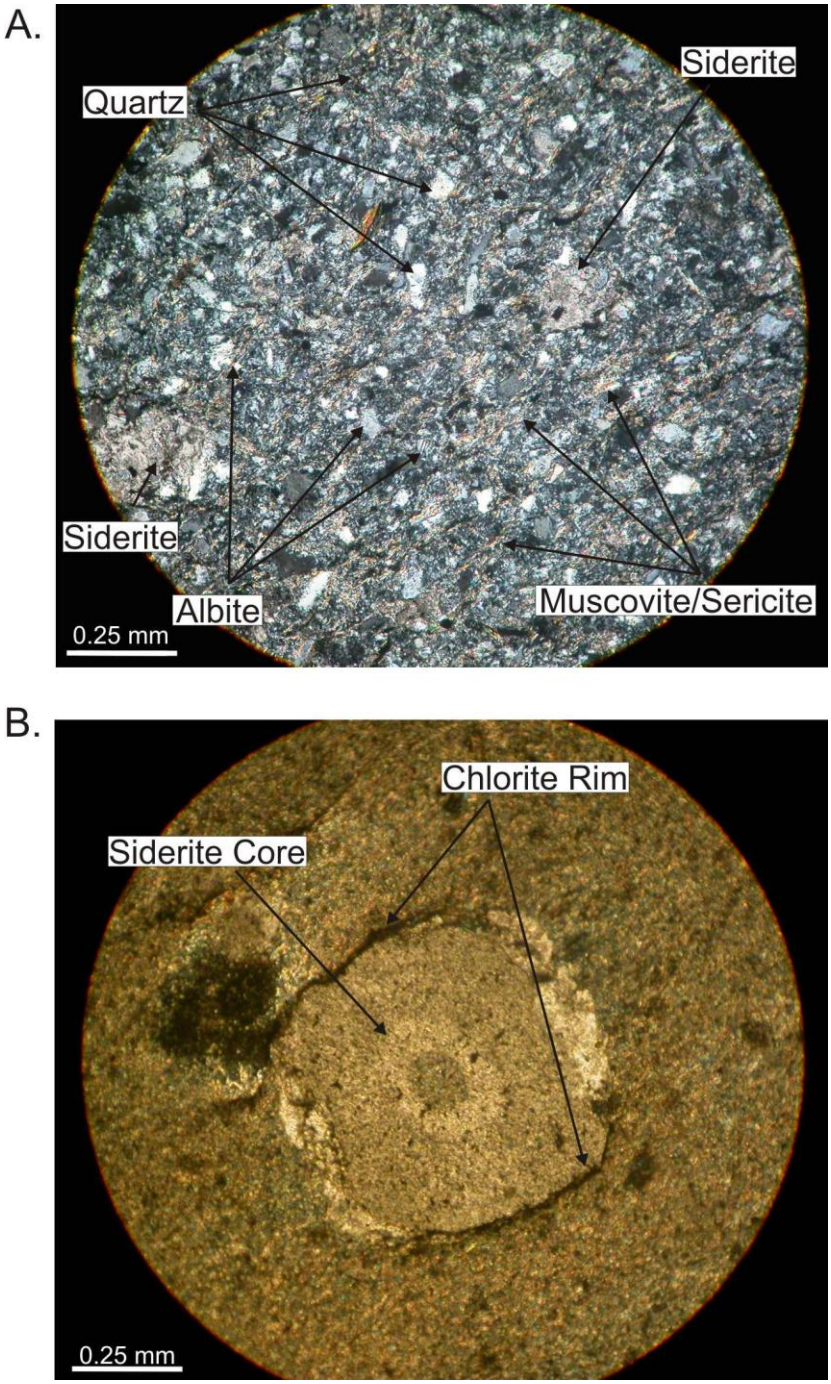

Figure 4.6: **A.** Thin section photograph of a siltstone unit under cross-polarized light. The photo shows fine-grained quartz and albite. Muscovite/sericite is common and occur as platy grains, defining a foliation. Disseminated siderite spots show larger grain sizes. The siderite alteration spots overgrows the quartz and albite of the matrix, which now occur within the alteration spots. **B.** Thin section photo of (cross-polarized light) a carbonate alteration spot in a siltstone. The alteration spots shows concentric zoning made up of a lighter coloured siderite core, surrounded by a thin, dark Fe-rich chlorite rim.

4.2.3 Greywacke unit

Description

Greywacke units occur as more massive beds, with sharp to, in places, graded contacts with either pelites or siltstones. In the saprolite zone, the coarser-grain size and higher quartz content is a diagnostic feature that allows identifying greywackes in the field.

In core samples, greywacke beds contain fine-grained (<1 mm) sulphides. When fresh, greywacke units are light- to dark-grey in colour. In the saprolite zone, the weathering profile influences the colour of the beds that may show variations of brown, light-brown and light-yellow to almost white between different parts of the open pits. Up to 10 cm large pelitic rip-up clasts are found at the base of greywackes, in both the weathered units as well as in core samples (Figs. 4.7.A-C). Flute clasts were also observed at the bottom of some fresh beds at the bottom of Bidini pit.

Distribution

Greywacke units are distributed throughout the Siguiri Mining Complex. The greywacke units are, on average, thicker than pelites and siltstones and individual greywacke beds may reach a thickness of > 6 m, as observed in Kossise open pit (Fig 4.8). Similar to pelites and siltstones, the greywacke units also tend to form packages of massive beds that are locally interlayered with the finer-grained rocks. These packages may reach a thickness of up to ca. 40 m. Prominent packages are developed in Kossise and Eureka North pits and these units are distinguished on the geological maps of individual open pits. Most importantly, auriferous quartz veins show a closer spacing in these coarser-grained greywacke packages compared to the finer-grained lithologies. This aspect will be further discussed in Chapter 6.

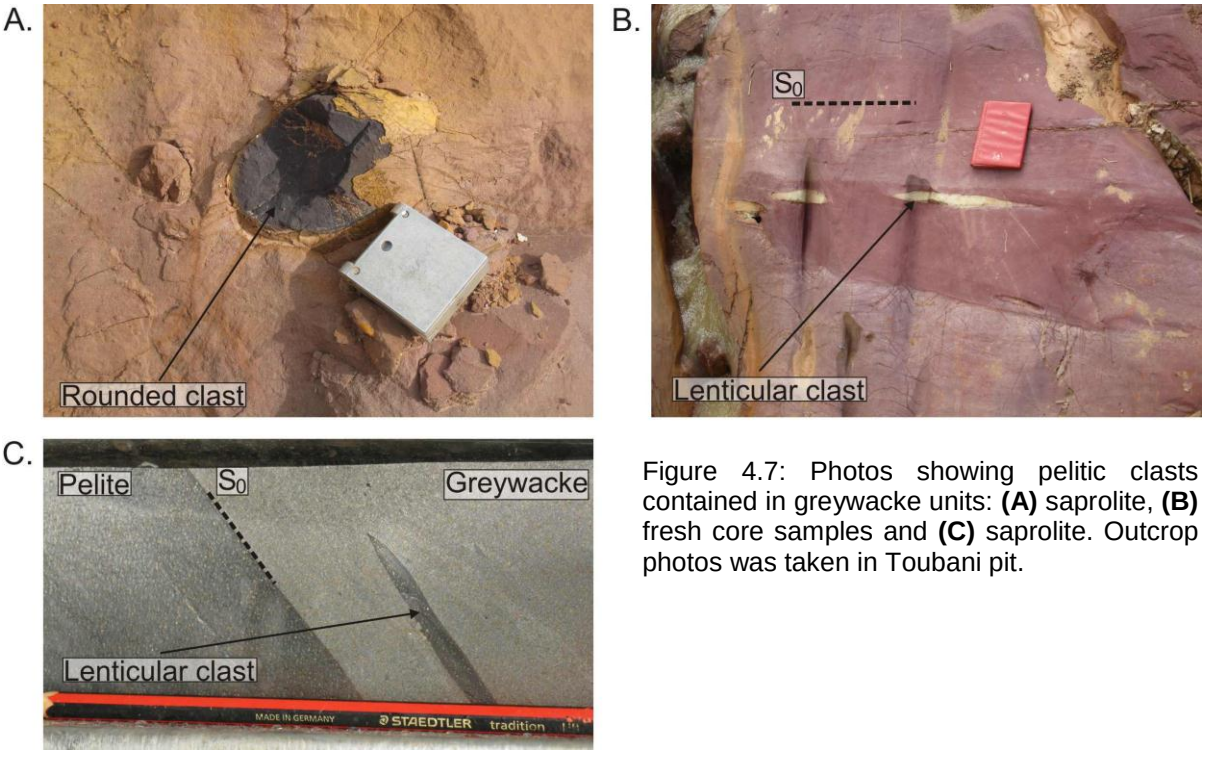

Figure 4.7: Photos showing pelitic clasts contained in greywacke units: **(A)** saprolite, **(B)** fresh core samples and **(C)** saprolite. Outcrop photos was taken in Toubani pit.

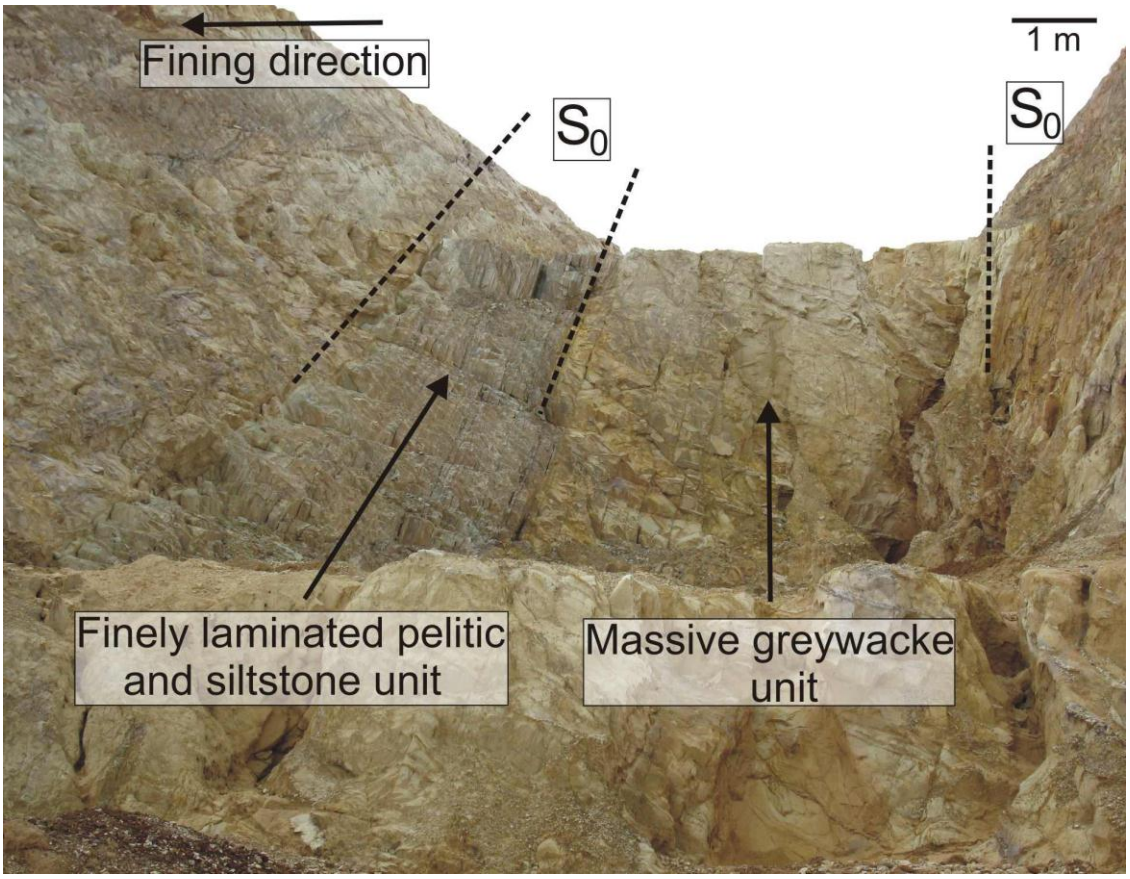

Figure 4.8: Photo showing a massive greywacke unit, which is capped by finely laminated shale and siltstone units. Photo was taken in the central domain of Kossise pit, looking north. The photo is distorted to the bottom; scale is at the top of the photo. Also note the sharp contact between the greywacke- and laminated units.

Petrography

Greywacke units consist of well sorted sand- to silt-sized grains (< 0.5 mm) of albite and quartz, which make up the bulk of the mineral composition of the rocks (Fig. 4.9.A). The finer-grained quartz-feldspathic matrix also commonly contains abundant amounts (10%) of muscovite/sericite. The grain-shape preferred orientation of the platy minerals defines a foliation. In some instances, the matrix is riddled with disseminated siderite alteration spots, with larger quartz and albite grains still preserved in the siderite spots. The greywacke units contain abundant mm- to cm-thick quartz-carbonate veins. Very fine-grained (< 0.03 mm), euhedral tourmaline grains are commonly associated with pervasive veining and sulphide mineralization in greywacke units (Fig. 4.9.B) (Theron and Coetzee, 2010).

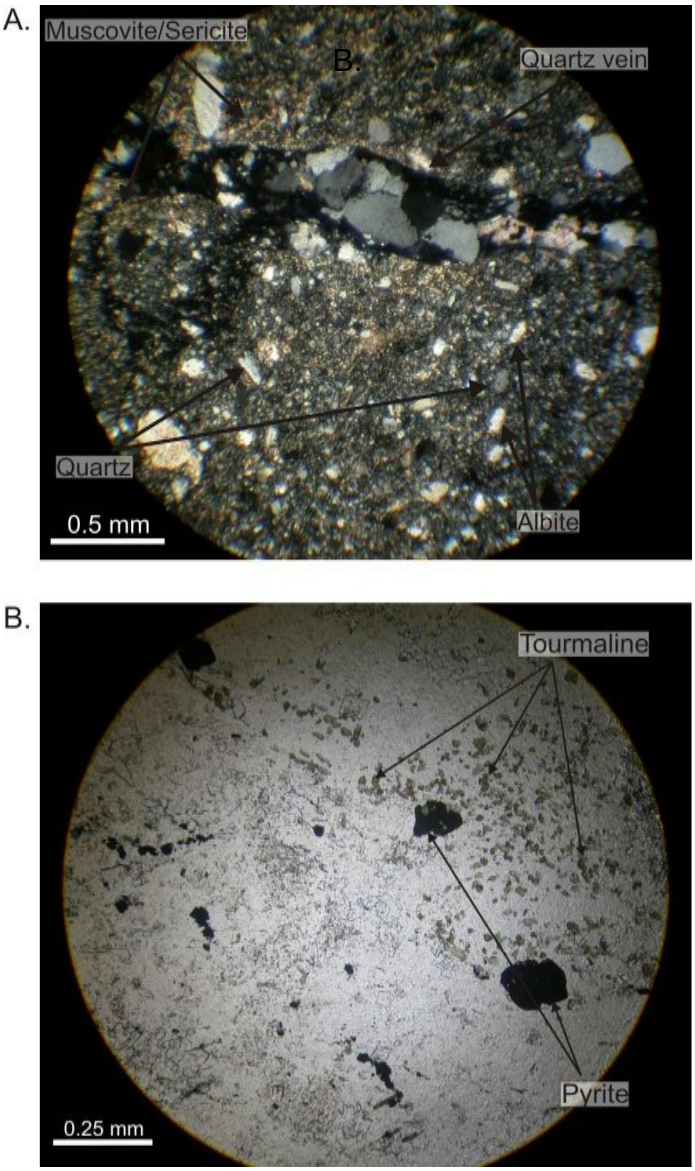

Figure 4.9: **A.** Petrographic slide showing a typical greywacke unit (cross-polarized light). The greywacke are dominantly made up of angular- to subrounded quartz and albite and significant amounts of muscovite/sericite. The photo also shows a quartz vein truncating the sample. **B.** Photo of a greywacke unit, taken under plane polarized light. In this greywacke unit significant amounts of tourmaline grains are developed. Here tourmaline occurs as small euhedral- to subhedral grains, commonly associated with nearby truncating quartz veins. Also note the development of pyrite.

4.2.4 Breccia unit

Description

Breccia units can be mapped in only two open pits, namely Sanu Tinti and Eureka North. The breccia units show sharp contacts with the surrounding lithologies that are (in places) erosive into the underlying units (Fig 4.10). Breccia units are also commonly more resistant to the saprolitic weathering.

The breccia units vary from clast-supported to matrix-supported (Fig 4.11). The majority of breccias are polymict, showing angular- to subrounded fragments of

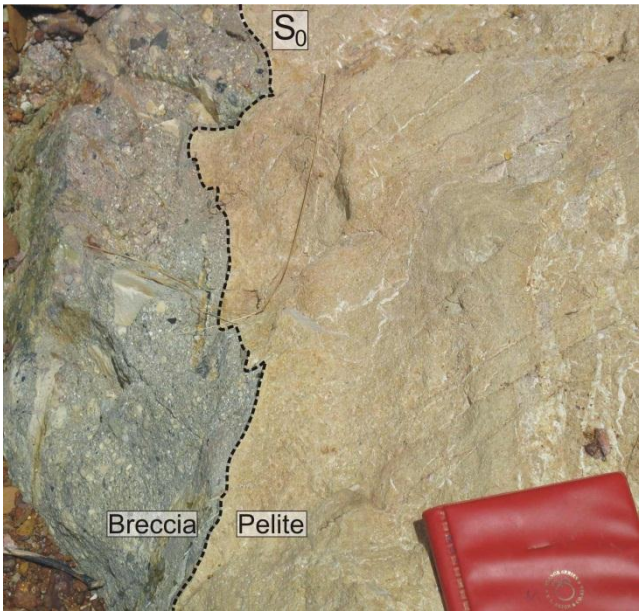

Figure 4.10: Photo indicating sharp and erosive contact between a breccia unit and adjacent pellitic bed. Oblique plan-view, taken in the northern extent of the Sanu Tinti open pit.

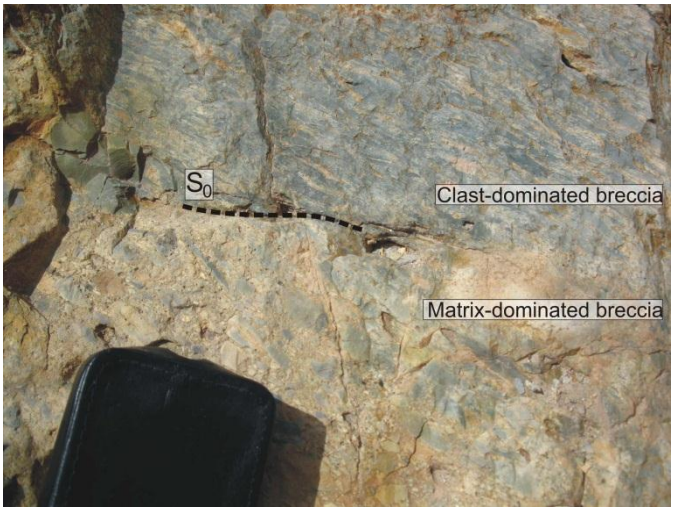

Figure 4.11: Photo showing the abrupt change between clast-dominated and matrix-dominated parts within a breccia unit. Photo was taken in Sanu Tinti.

laminated and/or homogeneous pelite, dark chert, and greywacke in a commonly sandy- to gritty matrix. Breccia clasts show no or only limited preferred orientation. Transitions from clast- to matrix-supported breccias are observed in the thick breccia unit in Sanu Tinti. The poorly sorted angular clasts range in size from a few millimetres to up to 7 cm. The largest clast observed in a breccia from the Eureka North open pit was an angular fragment of greywacke, measuring 45 cm in diameter. The polymict nature of most breccias, evidence of bedding in the breccia units and the lack of cataclastic features that would point to a structural origin, suggests that the breccias are sedimentary in origin. There are, however, cases where sedimentary breccias have been structurally overprinted, such as at Eureka North (see below). The breccia units located in the saprolite show similar textures compared to breccias in fresh samples (Fig 4.12.A-C).

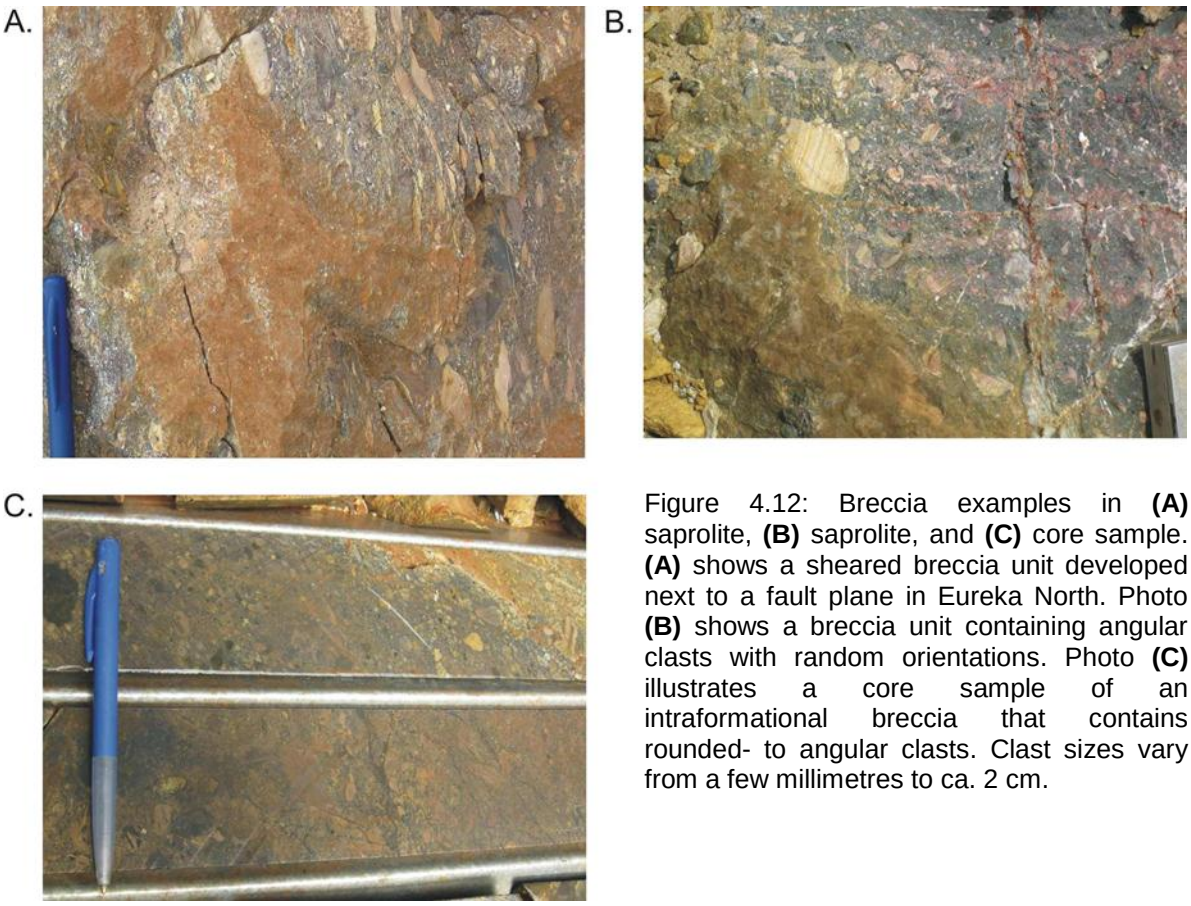

Figure 4.12: Breccia examples in **(A)** saprolite, **(B)** saprolite, and **(C)** core sample. **(A)** shows a sheared breccia unit developed next to a fault plane in Eureka North. Photo **(B)** shows a breccia unit containing angular clasts with random orientations. Photo **(C)** illustrates a core sample of an intraformational breccia that contains rounded- to angular clasts. Clast sizes vary from a few millimetres to ca. 2 cm.

Distribution

The breccia unit in Sanu Tinti occurs as a lenticular body, reaching a maximum width of ca. 10 m. The unit pinches out to the north and south. In Eureka North, the unit is located around the shear zone found in the southwestern parts of the pit. Adjacent to the shear zone, the clasts in the breccia unit are highly sheared and flattened in the plane of the foliation (Fig 4.12.A). The brecciated unit follows the local stratigraphy away from the shear zone which also indicates the unit to be of sedimentary origin. The unit has a maximum thickness of ca. 10 m adjacent to the shear zone and the thickness of the unit ranges between 1 and 2 m outside the shear zone.

Petrography

The clast population of the breccias unit consists of anhedral- to sub-euhedral clasts of greywacke, laminated pelites and siltstones and banded cherts, contained in a fine-grained matrix. The clasts are commonly larger than 5 mm. The matrix is made up of fine-grained (0.1-0.3 mm) anhedral albite and quartz, together within muscovite/

sericite, chlorite, siderite, euhedral sulphides (mainly pyrite) and very fine-grained tourmaline (Fig. 4.13). The latter are distinct, but are volumetrically only minor.

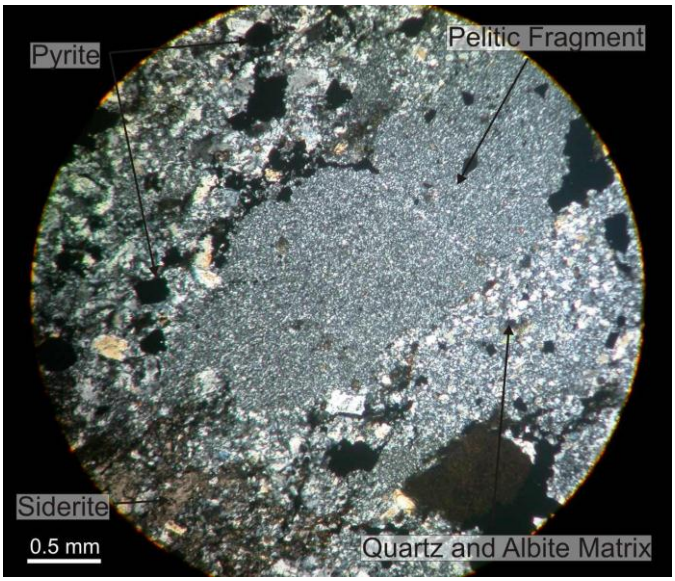

Figure 4.13: A photo taken of a breccias unit, under plain polarized light. Here a pelitic fragment is observed. Surrounding the pelitic fragment is a quartz and albite matrix, showing sand- sized gains. Decimated siderite grains are also commonly developed in the breccias units. Here the grain shows inclusions of quartz and albite. Sulphides are commonly developed in the breccia units and mostly occur as pyrite.

4.2.5 Volcanic unit

Description

Volcanic units occur as volumetrically very subordinate dykes and sills that intrude the sedimentary sequence. The mafic volcanics are dark in colour in the saprolite zone. The intrusions are fine-grained and weather positively, showing a characteristic columnar jointing (Fig. 4.14). Volcanics were not observed in core.

Distribution

The only evidence of volcanic intrusions in the Siguiri Mining Complex is confined to Eureka North pit. These mafic volcanic intrusions are not more than 30 cm thick and only locally developed. The intrusives are spatially associated with shear zones that truncate the Eureka North pit. Here the intrusive dykes intrude along the shearing plane as well as along the lithological contacts adjacent to it (Fig 4.15).

4.3 Overview of lithostratigraphy

Previous workers have suggested a turbidite-like origin for the rocks of the Siguiri Mining Complex, which seems entirely feasible. The abundance of rip-up clasts at the base of greywacke and siltstone units and the prominent sedimentary breccias all

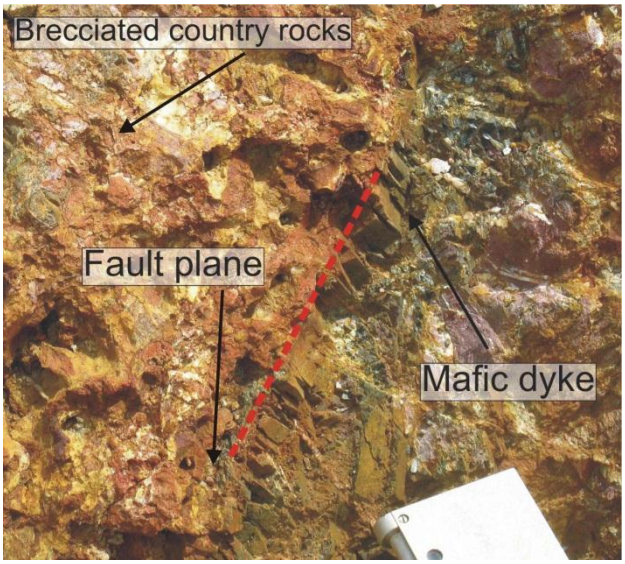

Figure 4.14: Mafic dyke intruding along a shear plane in Eureka North pit. The dyke is ca. 10 cm at its thickest. The shear plane dips towards the left corner of the photo. Also note the columnar weathering of the dyke.

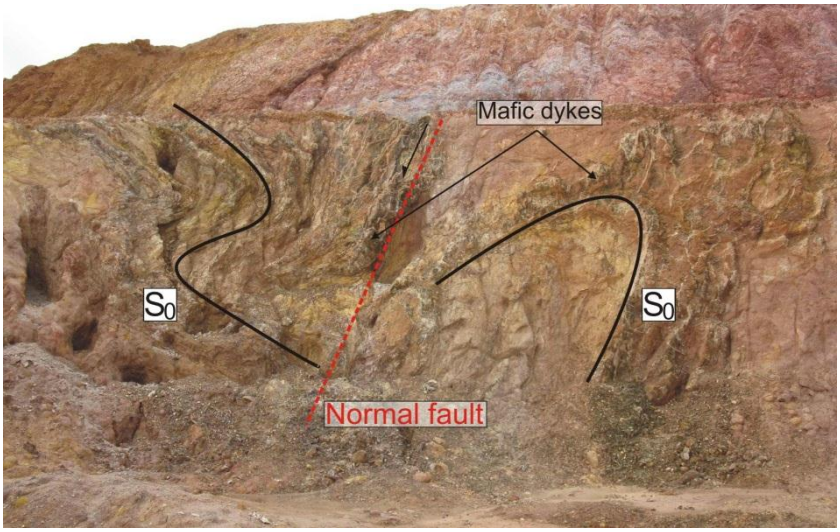

Figure 4.15: Photo of mafic dykes intruding bedding-parallel, adjacent to shear plane, as well as along it. Photo was taken in the western corner of Eureka North, with the view to the west. The shear plane shows a normal displacement along its trace.

point to an energetic sedimentary environment. For the regional mapping, pelite and siltstone-dominated units were grouped together, although greywacke layers do occur in these packages. These units were contrasted with greywacke-dominated

units. This rather simplified subdivision is aimed at highlighting the controls of gold mineralization, rather than a detailed lithological subdivision that is severely hampered by the deep weathering profile and the lack of outcrop outside the open pits. The simplification still allows for the, at least, tentative correlation of units across adjacent pits such as between Kami North, Kami South and Kossise.

Individual packages distinguished in this study vary between 20 to 120 m in thickness. Large, upward-fining turbidite sequences can locally be identified. These upward-fining packages are not more than 20 m thick and consist of a greywacke-dominated base, commonly interlayered with siltstones, grading into a siltstone-

dominated central portion that is capped by finely interlayered laminations of pelites and siltstones. In places, these fine-grained upper portions showed well-developed cross-bedding. Graded bedding in individual beds and large-scale upward-fining cycles were taken as the main indicators of the younging direction of bedding, indicating a normal sequence in shallowly dipping strata (Kami North and Eureka North).

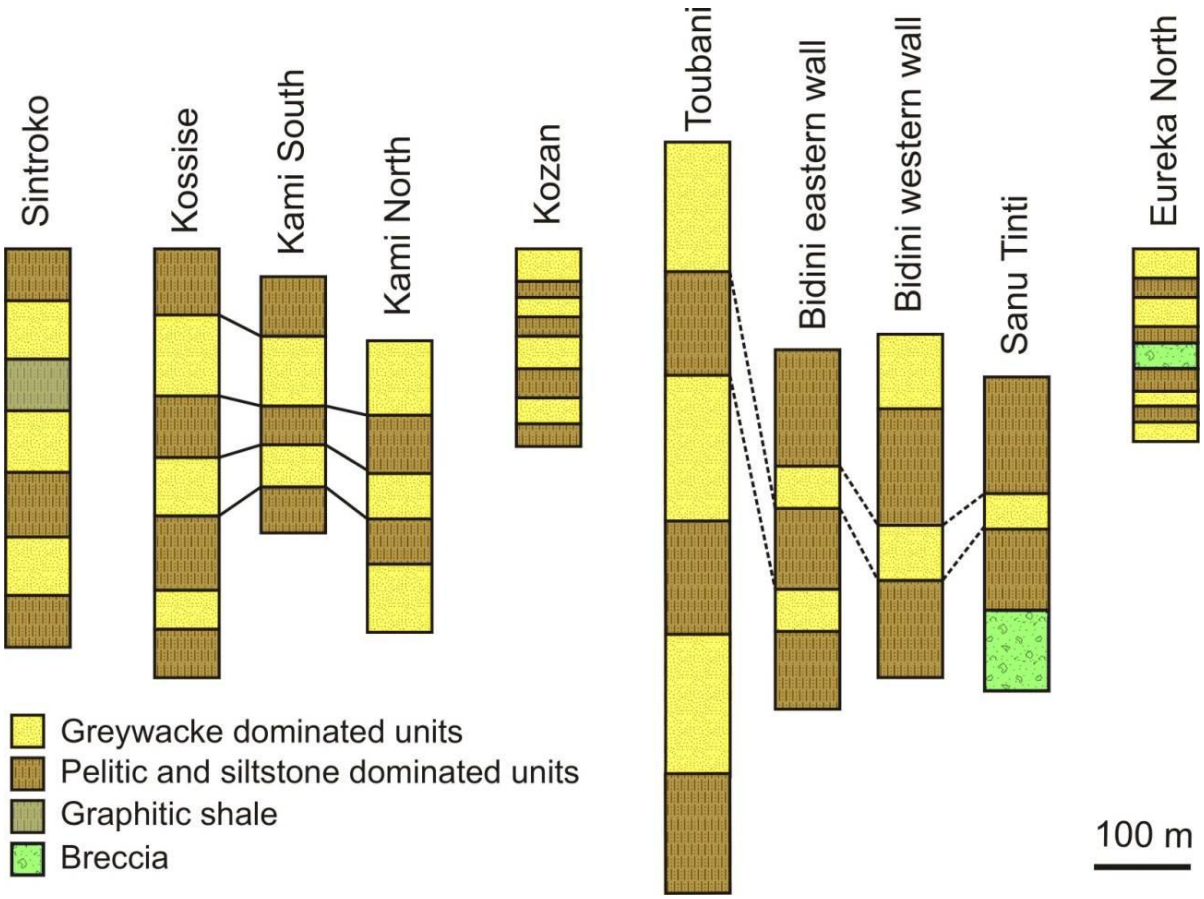

Figure 4.16: Generalized lithological profiles of the nine pits of the Siguiri Mining Complex, from Sintroko in the south to Eureka North, in the north. Correlation of units between pits were established for the Kami-Kossise Complex and inferred for the Bidini-Toubani-Sanu Tinti Complex

Chapter 5 Structure

5.1 Introduction

The following chapter describes and defines the main fabric and structural elements, followed by a more detailed account of individual pits. Rocks in the Siguiri Mining Complex show generally northerly trends. A change to more northwesterly trends is, however, evident in the northern parts of the mine workings in the Eureka North pit. The north-south structural grain of the Siguiri Mining Complex is determined by (1) northerly-trending mine-scale folds, and (2) up to several hundred metre wide domains of subvertical, northerly-trending and gently anastomosing bedding. The steep domains not only separate and bound folded domains, but fold styles (interlimb angles, vergence direction and plunge) also show systematic variations across them, suggesting that steep belts and folded domains are related. The formation of steep belts and folds are assigned to a D_2 phase of deformation, details of which are provided in the following.

It should be emphasized that many of the particularly secondary fabrics seem to have been partly or completely obliterated by the deep saprolitization. This becomes clear during the logging of core samples or where unaltered bedrock is preserved. The fresh samples show details of not only sedimentary structures, but also tectonic fabrics that are only rarely preserved in the saprolite profile. Hence, much of this detail cannot be appreciated and documented during regional mapping.

5.1.1 Bedding (S_0)

Bedding (S_0) is the most common planar feature and preserved throughout the mine complex. The mapping of bedding planes and contacts between sedimentary packages forms the basis for this structural analysis. S_0 is most prominent in well-bedded siltstone and pelitic units, where sharp contacts between different lithotypes accentuate bedding. Compositional and grain-size variations are also well expressed between different lithological packages of greywacke- or pelite-dominated units, which formed the basis for the lithostratigraphic subdivision in individual pits of the Siguiri Mining Complex (Chapter 4). Colour variations as indicators for bedding can only be used with great caution, since the deep weathering, associated leaching and oxidation have pervasively affected all rocks.

5.1.2 Secondary tectonic fabrics (S_1, S_{2a}, S_{2b}, L_2)

S_1 – *Bedding-parallel foliation*

A bedding-parallel foliation (S_1) is only rarely observed, but is more prominent in the steeply dipping rocks and recorded at Sintroko (see below). Here, S_1 is developed as an axial planar foliation to intrafolial folds (F_1) (Fig. 5.1.A). S_1 is only developed in the silty and pelitic units. It is not pervasive and can only be traced intermittently for a few metres. This fabric is defined by the alignment of white clay minerals, pseudomorph after muscovite/sericite, with a mm- to cm-spacing.

S_{2a} – *Steep, axial-planar (transecting) foliation*

S_{2a} denotes a steep, mainly E and SE-dipping foliation, but western dips are also observed. This foliation was only found in the steeply dipping rocks of the Bidini, Sintroko, Kossise, Kozan, and Toubani pits. On a regional scale, S_{2a} has an approximately axial-planar to transecting orientation to F_2 folds, (Fig. 5.1.B). In the saprolite zone, S_{2a} is defined by the alignment of alteration spots as well as the preferred orientation of pressure shadows around the carbonate spots in silty and greywacke layers. In thin sections of fresh samples, a very pronounced and closely spaced, commonly anastomosing foliation is defined by the alignment and grain-shape preferred orientation of chlorite, sericite and shale clasts (Fig. 5.2.A). This foliation also anastomoses around carbonate alteration spots and the foliation is accentuated by elongated pressure shadows around the alteration spots, but also sulphides, mainly pyrite. The pressure shadows mainly comprise intergrown quartz and carbonate, whereas strain caps are made up of fine-grained muscovite/sericite (Fig. 5.2.B).

S_{2b} – *Fracture cleavage*

S_{2b} denotes a shallower foliation (20-50° dip) that is most commonly developed as a fracture cleavage (Fig. 5.1.B). The S_{2b} foliation shows mainly westerly dips in the western parts of the mining complex in,, Sanu Tinti, Bidini and Toubani, but east to southeastern dips are also recorded in the pits of Sanu Tinti and Bidini. In the eastern parts of the Siguiri Mining Complex, easterly dips prevail

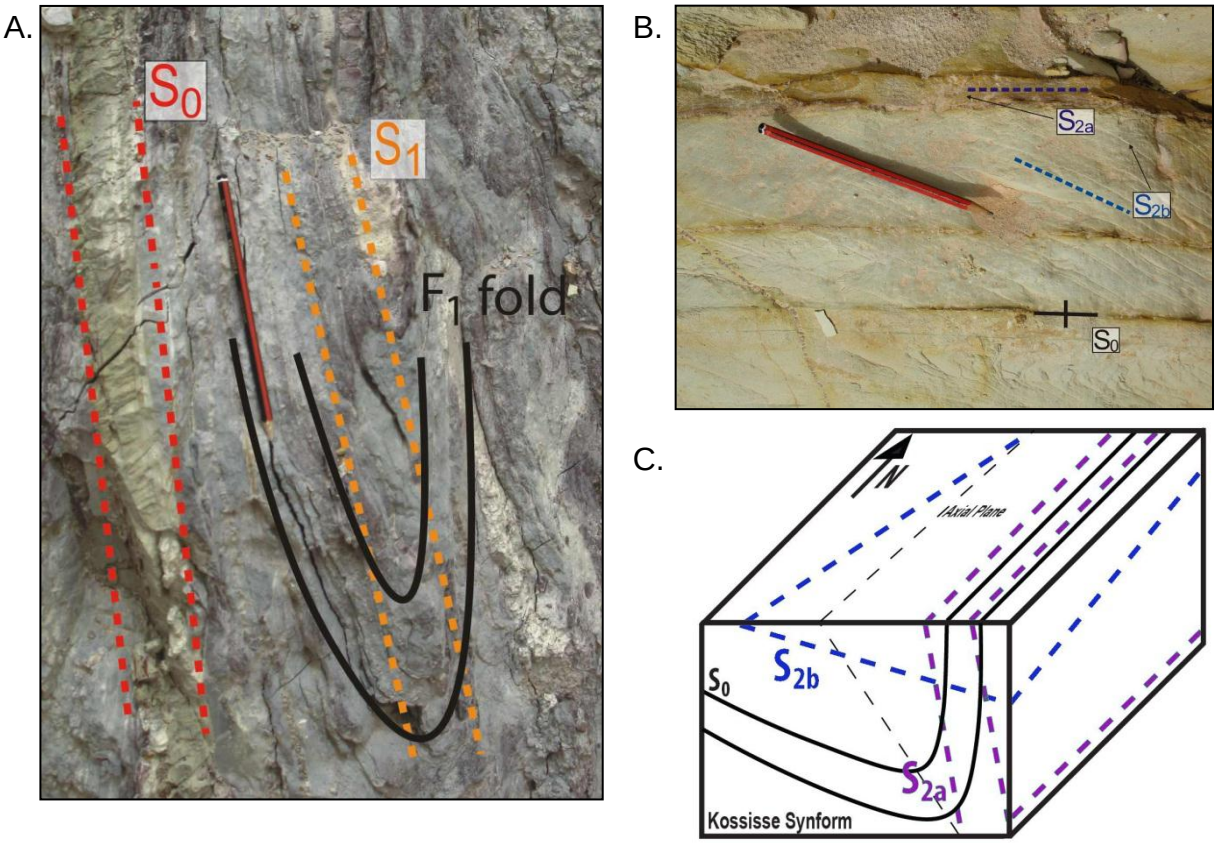

Figure 5.1: **A.** F_1 fold in the southern extent of the central domain of the Sintroko pit. The photo was taken looking south and shows a F_1 intrafolial fold, with an axial-planar S_1 foliation. S_0 trends north-northeast and dips steeply on either side of the F_1 fold. The F_1 fold shows a shallow plunge to the south-southwest. Use pencil for scale. **B**. The S_{2a} and S_{2b} foliations, here in the eastern extent of Kossise, plan view. In this case, S_{2a} shows steep dips, trending sub-parallel to the steep north-south trending bedding (S_0) and the axial plane of the larger F_2 Kossise Synform. S_{2b} is developed as a fracture cleavage that dips shallowly to the east-southeast (different dip-directions were developed in other pits). Use pencil for scale. **C**. A simplified block diagram of the Kossise Synform, showing the relationship between the bedding (S_0) and secondary foliations in the Kossise pit.

in Kossise and the Kami Complex. In the far north of the Siguiri Mining Complex, in the Eureka North pit, the foliation orientation changes to more southerly dips.

This is consistent with a change in the structural grain in the northern extent of the Siguiri Mining Complex, from north-south trends to northwest-southeast trends. The S_{2b} fabric is defined as a fracture cleavage. The intersection between S_{2b} and S_0 or S_{2a} forms the pencil weathering that is present in the pelitic layers in some pits (Bidini), and emphasizes the presence of pervasive

secondary fabrics in the rocks. The spacing of this fabric is on a mm- to cm-scale and is developed best in pelitic layers. The regionally developed S_{2b} foliation is a clearly transecting cleavage with respect to F_2 folds and forms most commonly in close proximity of D_2 reverse faults, present in the steep dipping zones (see below).

L_2 – *Linear fabrics*

Linear fabrics were rarely observed in the Siguiri Mining Complex, which is possibly also a result of poor preservation in the saprolite. F_2 fold hinges define an L_2 form lineation.

5.1.3 Folding (F_1 and F_2)

Folding is the most common manifestation of deformation in the Siguiri Mining Complex. The scale of folds ranges from wavelengths of a few metres to 10's of metres to 100's of metres. Two fold generations were distinguished in the Siguiri Mining Complex.

A. B.

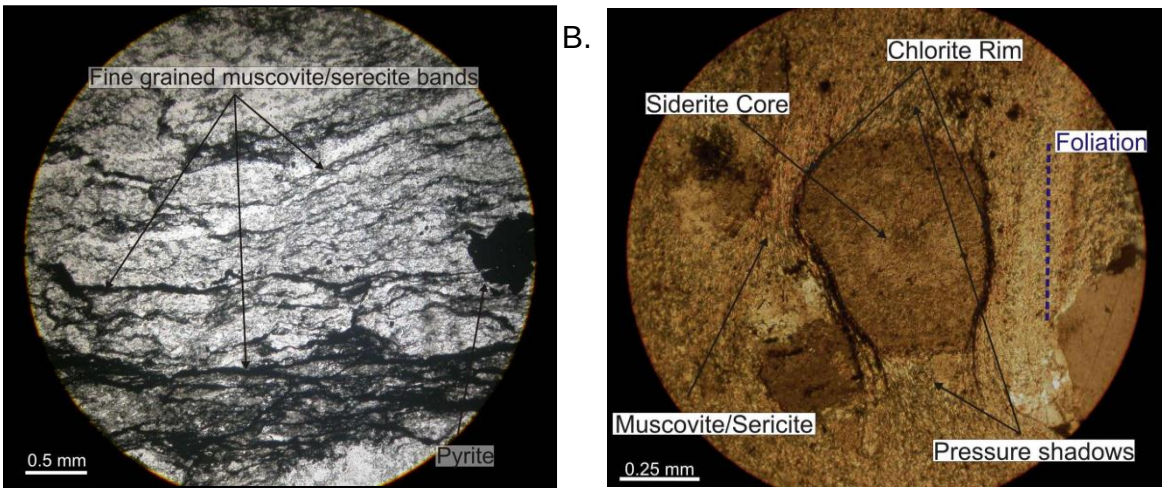

Figure 5.2: **A.** A photo taken of a greywacke unit, using plane polarized light. Here dark lines define a well-developed S_{2a} foliation. Dark material is developed as large irregular shapes and is also concentrated along the foliation planes. The dark material is suggested to be remnants of fine muscovite/sericite or fine-grained pelites. Lenses of less strained greywacke, are bounded by higher strained foliation planes. The greywacke unit consist of predominantly quartz and albite. **B.** A photo taken of a finer-grained siltstone, using cross polarized light. Here siderite nodules define a weak S_{2a} foliation. Purple dashed line show the foliation and is defined by the shape of the siderite grains and pressure shadows formed at the ends of the grains, as well as chlorite and muscovite/sericite wrapping around the grains. The pressure shadows consist of fine-grained silty and muscovite/sericite matrix.

F_1 – *Intrafolial folds*

Bedding-parallel and intrafolial folds represent the earliest fold generation mapped in the Siguiri Mining Complex and are referred to as F_1 folds (Fig. 5.1). These folds are tight- to isoclinal and are contained in zones of steep bedding. The folds assume shallow plunges and wavelengths between 0.5 and 1 m, but cm-scale folds were also observed. It is uncertain whether the folds represent early diagenetic slumping structures in the meta-turbiditic sequence. The fact that they are invariably developed in zones of steep bedding and the presence of an S_1 axial-planar foliation suggests that they are tectonic in origin.

F_2 – *Mine-scale folds*

F_2 folds are the dominant structures of the Siguiri Mining Complex (Fig. 5.3). The folds show half-wavelengths between ca. 10 and 350 m. The largest F_2 fold underlies the central-western parts of the Kossise open pit with a half-wavelength of ca. 350 m, but half-wavelengths of the folds are more commonly between 10 to 100 m. F_2 folds trend north to north-northwest. Rare examples of east-west trending folds are recorded at Kami North and Toubani. The latter are also referred to as F_2 folds, despite their different orientation, for reasons developed further below in this chapter. To the north of the Siguiri Mining Complex, in Eureka North, the orientation of F_2 folds changes to more northwesterly trends. This follows an overall change in the direction of the structural trend to the north of the Siguiri Mining Complex.

F_2 folds show no uniform vergence direction. Westerly verging folds dominate the eastern parts of the Siguiri Mining Complex in Kossise and Kozan, whereas F_2 folds tend to verge to the east in the west, such as in Sanu Tinti. The vergence of F_2 folds is most prominent adjacent to zones of steep bedding (Fig. 5.4, and see below). F_2 folds away from these zones tend to be upright and openly folded (Fig. 5.4). This already suggests a relationship between north-south steep dipping zones and F_2 folds (see below).

The plunges of F_2 folds are commonly shallow (<15-20°) and both to the north and south. This also emphasizes the non-cylindrical geometry of F_2 folds that may be doubly-plunging or that show adjacent folds in fold pairs with opposite plunges. Good examples of F_2 antiform-synform pairs with opposite plunges are developed in the Bidini pit, whereas doubly-plunging dome-like structures underlie much of the Kami

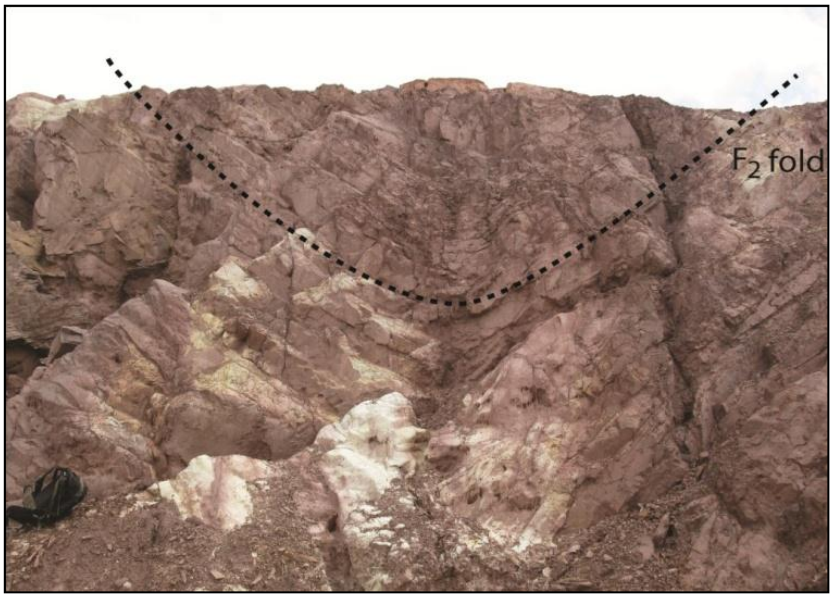

Figure 5.3: Cross-sectional view of an F_2 fold at Kozan, looking north. The fold forms part of a series of shallowly plunging, north-south trending F_2 folds. The fold has a wavelength of 15 m. Use rucksack as scale (lower left hand corner of photo).

Complex. Variations in plunge direction also results in fold axial depressions and -culminations, most prominently developed in the central Kami Complex. The axial depressions/culminations trend at high-angles to F_2 folds (east-northeast orientation). Moreover, large-scale folds describe an en-echelon arrangement in the vicinity of axial depressions and -culminations, examples of which can be mapped in the Kami Complex.

Notable exceptions of steep and subvertically plunging F_2 folds are developed in a number of pits and most prominently in Bidini, Toubani and the eastern and western parts of Sintroko. Notably, all steeply plunging folds are contained in zones of steep bedding. Moreover, steeply plunging folds contained in steep belts are commonly tight, whereas F_2 folds outside the steep belts show gentle- to close interlimb angles.

The S_{2a} foliation is approximately axial planar to F_2 folds, but variably developed across the Siguiri Mining Complex (Fig. 5.1.C).

5.1.4 D_2 steep belts

D_2 steep belts referred to in this study are up to several hundred metre wide zones in which the bedding assumes subvertical- to vertical dips (Fig. 5.5.A and Fig. 7.1) The zones of vertical bedding may also be much more localized and narrower (5-10 m wide) developed as in Bidini and Sanu Tinti. For the most part, bedding trends north-

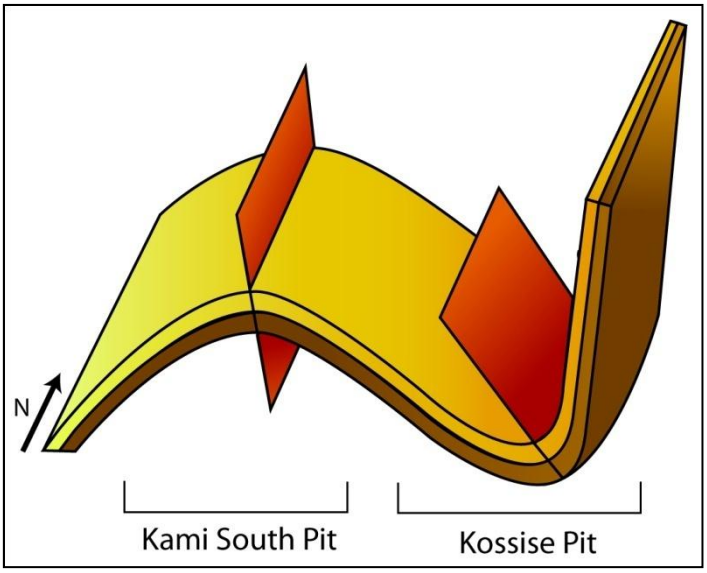

Figure 5.4: A simplified illustration of the north-south trending F_2 folds in the Siguiri Mining Complex, showing the characteristic relationship of F_2 folds with steep belts (see below). Folds are tighter and asymmetric close to steep belts (right hand side of sketch), but become more open and upright with vertical axial planes (red planes) away from the steep-D_2 zones (here sketched from the eastern extent of Kossise). F_2 folds show most commonly shallow plunges

south in the steep belts, assuming more north-northeasterly trends in the southern part of the Siguiri Mining Complex at Sintroko.

Two main steep belts can be mapped, which form, in the central parts of the mining complex, the eastern and western boundaries of the Siguiri Mining Complex, respectively. An eastern steep belt can be distinguished from a less well-developed and anastomosing western steep belt. The eastern belt forms the eastern boundary of the open pit workings of Kossise and Kozan. At Kossise, the zone of subvertical to, in fact, overturned bedding is, at least, 300 m wide. The steep zone that forms the eastern boundary of Kozan seems to be the direct along-strike continuation of this zone, so that the eastern belt can be traced for, at least, 2 km. If the belt is extended to the south and into Sintroko, this eastern steep belt shows an along-strike extent of > 6 km and, given its considerable width (> 300 m in some places), probably much further than this.

The western belt is less well exposed and describes a more anastomosing pattern. It is well developed in Toubani (Fig. 5.5.A), being exposed over a width of ca. 250 - 300 m showing subvertical westerly dips. North and north-northwest of Toubani, the steep belt appears to bifurcate into narrower belts that are only 1 to 60 metres wide. The steep zones enclose, but also truncate folded domains (F_2).

These D_2 steep belts show evidence of higher strain intensities than in adjacent folded areas. Deformed strata and clasts within the strata are common in the pits of Kossise, Toubani and Sintroko (Figs. 5.5.A and B).

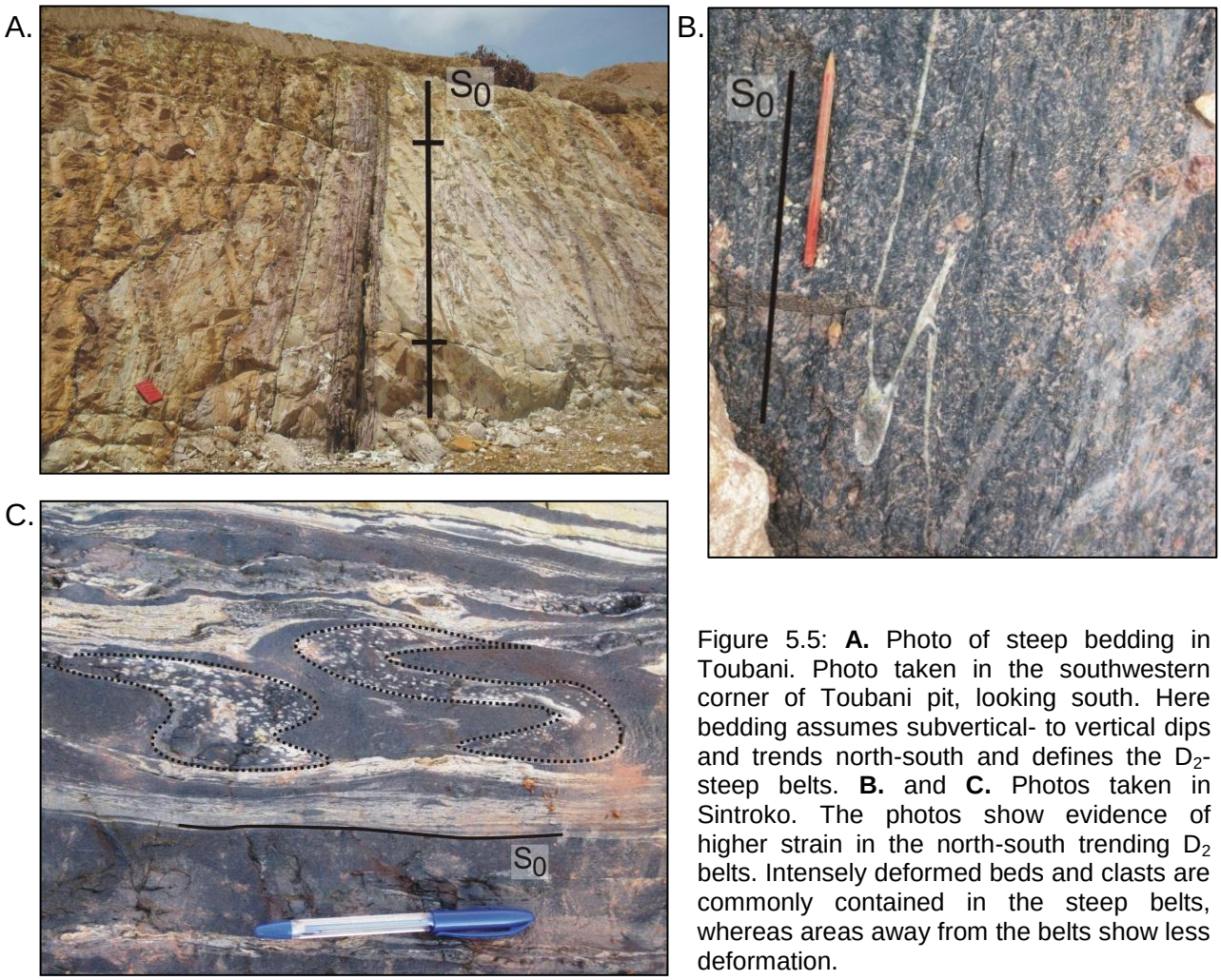

Figure 5.5: **A.** Photo of steep bedding in Toubani. Photo taken in the southwestern corner of Toubani pit, looking south. Here bedding assumes subvertical- to vertical dips and trends north-south and defines the D_2-steep belts. **B.** and **C.** Photos taken in Sintroko. The photos show evidence of higher strain in the north-south trending D_2 belts. Intensely deformed beds and clasts are commonly contained in the steep belts, whereas areas away from the belts show less deformation.

5.1.5 Faults

Faults occur in all pits of the Siguiri Mining Complex. Two main generations of faults can be distinguished, including earlier (D_2) reverse-, strike-slip faults, and (D_2) normal faults, as well as later (D_3) high-angle normal faults (Figs. 5.6 A and B).

D_2 faults: D_2 Reverse faults are particularly common in the steep belts (Fig. 5.6.A), where the displacement of markers by the moderate- to steeply dipping faults is most prominent. The reverse faults trend north-south and show dips to both the east and west, defining a (on a mine-scale) conjugate pattern about the vertical bedding of the steep belts. Displacement is minor and, where marker horizons could be identified, does not exceed 10 metres.

Good examples of D_2 reverse faults can be mapped in Sintroko and Kossise. Due to weathering and the nature of the outcrop, the offset of marker beds cannot be followed across the fault plane in several of the open pits. In these cases, reverse faults can still be recognized by the drag of bedding adjacent to the fault plane. D_2 reverse faults are rather localized structures that cannot be followed or correlated between different pits of the Siguiri Mining Complex.

D_2 strike-slip faults in the Siguiri Mining Complex show dips >80°and the strike of these faults varies from N-S to NE-SW (Fig. 5.6.B). Strike-slip faults either occur as

A.

B.

Figure 5.6: **A.** Outcrop of a narrow, north-south trending steep D_2-belt (fault zone), truncating bedding in the Bidini open pit (cross-sectional view, looking south). Black line in bottom corner measures 1 metre in length. **B.** An east-west cross-sectional view of the eastern part of the Kossise pit, looking north. Here north-south trending reverse faults truncate the steep dipping bedding of the eastern extent of Kossise. The fault shows top-to-the-west displacement.

bedding-parallel faults, in Toubani, or as highly discordant faults truncating bedding and separating distinct structural domains within individual open pits. This latter pattern is very prominent in Bidini, Sanu Tinti and Sintroko. Bedding-parallel strike-slip faults are difficult to recognize in the weathered saprolite zone. In Sintroko, bedding-parallel strike-slip faults are associated with a brecciation of wall rocks. The breccia zones that mark the fault traces are commonly less than 2 m wide. In Toubani, strike-slip faults are indicated by the negative weathering of rocks and the slightly different, whitish colouration of the rocks. Discordant strike-slip faults are more easily recognized and most obvious on a map scale through the abrupt and often high-angle termination of bedding against them. In places, the drag of the bedding along the faults indicates a dextral sense of displacement, which is well preserved in Sintroko. The offset of bedding along strike-slip faults could not be measured and is only inferred.

A set of steeply dipping D_2 normal faults is only developed in Kami South. The faults trend east-northeast, indicating a component of north-northwest extension normal to the plunge direction of the underlying F_2 folds. This aspect is developed in Chapter 7.

D_3 faults: D_3 normal faults truncate and displace all earlier structures. These faults are common throughout the Siguiri Mining Complex (Fig. 5.7.). The fault traces are commonly marked by a greenish-blackish colouration with minor quartz- and/or carbonate veining. The faults commonly show a negative weathering profile in the pit walls. Most D_3 faults trend north-south and dip at steep angles to both the east and the west, thereby defining a pattern of conjugate graben and half-graben structures. The D_3 faults are considered to be distinct from the ENE-trending D_2 normal fault set developed in Kami South. Displacement along these faults is between 0.5 m to 10 m, with the largest displacement observed along a north-south trending normal fault in the western part of Kami North. This fault could be followed from Kami North through Kami South and into Kossise. These normal faults truncate earlier D_2 structures and are related to a younger extensional event (D_3).

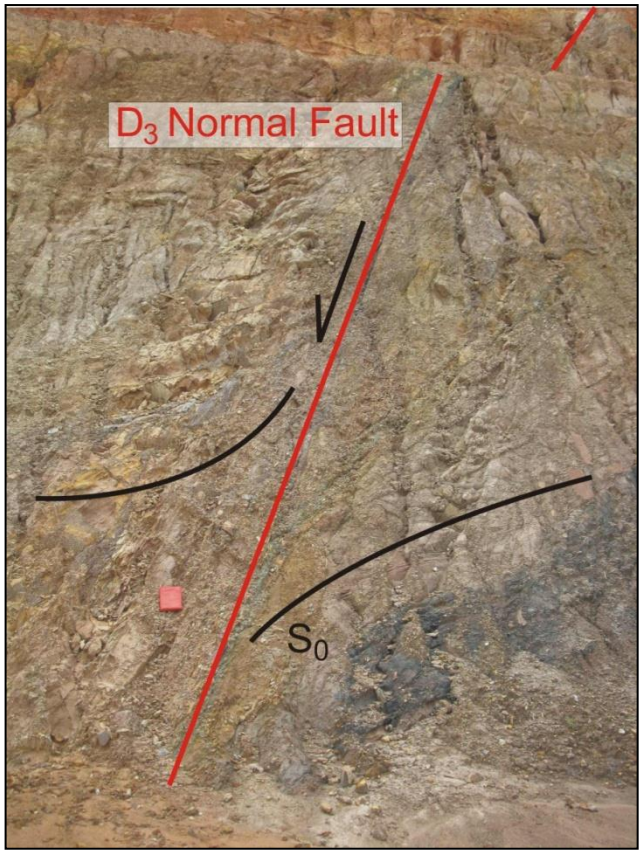

Figure 5.7: Photo of a D_3 normal fault taken in the eastern part of Kami-North, looking north-northeast. Here the fault shows moderate dips to the west. Bedding is dragged into the fault plane, with marker horizons across the fault plane showing a displacement of ca. 10 m. Darker weathering along fault trace is due to chlorite alteration. The darker bed, left of fault-plane, is a graphitic schist bed and is dragged down by fault. Use red book as scale.

5.2 Detailed structural overview of the individual pits

5.2.1 Sanu Tinti

The Sanu Tinti open pit can be subdivided into a western, central and eastern structural domain (Fig. 5.8.A). The three domains are distinguished by distinct and, along the central domain, abrupt changes in the dip and dip directions of the strata and the underlying structures.

The western domain is underlain by north-south trending, moderate- to steep east-dipping (30° to 60°) bedding, rotating to more northeasterly trends towards the north. Here bedding may form part of the central synformal structure, but outcrop is very limited in this part. A north-south trending reverse fault is also inferred in the western part of the pit, forming the contact between the shale- and siltstone- dominated lithologies in the far west and the breccia unit (Fig. 5.8.B).

A.

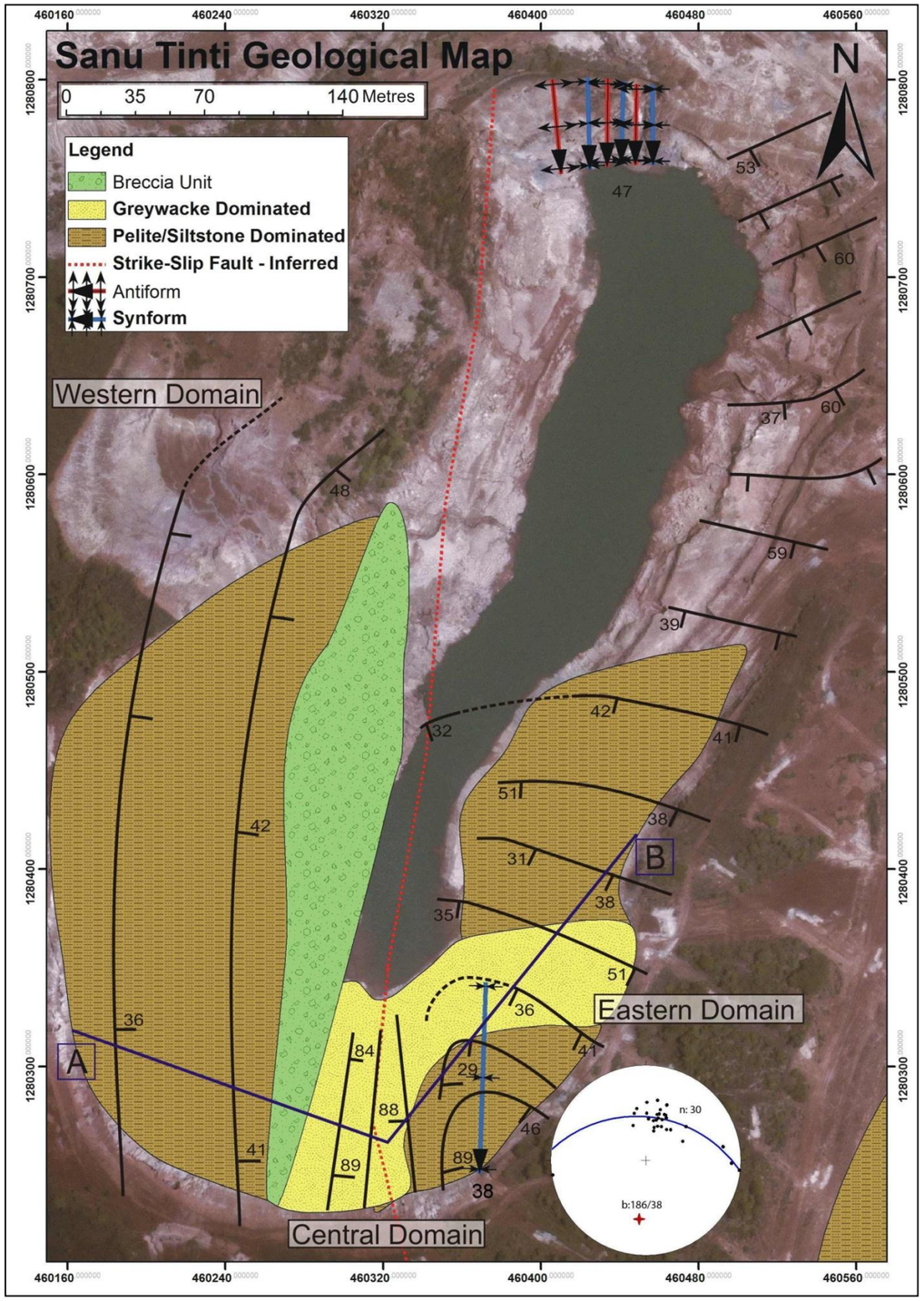

B.

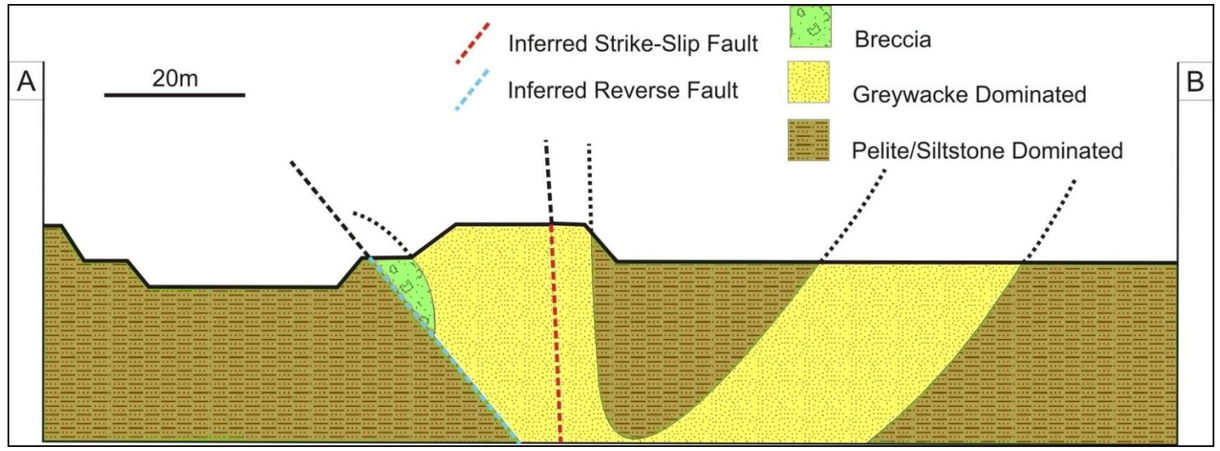

C.

D.

Figure 5.8: **A**. Formline map of Sanu Tinti. The lithologies in the map consist of greywacke dominated, pelite/siltstone-dominated lithotypes and a lens of breccia. Stereographic projection shows the orientation and plunge of the synform in the southeastern extent of the pit (here and elsewhere: the poles to bedding are plotted). Note the parasitic folds in the northern extent of the pit. **B**. Cross-section drawn through Sanu Tinti from west to east, along the purple line included in figure 5.8.A. Here an inferred reversed fault is included in order to account for the presence of the breccia lens. The cross-section shows the shallow south-plunging synform, located in the eastern domain of the pit. The inferred strike-slip fault in the central steep domain is also shown. **C**. Photo taken in Sanu Tinti looking east-southeast showing the development of a moderately south-plunging F_2 synform, with a subvertical, north-south trending western limb, and a moderate south-dipping eastern limb. Rocks are deeply weathered in this old pit. **D**. Photo taken in the northern extent of Sanu Tinti, looking north, showing a parasitic antiform, which forms part of a series of south-plunging fold pairs. These small-scale folds are interpreted as being M-folds developed in the hinge of the larger synform towards the south.

Towards the east, the moderate dips of the western domain abruptly terminate against subvertical and north-south trending beds of the central domain. This relationship is well exposed in the southern extent of the pit. In the north, these steep dips cannot be recorded, but this may also be a function of the very poor outcrop. The abrupt change from moderate easterly-dipping beds in the west, to steep- and subvertical dips is tentatively related to a north-trending fault zone (D_2) in these central parts of the pit. However, high-strain fabrics or fault rocks are not evident.

The eastern domain of the pit consists of moderate- to shallow (40°), E- to SE- and S-dipping strata. The rotation of bedding defines a large-scale (120 m wavelength), south-plunging (ca. 186/38°), east-verging F_2 synformal structure (Fig. 5.8.C). A subvertical foliation (S_{2a}: 264/86°) developed close to the hinge of the synform is suggested to be axial planar, although this would indicate a more upright geometry of the fold than is suggested by the asymmetry of the fold limbs. A moderately SE-dipping fracture cleavage (S_{2b}: 134/51°) is also developed. The far northern extent of the pit is underlain by three synform-antiform pairs, plunging at shallow- to moderate angles (10 to 50°) towards the south (Calculated: 196/22°). These open folds have short wavelengths between 10 m and 20 m and upright axial planes. The folds are interpreted to represent parasitic M-type folds, located in the hinge of the main synform developed in the southern extent of the eastern domain in Sanu Tinti (Fig. 5.8.D).

5.2.2 Bidini

Bidini is subdivided into three north-south trending domains, henceforth referred to as the western, central and eastern Bidini domains, which are separated by two subvertical, N- to NE-trending D_2 strike-slip faults (Figs. 5.9.A-D). The faults not only truncate bedding of the adjacent wall rocks, but the domains in between the faults also show distinctly different structural styles.

The western domain is underlain by steep- to subvertical, E-W to ENE-trending bedding in the southern parts of Bidini that finds its continuation with bedding of the eastern domain of Sanu Tinti. The bedding between the two pits combines to form an openly folded, steep NW-plunging (b: 321/71°) synform (Fig. 5.10.A). Along the northwestern wall of Bidini, bedding trends north-south and defines the eastern limb of the steeply plunging synform. Bedding continues to stay subvertical along the

central-western wall of Bidini, but becomes shallower (40 to 70°) towards the far north. A localized, small-scale fold was observed in the zone of steep, east-west trending bedding along the southwestern wall of Bidini. This tight, overturned fold, shown in figure 5.10.D, has a wavelength of ca. 6 m and plunges towards 241/25°.The central domain of Bidini contains a series of small-scale, N-NNW trending fold pairs (Fig. 5.9.B; Fig. 5.10.B). It is common for adjacent folds to have opposite plunge directions. Fold plunges are shallower (8 to 40°) in the northern extent of the pit, steepening (50 to 60°) towards the south. The small-scale folds also show an increase in wavelength in the central part of the pit, from west to east (Fig. 5.9.D). This is better defined in the southern set of folds and wavelengths increase from 20 m in the west to 200 m in the east, whereas the set of folds in the northern part of the pit tend to have smaller wavelengths (10 to 40 m). Throughout Bidini, a moderate- to steep ESE-dipping secondary foliation (S_{2a}) is developed, more or less axial planar to the north-south trending small-scale folds in the central domain. The S_{2a} foliation has a calculated orientation of 110/75°. The S_{2b} fracture cleavage is prominent in Bidini and dips at shallow- to moderate angles to the west, showing a calculated orientation of 260/34°. S_{2b} is locally developed, showing shallow easterly dips with a calculated orientation of 92/26°.

The eastern domain of the Bidini pit is structurally complex. The far northeastern corner of the pit is underlain by north-south trending, subvertical strata (calculated dip: 254/89°). Towards the south, bedding assumes shallower (30 to 60°) dips, with very shallow dips (12°) further south. In the central-eastern part of the pit, bedding is rotated to northwest-southeast trends. Bedding orientations rotate towards the east to form a synformal, doubly-plunging, basin-like structure with shallow- to moderate (9 to 50°) dipping strata. To the immediate south of the doubly-plunging synformal structure, a set of NNW-plunging (calculated plunge direction and plunge: 352/07°) folds are developed ((Fig. 5.9.C and 5.10.C). This shallow- to moderately plunging antiform-synform pair is openly folded, with subvertical axial planes and wavelengths between 30 and 40 m. Along the southeastern wall of Bidini, bedding trends northeast-southwest and has a slightly arcuate geometry. The central domain of the Bidini pit is bounded by two steep (80°), north-south trending fault zones (Fig. 5.11.A). The faults are defined by subvertical bedding and the abrupt truncation and/or steepening of bedding from shallower dips into the faults. The truncation of

A.

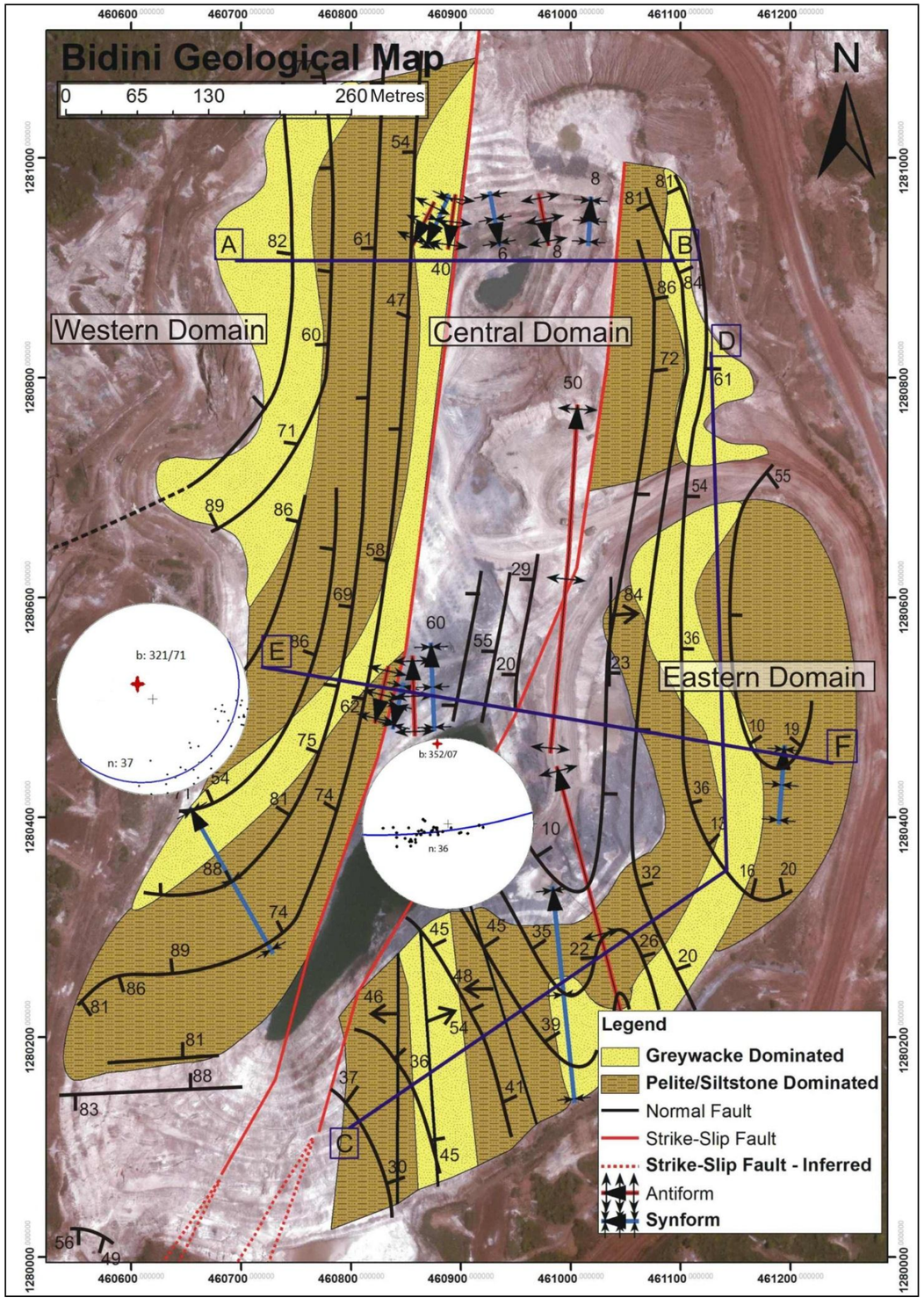

B.

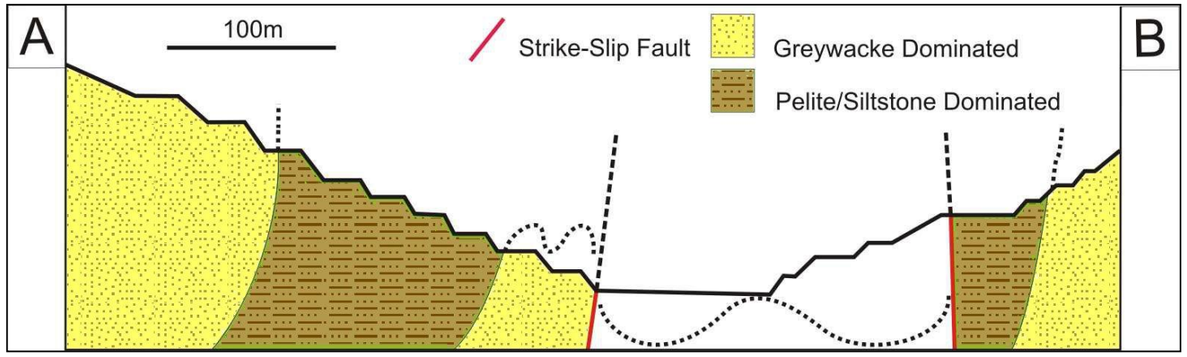

C.

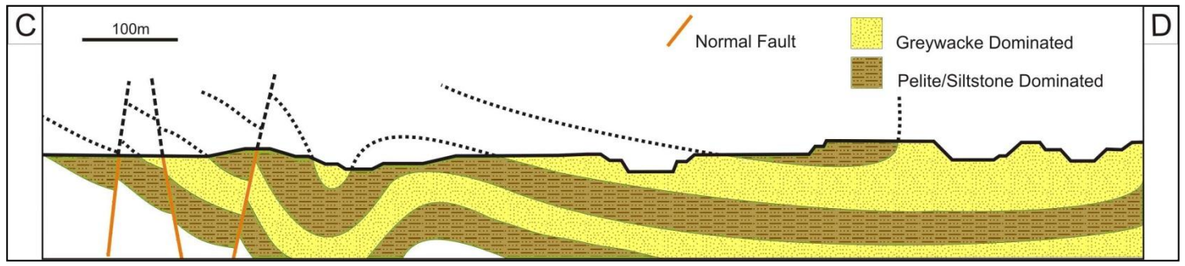

D.

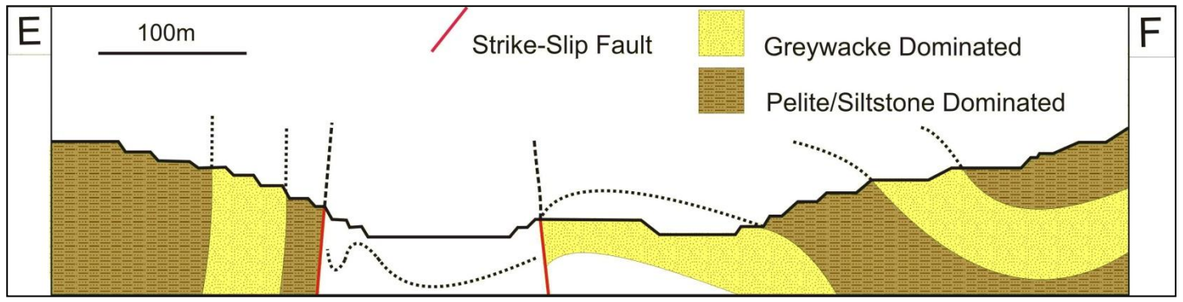

Figure 5.9: **A**. Formline map of Bidini. Stereographic projections show the orientation and plunge of the synform along the western wall of Bidini, as well as that of the fold pair in the southeastern part of the pit. Section lines used in Fig. 5.9 B-D are indicated. **B**. West-east cross-section drawn through the northern extent of Bidini, along line A-B. The cross-section shows steep bedding along the western and eastern wall, with bedding along the western wall becoming shallower with depth. Lithologies in the central domain of the pit were not distinguished in detail, but small-scale F_2 folds are indicated with a dotted line. **C.** Cross-section drawn from the southern parts of Bidini, along the southeastern and eastern walls, to the northeastern extent of the pit. The cross-section was drawn along line C-D in figure 5.9.A. The section includes a set of opposite dipping normal faults, and the small-scale fold pair observed along the southeastern wall of the pit. Further north along the eastern wall, shallowly dipping bedding defines a basin-like structure, with steeply dipping, north-south-trending bedding to the northeast of the Bidini. **D.** Cross-section drawn through the central parts of Bidini, from west to east, along line E-F included in figure 5.9.A. The cross-section shows the steep north-south trending bedding along the western wall of Bidini, with the moderate- to shallowly dipping bedding of the basin-like structure in the central-eastern part of Bidini. To the west of the basin structure is a small-scale, north-south trending, openly-folded synform. The central domain is bounded by two north-south trending D_2 strike-slip faults and is underlain by a series of small-scale folds. These folds become larger and more openly folded from west to east.

Note, here and in other maps, structural formlines and the actual outcrop pattern of lithological packages may deviate from each other. This is a function of the surface topography of the open pit workings.

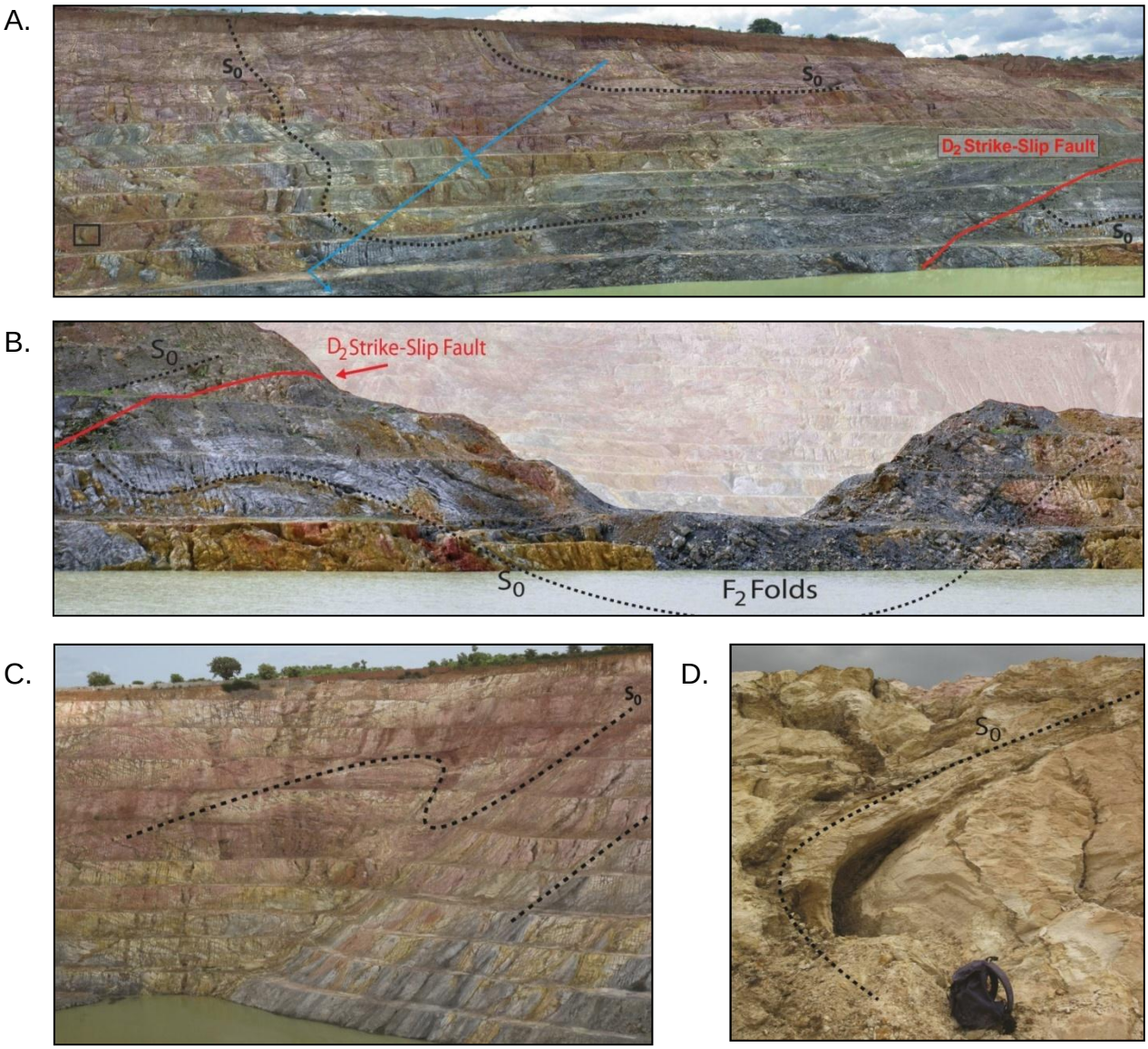

Figure 5.10: **A.** View of the western wall in the central parts of Bidini, looking east-northeast. Bedding can be seen following east-west trends from Sanu Tinti in the west, but assumes subvertical northern dips in Bidini. Close to the north-south trending strike-slip fault, bedding is folded by a steeply NW-plunging synform to steep north-south trends. Black box drawn in the bottom left corner shows the location of figure 5.10.D. **B.** Photo taken in the central parts of the central domain in Bidini, looking north. Here, small-scale folds (bedding annotated by stippled line, S_0) formed in between two north-south trending strike-slip faults. The folds trend north-south and adjoining folds commonly have opposite plunges. As can be seen in the photo, folds become more open and show larger wavelengths away from the western fault. **C.** Photo taken in the central part of the eastern domain of Bidini, looking east, showing a small-scale F_2 fold pair. The folds show an open geometry, with upright axial-planes and plunges to the north-northwest. **D.** Photo showing a tight, overturned fold, which has a shallow western plunge. The fold is interpreted to be formed as a parasitic Z-fold on the east-west trending limb of the larger synformal structure formed here. Photo was taken in the southern parts of the western domain in Bidini, looking west.

A.

B.

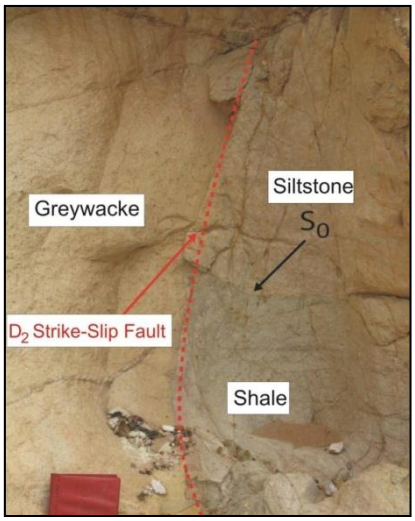

C.

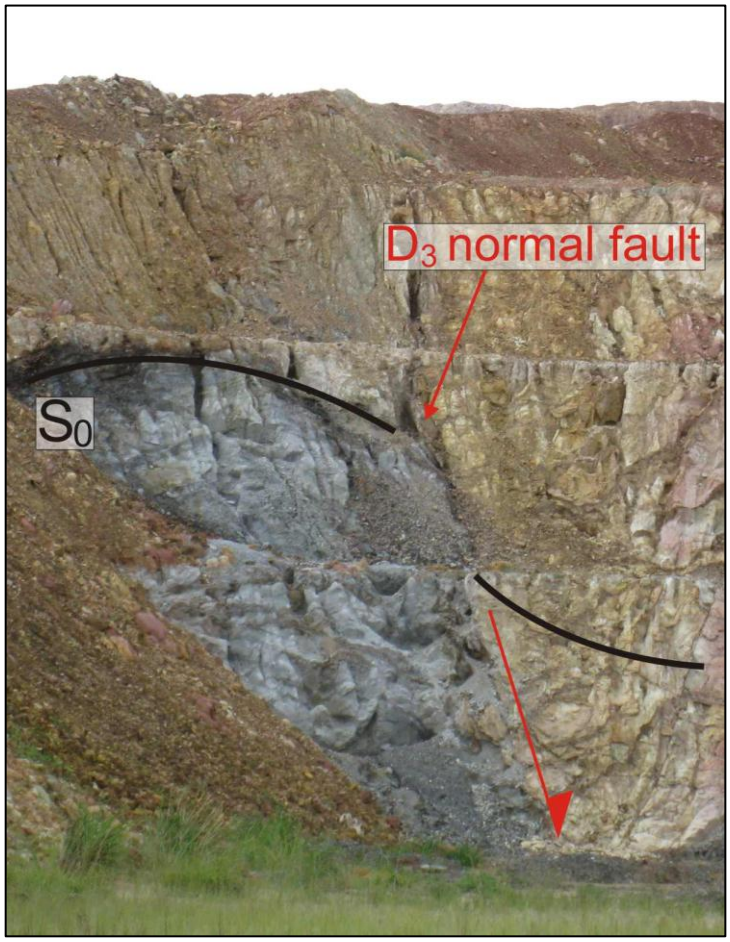

Figure 5.11: **A.** Photo showing D_2 strike-slip faults in the southern extent of Bidini, looking southeast. Two NNE-trending D_2 strike-slip faults truncate the pit. The adjacent bedding terminates against the subvertical faults. To the east of the eastern fault, bedding assumes moderate dips to the northeast, whereas to the west of the western fault, bedding trends east-west and dips steeply to the north and south. The black rectangle shows the location of figure 5.11.B. **B.** Photo showing the sharp termination of bedding against the steeply dipping eastern shear, from the west, taken in the southern extent of Bidini, looking south-southeast (see Fig. 5.11.A). In the southern extent of the pit, weathering and local mining activity made mapping in between the shears difficult and the photo shows the only bedding (S_0) mapped between the faults. Here bedding assumes subhorizontal dips on the western side of the fault. See red book for scale. **C.** Photo taken in the central part of the eastern domain, looking north. A steeply east-dipping, north-south trending shear is interpreted as being a normal fault, inferred from the sigmoidal drag of bedding adjacent to the fault, with hanging wall showing evidence of being dragged down.

bedding against the faults is particularly well developed in the central and southern parts of the pit (Fig. 5.11.B), but the faults show subparallel trends with the wall rocks further north. The fault zones thus defined are 2 to 3 m wide. The faults are interpreted as D_2 strike-slip faults, indicated by the drag of bedding along the fault planes along the western wall of Bidini. A dip-slip component along these faults seems likely, judging from the drag of bedding against the shear. Along the western shear (dip and dip direction: 276/79°), bedding has been deformed into an antiform on the western side of the shear and a synform on its eastern side. These faults can be traced into the Toubani open pit in the south. Although these faults are termed strike-slip, a dip-slip component cannot be excluded. Since this may indicate a sigmoidal bedding pattern as a result of fault drag, which, in turn, would point to a reverse component of slip along the fault zone.

North-south trending D_3 normal faults are particularly common in the south-eastern parts of the Bidini open pit (Fig. 5.9.C). Bedding is commonly openly folded along the moderate (45 to 55°) east-northeast and west-dipping faults as a result of the drag along the fault. These folds trend subparallel to the normal faults and show a plunge direction and plunge of 330/22°. In the central-eastern domain of Bidini, a north-south trending, steep (84°) east-dipping normal fault offsets the bedding in the area west of the basin structure (Fig. 5.11.C).

5.2.3 Toubani

The current Toubani open-pit operations can be divided into three structurally different domains, namely a southwestern domain, a central-northern domain and an eastern domain (Fig. 5.12.A).

In the southwest of Toubani, the northerly-trending bedding is subvertical (80° to 90°) with dips both to the east and west (Fig. 5.5.A; Fig. 5.12.B). Towards the northwestern part of the pit, bedding undulates showing steep dips and north-northwest trends, assuming more northerly trends again in the far northwestern parts of the pit. This steep zone can be linked to the central steep domain in Sanu Tinti (Fig. 5.8.A). Two closely-spaced (3 to 4 m spacing) D_2 reverse faults are developed in the southwestern corner of the pit. The reverse faults dip at moderate angles (40 to 60°) to the west (Fig.5.12.B).

A.

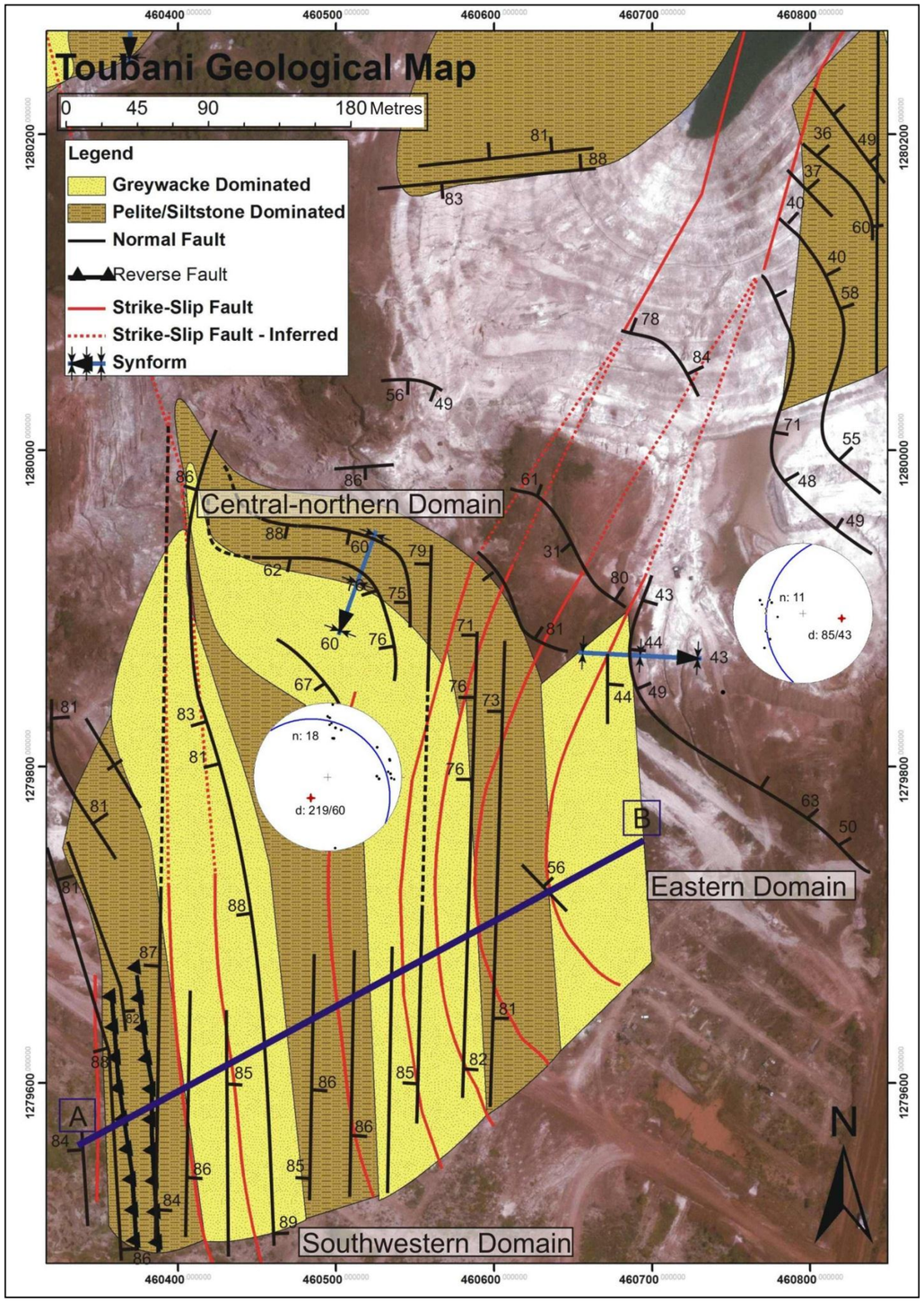

B.

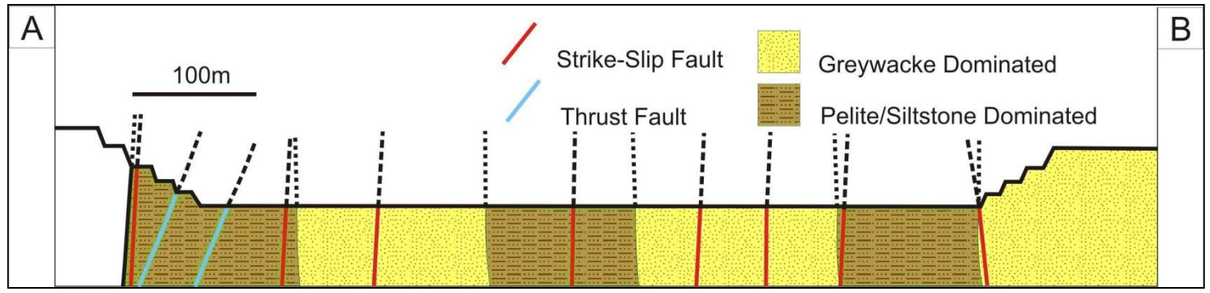

C.

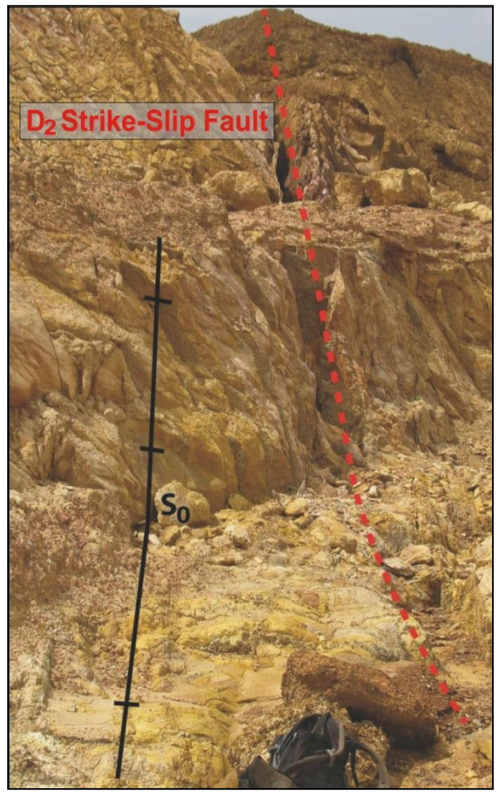

D.

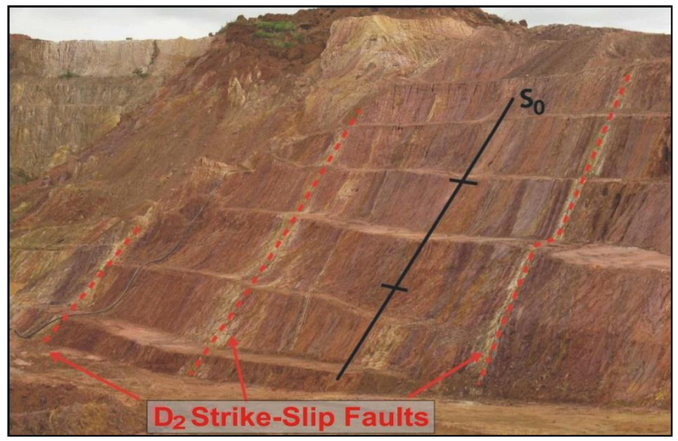

Figure 5.12: **A.** Formline map of Toubani. The lithologies in the map consist of greywacke-dominated and pelite/siltstone-dominated lithotypes. Stereographic projections show the orientation and plunge of the two synformal structures in Toubani, located in the central-northern and eastern parts of the pit. Note the either abrupt truncation or drag of bedding against D_2 strike-slip faults. **B**. Cross-section drawn through the southern parts of Toubani, from southwest to northeast, along line A-B in Fig. 5.12.A. The cross-section shows the steeply dipping, north-south trending bedding underlying most of the Toubani pit operations. In the southwestern extent of the pit, a pair of west-dipping reverse faults is developed. The section also shows a series of bedding-parallel strike-slip faults truncating the pit. **C.** Photo showing a north-south trending strike-slip fault in the southwestern domain of Toubani. Here, the bedding-parallel strike-slip fault shows pronounced negative weathering compared to the surrounding rocks. **D.** Photo taken in the central-eastern domain of Toubani, looking north-northeast, showing subvertical, northerly-trending bedding and subparallel strike-slip faults (annotated as red, dotted lines). The traces of faults are marked by bleaching and their white colouration against the reddish-brown wall rocks. A fourth strike-slip fault was observed further to the southeast. Photo is slightly distorted to the left and right edges due to stitching.

The central-northern domain covers the area of the Toubani Old Pit. Here, bedding rotates to more east-west trends and steep southerly (60 to 90°) dips. This defines a steep SE-plunging F_2 synform (plunge direction and plunge: 219/60°) having a sigmoidal, S-shaped geometry. The eastern boundary of the central-northern domain is made up of a set of north-trending D_2 strike slip faults (Fig. 5.12.A). The drag of bedding against the faults points to a dextral strike-slip component along the faults.

The northern extent of the eastern domain shows shallower (50°), E-W to NW-SE trending bedding, deformed into gently folded strata. The structures include moderate- to steeply plunging open antiform and synform pairs. This rotation of the bedding may be due to the D_2 shears that seem to extend from Toubani in the south to Bidini in the north. In the far southeastern part of Toubani, steeply dipping (50 to 65°), NW-SE trending bedding is folded by an open, east-plunging synform (orientation: 85/43°) resulting in north-northeast trends.

S_{2a} dips at angles of 70 to 80° to both the east and west in rocks of the Toubani pit which is subparallel to the axial plane of the synform (F_2) in the central-northern domain. In addition, the S_{2b} fracture cleavage shows westerly dips (S_{2b}, calculated orientation 264/50°). Both these foliations are also present in rocks of the Bidini open pit (Chapter 5.2.2).

A series of bedding-subparallel D_2 strike-slip faults are developed in the subvertical bedding. The faults are identified by their whitish colouration (Fig. 5.12.D) and negative weathering (Fig. 5.12.C) compared to the surrounding beds, as well as the abrupt termination of adjacent structures to the northeast of Toubani and also in Bidini (see above). The shears describe an overall arcuate geometry from NW-SE trends in the south of Toubani to more north-northeast trends in the northeast. The dips of the shears are mostly between 80° and vertical. Dips are steep (ca. 70°) where the shears assume more NW-SE trends.

5.2.4 Kami North

The Kami North open pit is subdivided into two domains, namely a western and a central- to northeastern domain. The western domain is underlain by a N-S to NW-SE trending antiform (F_2) that shows a shallow (5°) plunge to the south-southeast. The closure of structural formlines (Fig. 5.13.A) to the north

A.

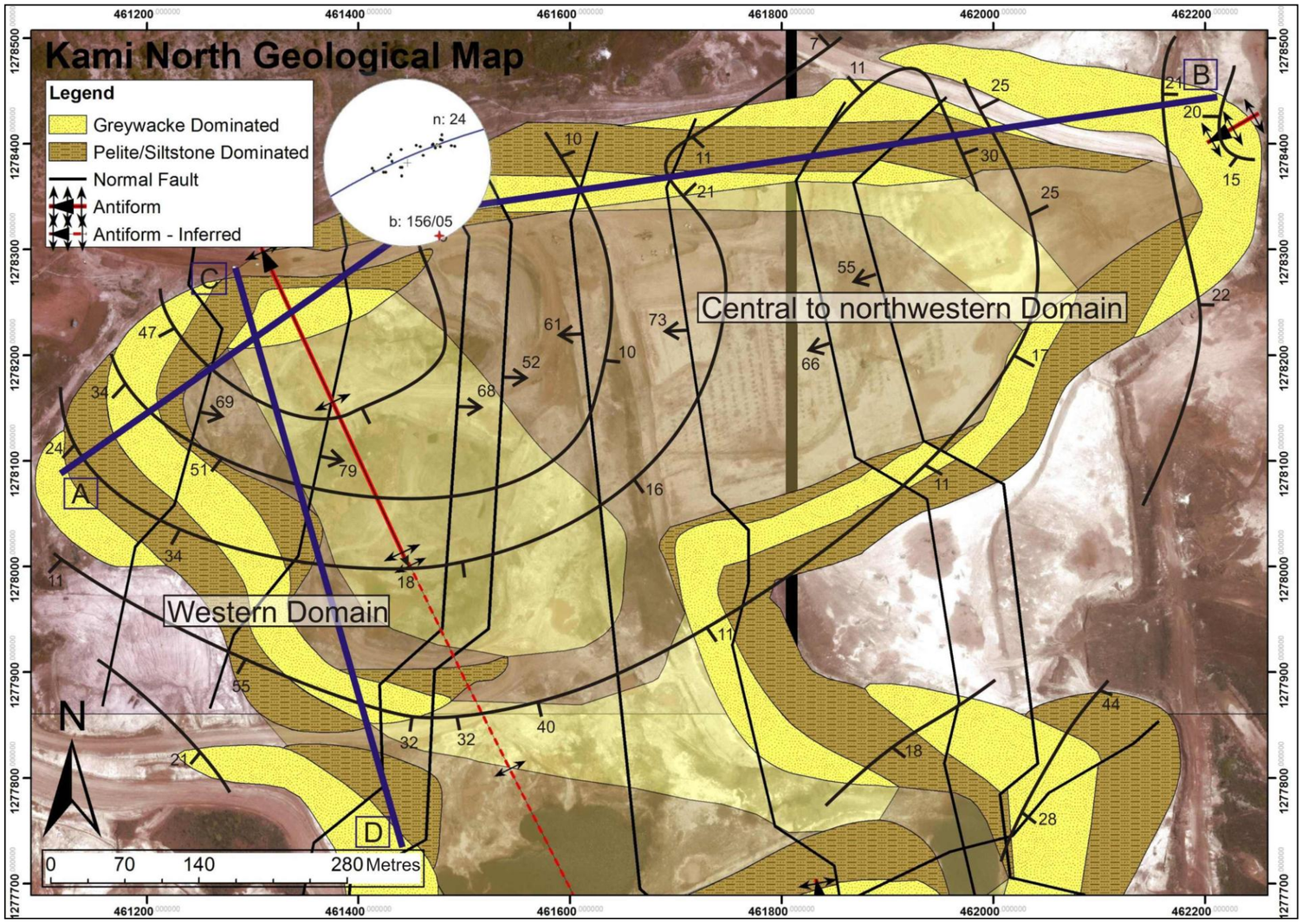

B.

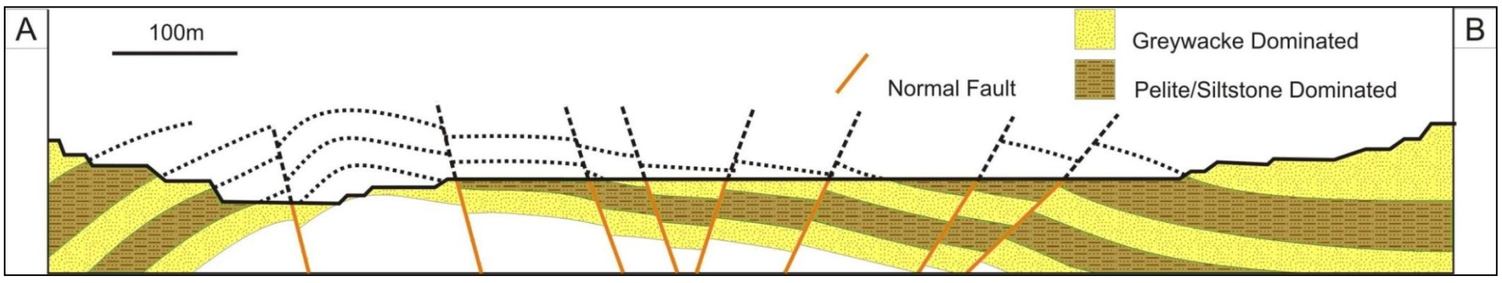

C.

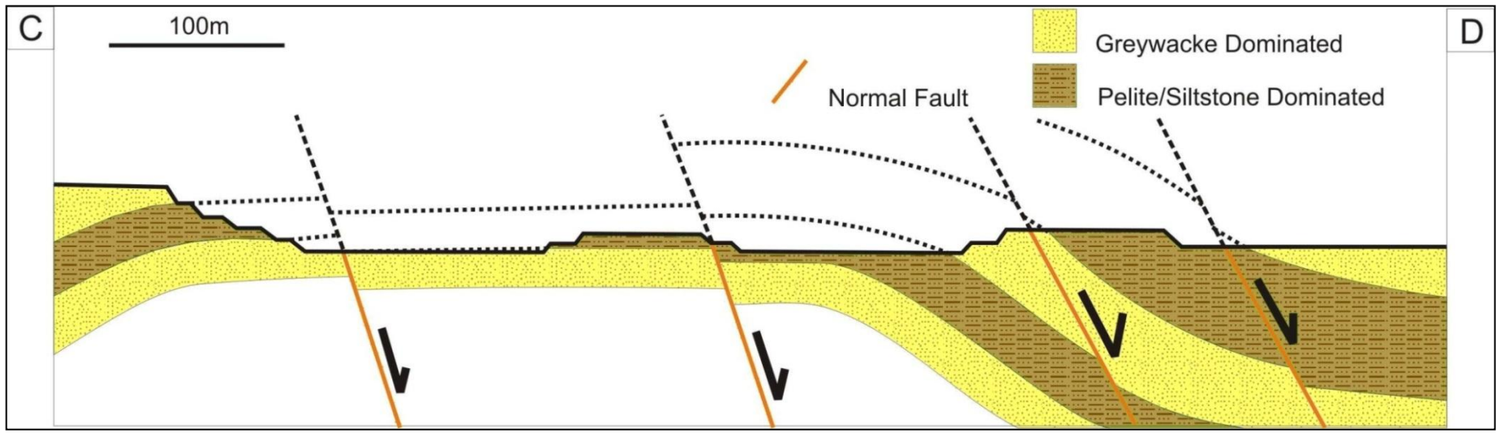

Figure 5.13: **A.** Structural formline map of Kami North. The stereographic projection shows the orientation and plunge of the NW-SE trending main antiform that underlies the western domain of the pit. **B**. Cross-section along the northern and northwestern wall of Kami North along the line A-B (Fig. 5.13.A). The cross-section shows the open, gently west-verging antiformal structure that underlies much of Kami North. A series of north-south trending normal faults truncates the pit. The easternmost fault has the largest displacement. The cross-section also illustrates the tilting of strata between normal faults. **C.** Section drawn parallel to the hinge of the antiform in the western domain of the pit, along line C-D (Fig. 5.13.A), illustrating the doubly-plunging, dome-like nature of the antiform. The section cuts obliquely through the D_3 normal faults.

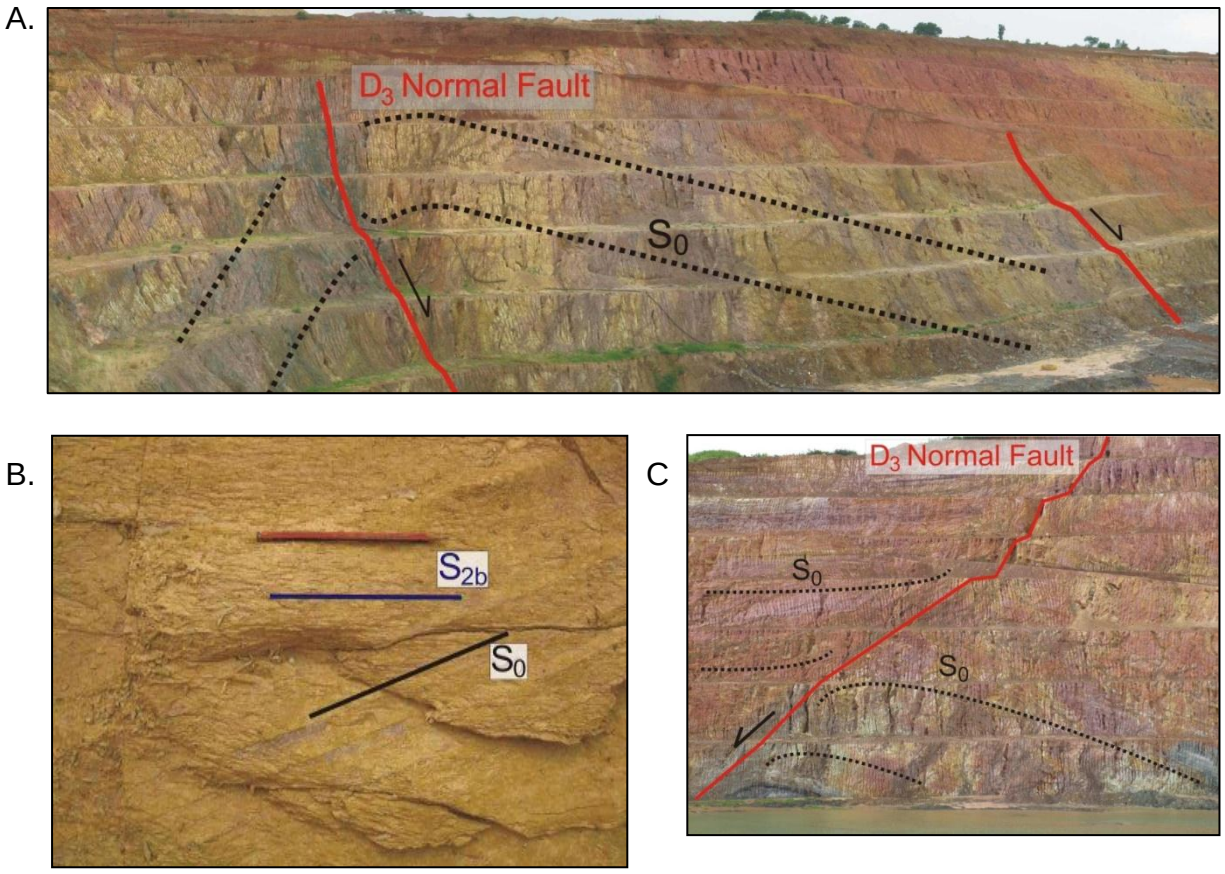

Figure 5.14: **A.** Photo taken in the western domain of Kami North, looking north-northeast, showing the main antiform underlying Kami North. The antiform trends north-northwest and plunges shallowly to the south-southeast. The western limb is slightly steeper than the eastern limb and results in an overall west-southwest vergence. Truncating the antiform is a series of east-dipping D_3 normal faults (red lines). **B.** Photo taken in the western domain of Kami North, on the eastern limb of the antiform, plan view. The S_{2b} foliation is developed as a spaced fracture cleavage, dipping moderately to the east-southeast. In the northwestern part of the pit bedding assumes shallow east-northeast dips, along the eastern limb of the antiform. **C.** Photo taken in the north-eastern part of the pit, looking north, showing the easternmost normal fault with a displacement of ca. 10 m. The bedding is dragged along the fault plane. The formation of half-graben structures involving a rotational component and tilting of the strata, as can be seen west and east of the fault.

indicates that this antiform is doubly-plunging. The open antiform has a shallower (10 to 25°) northeastern limb, underlying the central- to northeastern domain, and a steeper (25 to 50°) southwestern limb. This results in a slight west-southwesterly vergence of the fold (Fig. 5.14.A). The doubly-plunging antiform forms the core of a larger, ENE-trending dome structure underlying the whole of Kami North (Fig. 5.13.B). A minor parasitic antiform is developed in the far northeastern corner of the pit, where rocks are steeper, showing a calculated orientation of 125/30° (Fig.

5.14.B). The axial planar foliation (S_{2a}) is not developed in Kami North, which may relate to the very open fold shapes, in turn indicating a lower degree of shortening.

A set of north-trending normal faults (D_3) is developed in Kami North (Fig. 5.14.C). The normal faults show moderate- to steep (55 to 75°) dips towards the east and west, resulting in symmetrically arranged half-graben structures on both sides of a main graben structure that runs through the central parts of Kami North. Locally, bedding can locally be seen to be dragged along the fault planes. Individual normal faults show a maximum displacement of up to 10 m for the easternmost normal fault. The cumulative throw along the normal faults and into the central graben is at least 20 to 30 m. Bedding readings also change around the faults with the largest variation being along the easternmost normal fault, where predominantly shallow NW-dipping bedding changes to easterly dips towards the northeastern corner of the pit. This suggests that the normal faulting in the half-graben structures involved a rotational component and tilting of strata between normal faults (Fig. 5.14.C).

5.2.5 Kami South

The Kami South open-pit operations can be subdivided into a western-, central- and eastern domain (Fig. 5.15.A). A central antiform, with a half-wavelength of ca. 300 m, dominates the central domain of the pit and can be followed from Kami North. This antiform in Kami South shares its eastern limb with the western limb of the Kossise synform to the immediate east, showing moderate- to shallow (30 to 40°) easterly dips. The western limb of the antiform shows slightly steeper dips (40 to 50°) towards the west, giving the antiform an overall westerly vergence, with a steeply east-dipping axial plane (Fig. 5.15.B). The open antiform plunges at shallow angles to the north (plunge direction and plunge: 003/10°) (Fig. 5.15.C; Fig. 5.15.D). The southern extent of the open pit is mainly underlain by east- and west-dipping beds forming the limbs of the antiform. Here, the antiform shows subhorizontal plunges (147/01°), indicating the doubly-plunging geometry of the fold. Towards the north, the bedding systematically changes and dips are to the southeast in the eastern domain and SW-dipping in the western domain of Kami South. A pair of shallow NW-plunging F_2 folds is developed in the northwest, in vicinity of the Kami South ramp (Fig. 5.16.A). These are parasitic folds, with a wavelength of ca. 25 to 40 m and a calculated plunge direction and plunge of 330/10°. The eastern fold is a synform, consisting of a steep eastern limb and shallow western limb, resulting in a westerly vergence. The

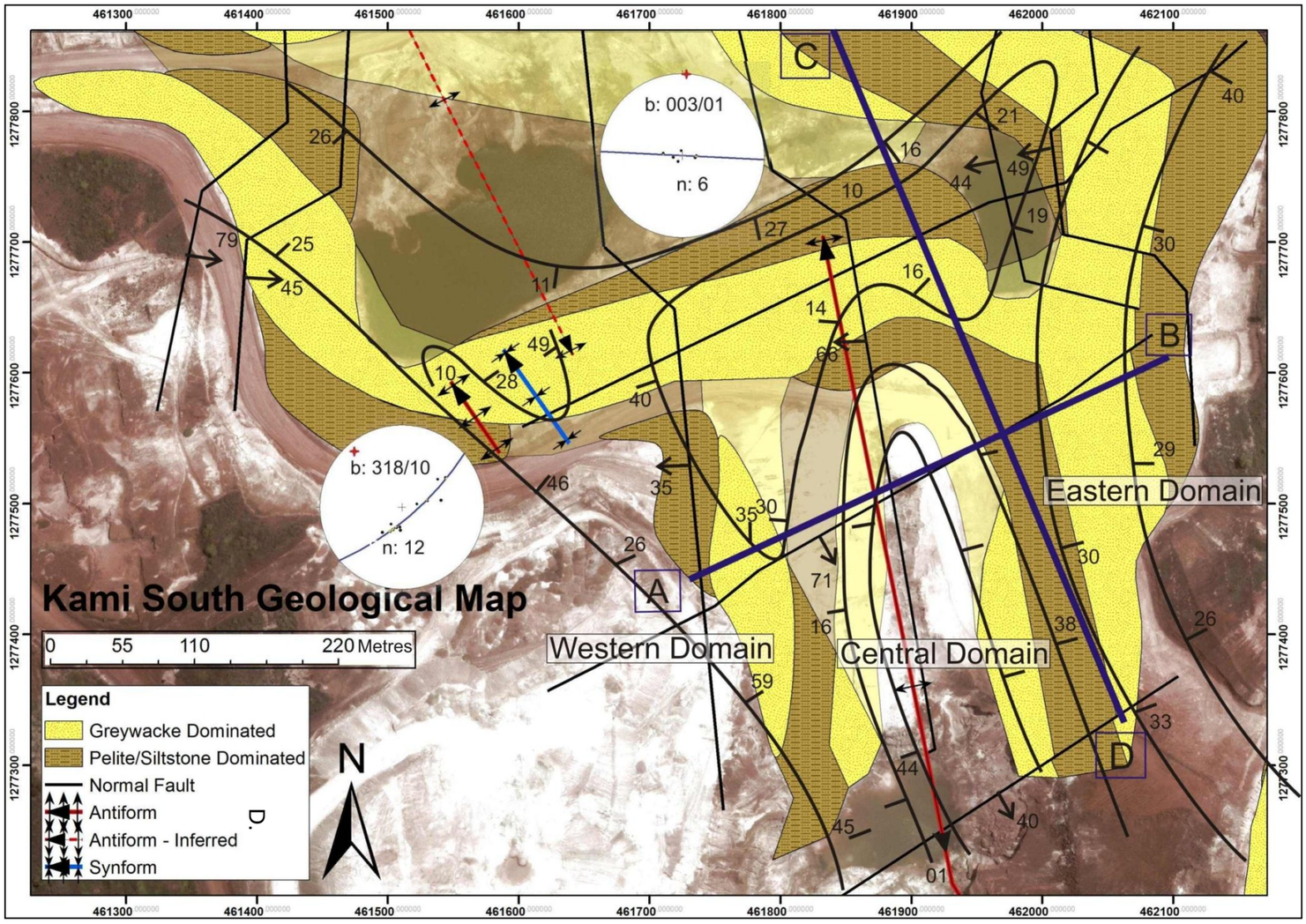

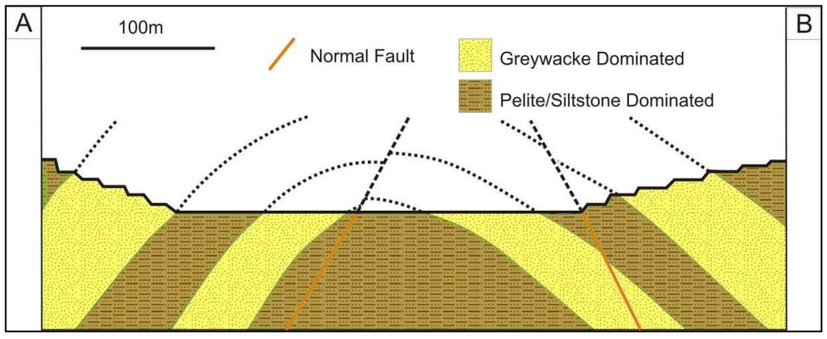

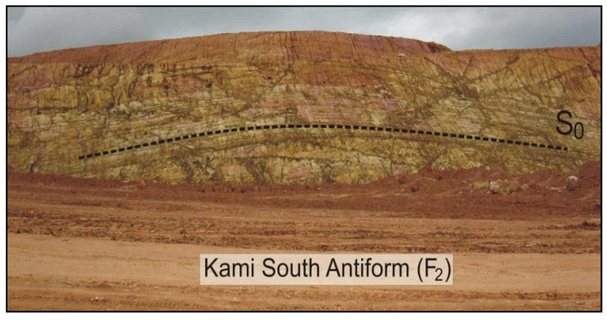

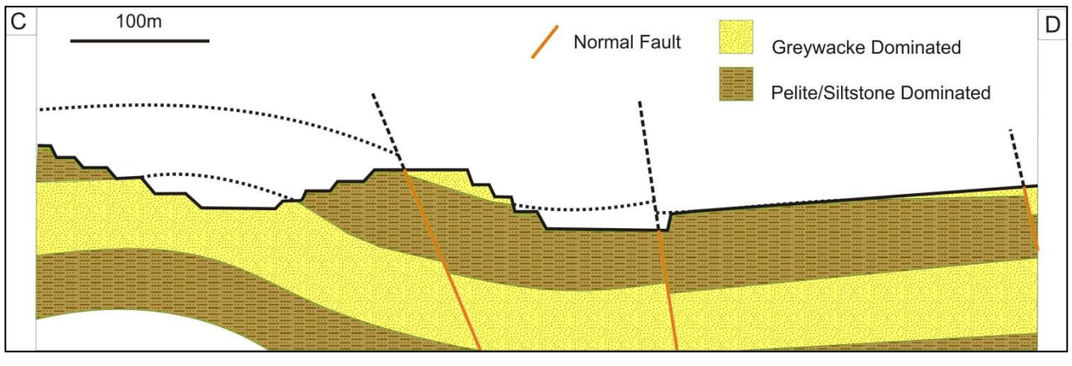

Figure 5.15: **A.** Structural formline map of Kami South, with Kami North to the north. The lithologies in the map consist of greywacke-dominated and pelite/siltstone-dominated lithotypes. Stereographic projections show the plunge direction and plunge of the N- to NNW trending antiform that underlies most of the pit and the parasitic fold pair in the northern part of the western domain of the pit. **B**. Cross-section through the central parts of the pit, from WSW to ENE, along the line A-B (Fig. 5.15.A). The cross-section shows the antiformal structure, underlying most of Kami South. The western limb is steeper than the eastern limb, resulting in a west to southwesterly-verging antiform. A series of north-south trending normal faults is developed in Kami South. The cross-section also includes an ENE-trending normal fault. This set of D_2 normal faults is only developed in Kami South. **C.** Section drawn along the eastern-wall of Kami South, from northwest to southeast, along line C-D included in figure 5.15.A. The section shows the shallow northerly plunge of the central antiform. The main dome structure of Kami North is located to the immediate north. The section cross-cuts two of the ENE-trending D_2 normal faults. **D.** Photo taken in the central domain of Kami South, looking north. The north-south trending, antiformal structure is shown. Here the antiform shows very gentle interlimb angles. The antiform is more open to the north of the pit where bedding changes orientation to southwesterly dips in the west and southeasterly dips in the east. It is also here where the antiform steps to the left, as it trends into Kami North, describing an en-echelon arrangement (Chapter 5.2.8).

A.

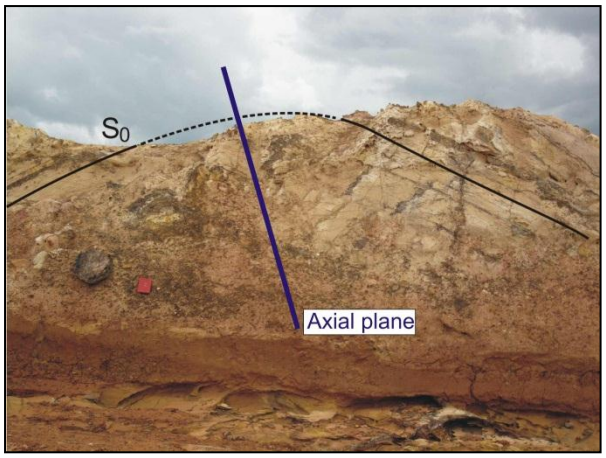

B.

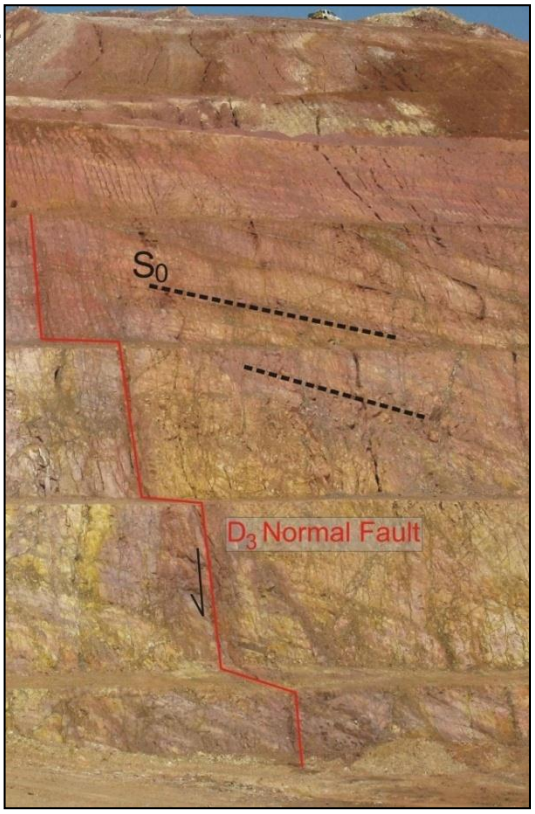

Figure 5.16: **A.** A photo taken to the north, showing a cross-sectional view of an open, west-verging antiform in the western domain of Kami South; bedding and the axial surface are annotated. **B.** Photo taken in the central parts of the western domain in Kami South, looking west. The ENE-trending D_2 normal fault is shown and dips steeply to the south-southeast. The fault truncates the moderately west-dipping strata of the western limb of the Kami South antiform.

adjacent parasitic antiform is more open and upright, with a subvertical axial plane. Transecting foliations (S_{2b}) with respect to the F_2 folds observed in Kami South show moderate-to shallow east-southeast dips, with a calculated orientation of 121/40° or with even shallower, west-northwest dips (calculated orientation of 292/20°). The absence of the steep S_{2a} fabric may again reflect the rather open fold geometries and a lower degree of shortening.

Normal faults show mainly two trends in Kami South, as opposed to the one set located in Kami North. A high-angle set of ENE-trending normal faults dips to the southeast at angles between 40 and 70° (Fig 5.16.B). These normal faults are interpreted to have developed during the main D_2 deformation event. The faults trend normal to the trace of the hinge, of the underlying F_2 antiform. North-south trending normal faults (D_3) dip between 35 and 65° towards the west. The actual displacement along these faults could not be measured due to lack of marker horizons.

5.2.6 Kossise

The central synformal structure in the Kossise pit trends north-south and has a half-wavelength of over 350 m (Figs. 5.17.B and C). The synform plunges shallowly towards the north (355/14°). The eastern limb of the synform consists of steep- to overturned bedding and has a calculated dip of 80° towards the west. The western limb has a much shallower dip of 40° towards the east-northeast. The steep- to overturned eastern limb and shallowly dipping western limb result in an overall westerly vergence of the fold. In the northern part of the pit, the fold hinge is well exposed and characterized by parasitic folds and m- to larger-scale out-of-syncline reverse faults (Fig. 5.18). The fold closure is not well exposed in the southern wall of the Kossise pit. The axial-planar foliation (S_{2a}) that is fairly prominent in the steep belts of the Siguiri Mining Complex, is also well developed in the steep limb of the synformal structure in Kossise. Where developed, S_{2a} shows steep east-southeasterly dips (calculated dip direction and dip: 100/84°; Fig. 5.2.B). The shallower S_{2b} shows moderate southeast dips with a calculated dip direction and dip of 125/40°.

The steep- to overturned eastern limb contains three reverse faults (D_2) that can be followed along their north-south trend throughout the open pit (Fig 5.17.D). These reverse faults dip to the east (calculated 100/45°), with a throw of between 1 and 6 m, recording top-to-the-west sense of displacement. The western pit wall exposes a moderate- to steeply dipping normal fault (D_3) located in the shallowly dipping western limb of the Kossise synform. This normal fault dips 60° towards the west and seems to represent the southern strike continuation of the easternmost D_3 fault in Kami North.

5.2.7 Summary of the Kami-Kossise Complex

There are a number of structural features that characterize the Kami-Kossise open-pit cluster. The complex is underlain by mainly gently folded (F_2) strata, bordering against the D_2 steep belt in the eastern parts of the Kossise pit. F_2 folds show a systematic change of their vergence direction with proximity to the eastern steep belt. Folds verge to the west in closer proximity to the steep belt and become progressively more upright away from the belt. The doubly-plunging geometry of F_2 folds results in distinct zones of axial depressions and culminations. The main dome

A.

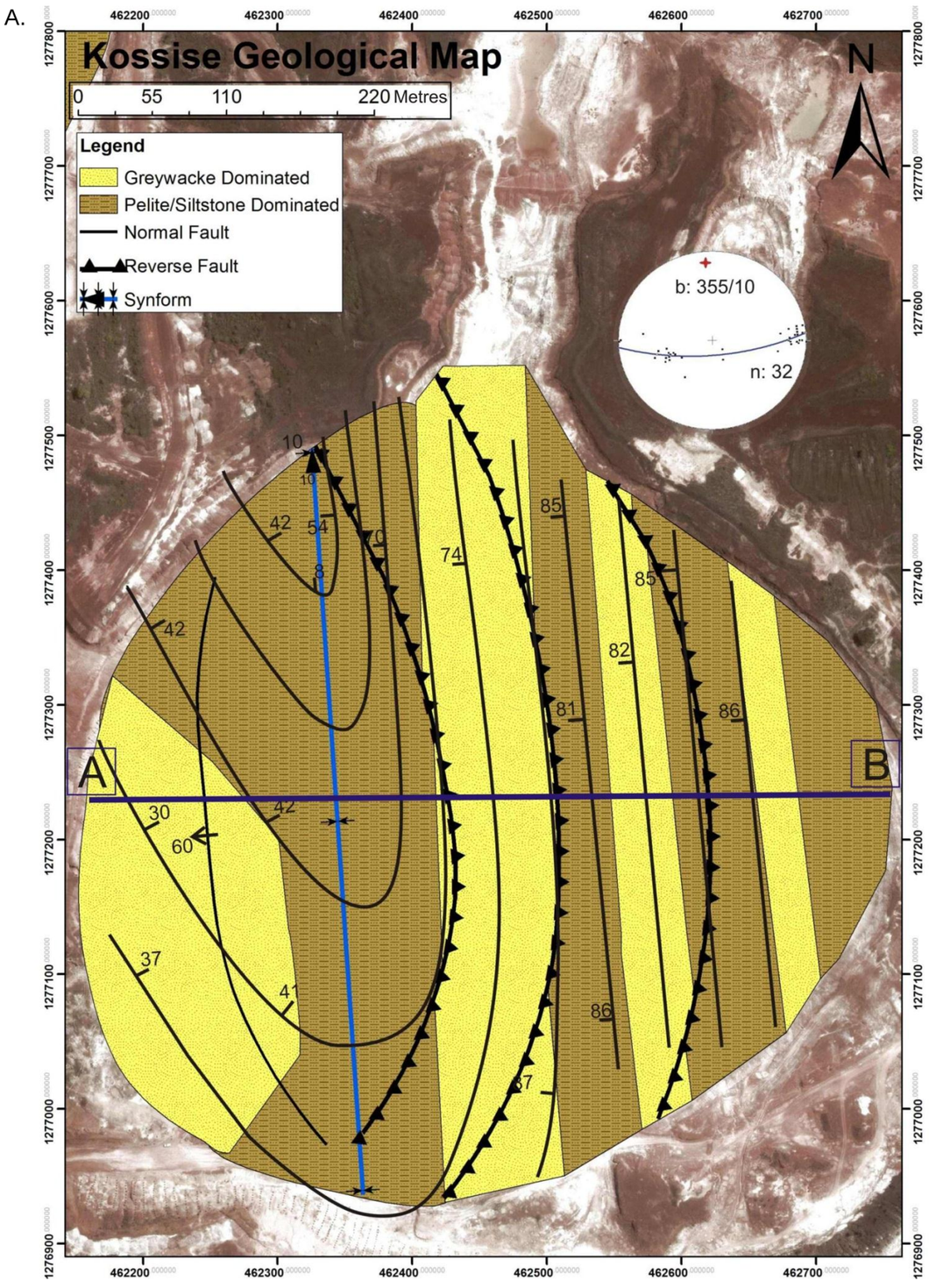

B.

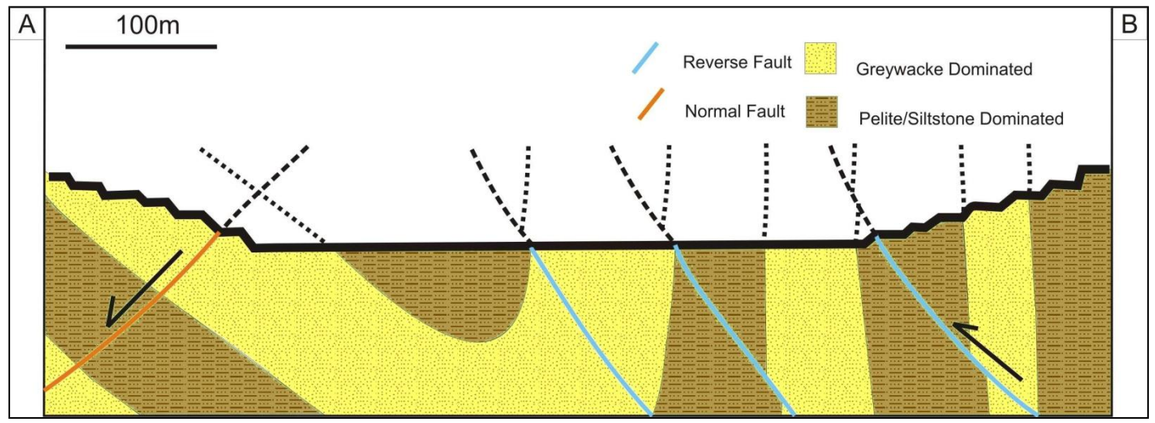

C.

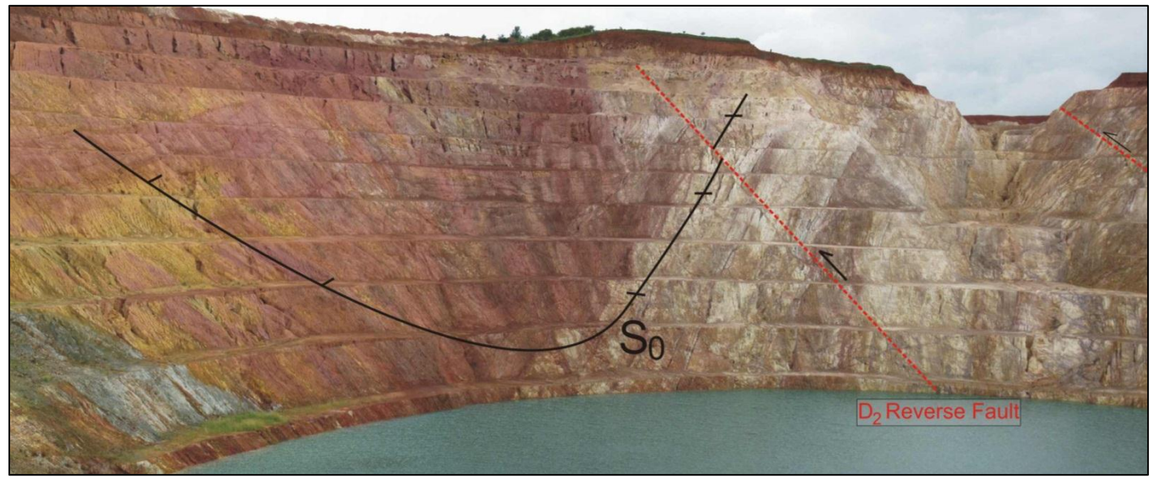

D.

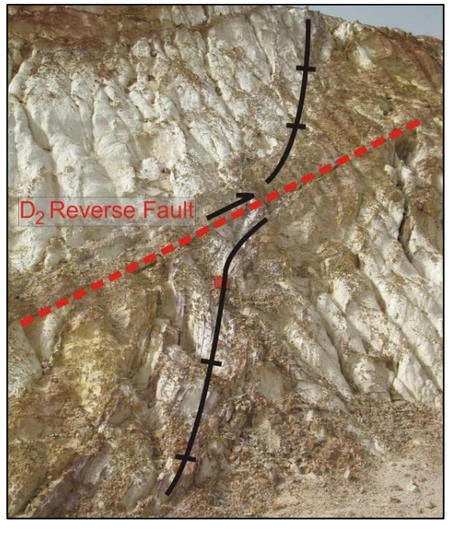

Figure 5.17: **A.** Structural formline map of Kossise. The stereographic projection shows the plunge and plunge direction of the Kossise Synform. **B**. Cross-section drawn through the central parts of the pit, from west to east, along line A-B indicated in figure 5.17.A. The cross-section shows the asymmetric, west-verging synformal structure underlying Kossise. North-south trending, upright- to overturned strata defines the eastern limb, whereas the western limb is underlain by shallower NE-dipping strata. A set of steeply east-dipping reverse faults cuts the eastern limb of the synform, with a single west-dipping normal fault truncating the western limb. **C.** Photograph of the northern pit wall of Kossise. The annotated bedding (S_0) delineates the west-verging synform. Photo is distorted to the edges, due to stitching. **D.** Photo of a part of the southern pit wall, showing an east-dipping reverse fault and associated drag of the bedding, particularly in the footwall of the reverse fault. The reverse faults can be traced for several hundred metres along strike through the pit, from north to south.

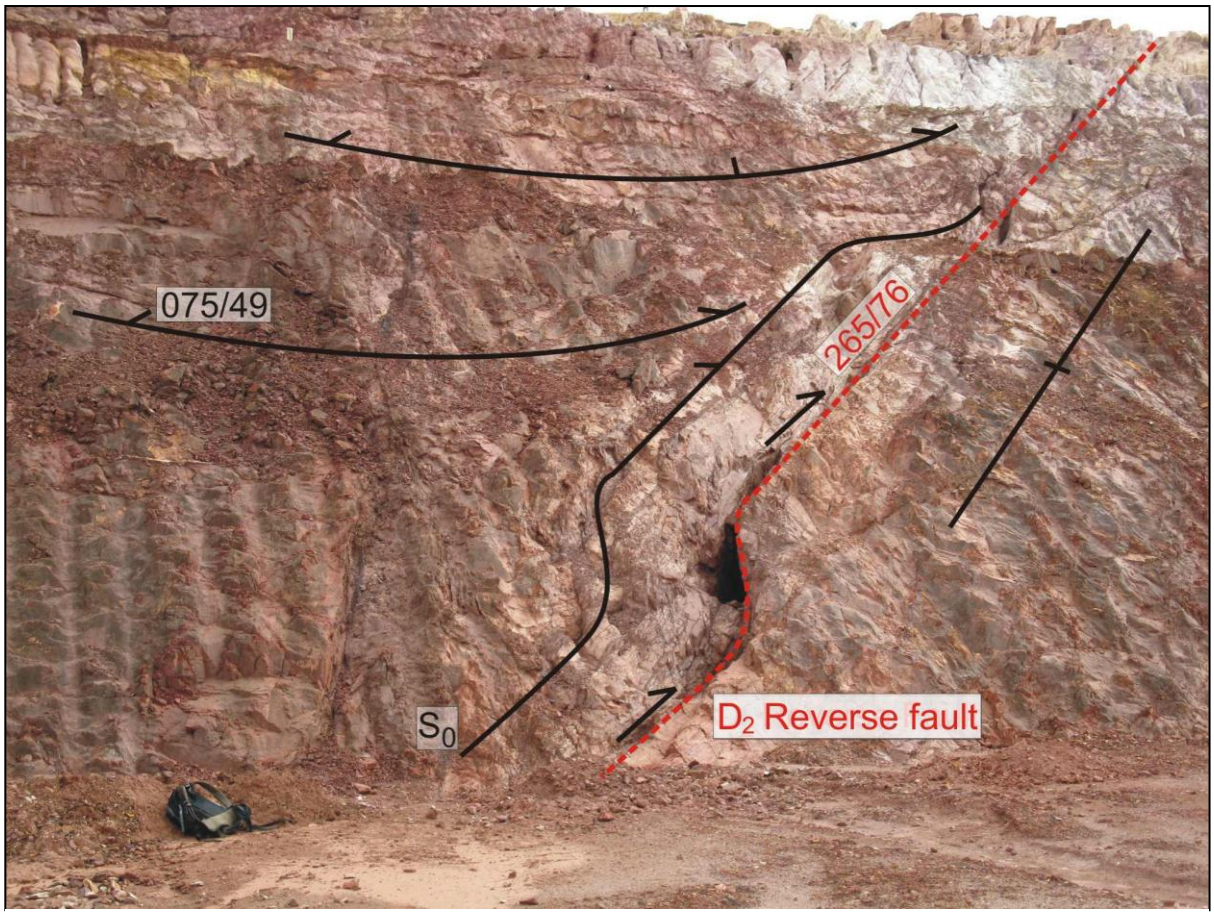

Figure 5.18 **A.** Photograph taken in the hinge of the synform along the northern pit wall (bedding annotated by black lines). The photo shows a small-scale, west-dipping, out-of-synform reverse fault (D_2). This reverse fault dips in the opposite direction of the main east-dipping set. Here, the reverse fault is developed on the steeper eastern limb and follows a flat-and-ramp staircase-like geometry (red dashed line). The hanging wall stratum develops a snake-head structure further up-dip.

structure at Kami North represents an axial culmination, bordered in the south by an elongated, E- to NE-trending axial depression. Within the axial depression, the axial traces of F_2 folds describe a left-stepping en-echelon arrangement. Notably, the orientation and location of the main pit operations coincide with the F_2 axial depressions and culminations, an aspect that will be developed in Chapter 7.

5.2.8 Kozan

The Kozan open pit is divided into an eastern-, central- and western domain (Fig. 5.19.A). The eastern domain consists of north-trending, subvertical (dips: 70 to 85° to the west) bedding (Fig. 5.19.B and C) forming the northern continuation of the D_2 steep belt in Kossise (Chapter 5.2.6). Immediately west of the steep zone, three closely spaced reverse faults occur. The D_2 reverse faults dip to the west at angles of 45 to 50° and occur over an area of 30 m (Fig. 5.19.D). Bedding in the hanging wall

A.

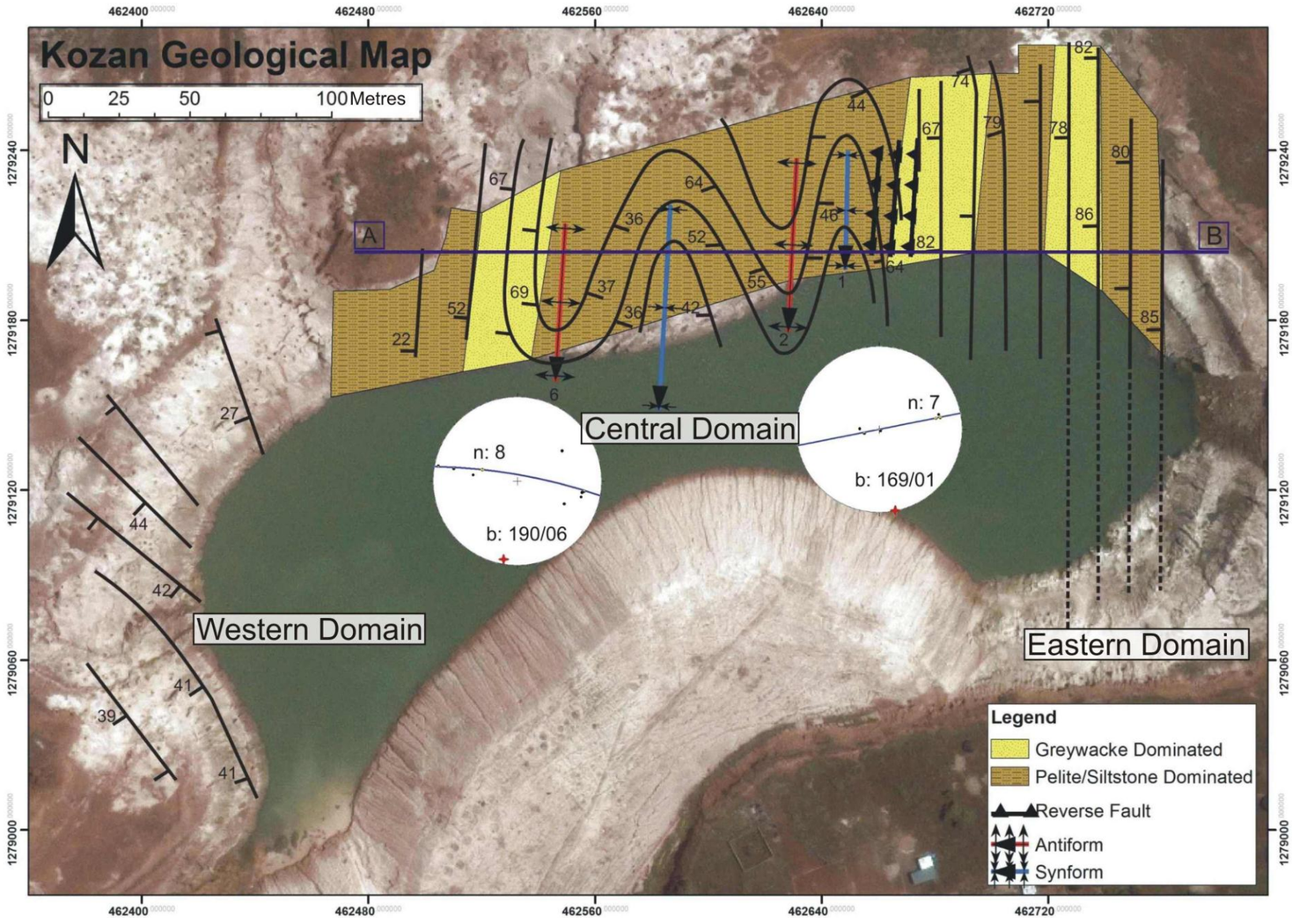

B.

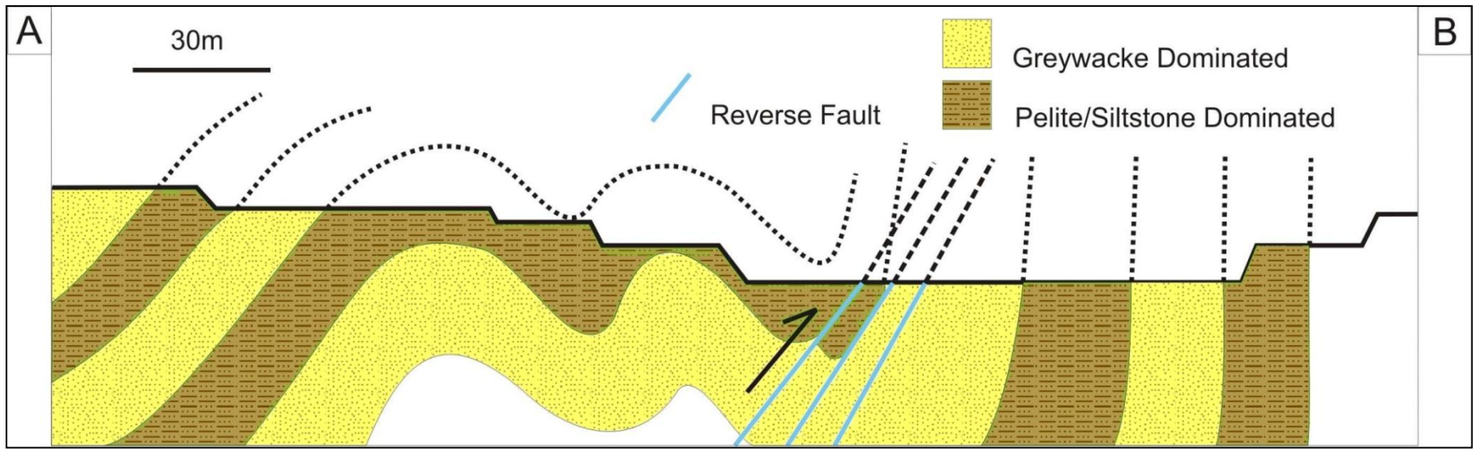

C.

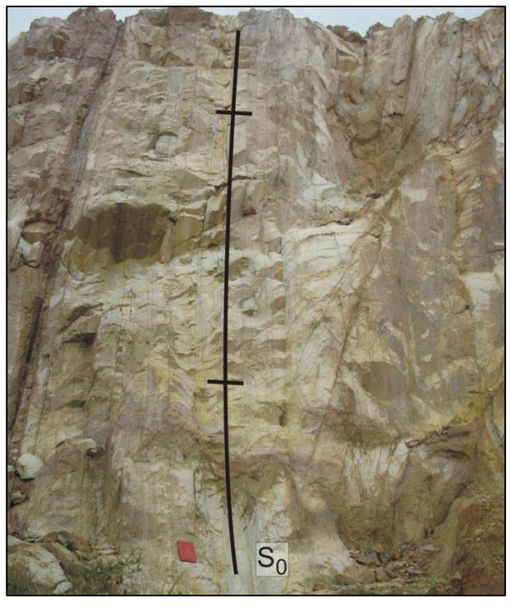

D.

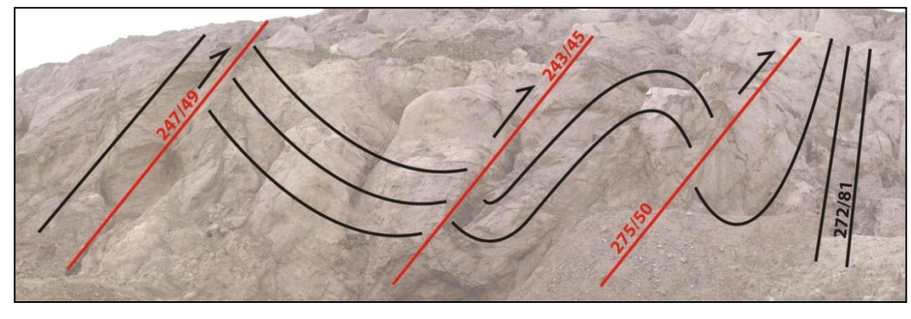

Figure 5.19: **A.** Structural formline map of Kozan. The stereographic projections show the plunge and plunge directions of the eastern- and westernmost folds (poles to bedding are plotted). **B**. Cross-section along the northern wall of Kozan, from west to east, along line A-B (Fig. 5.19.A). The cross-section shows the steep, north-south trending eastern domain. To the west of the steep zone, two north-south trending, synform-antiform pairs are developed. The eastern limb of the eastern synform is truncated by three moderately west-dipping reverse faults. This folded domain flattens out to the west, with bedding assuming moderate- to shallow dips and more northwest-southeast trends. **C.** A photo taken in the eastern domain of the pit, looking north. The photo shows the north-south trending, subvertical bedding, which characterizes the eastern domain of Kozan. **D.** Annotated photo of the three small-scale, west-dipping reverse faults bordering against the eastern steep belt (looking north, cross-sectional view). Reverse faults and bedding are annotated with red and black solid lines, respectively.

and the footwall of the reverse faults is dragged into the fault planes, also indicating the top-to-the-east sense of displacement. However, the lack of marker horizons precludes an estimate of the actual displacement along the faults.

Two antiform/synform pairs are located structurally above the reverse faults. These F_2 folds form the central domain of the Kozan pit. The folds plunge shallowly towards the south and have wavelengths of between 45 and 80 m. The easternmost synform, located in the immediate hanging wall of the reverse faults, has a slightly steeper eastern limb and a shallower western limb, resulting in an overall westerly vergence of the fold, which is opposite to that of the faults. This fold has a wavelength of 45 m and a plunge direction and plunge of 169/01°. A rather open, gently west-verging antiform follows to the immediate west of the synform, with a wavelength of ca. 50 m (plunge direction and plunge: 170/02°). Folds to the west become more open and are rather upright, maintaining overall northerly trends. The westernmost fold has a plunge direction and plunge of 190/06° and a wavelength of 80 m (Fig. 5.20). The S_{2a} foliation observed in Kozan is approximately axial planar to F_2 folds and dips steeply to the east-southeast with a calculated orientation of 115/85°.

In the western domain of the Kozan, bedding assumes shallower attitudes away from the folded area. The westerly dips in the eastern parts of this domain give way to more southwesterly dips in the far western extents of the pit (calculated dip direction and dip: 240/36°) (Fig 5.19.A).

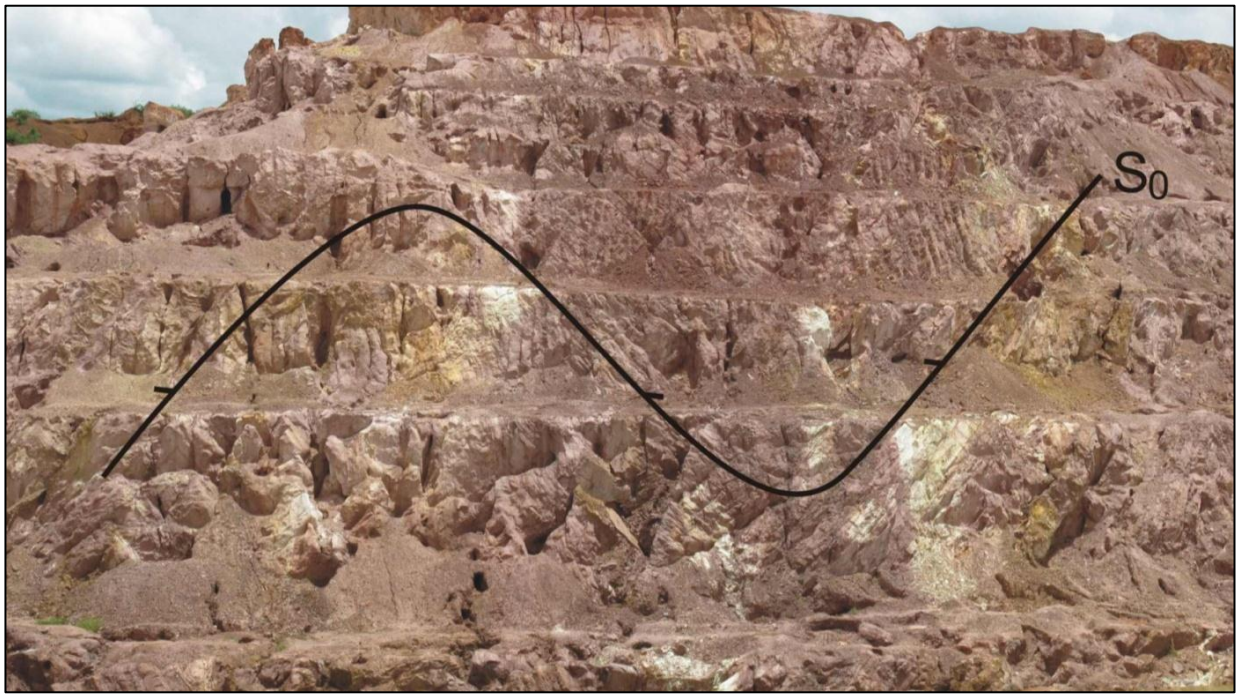

Figure 5.20: Photo of the western antiform-synform pair, cross-sectional view of the northern wall of the Kozan pit, bedding annotated. Here, the north-south trending folds assume an upright, open geometry, with steeply dipping axial planes and shallow plunges to the south.

5.2.9 Sintroko

The Sintroko open-pit operation can also be subdivided into three structurally different domains, namely an eastern-, western- and a central domain (Fig. 5.21.A). It is unique compared to other open pits of the Siguiri Mining Complex in that is located in steep- to subvertical strata, whereas the intervening and gently folded F_2 domains are not developed.

The central domain consists of steep, NNE-trending bedding (calculated dip direction and dip: 105/80°) (Fig. 5.21.B). This steep belt has a width of 140 m and is bounded in the east and west by north-south trending, bedding-subparallel shears (D_2), interpreted as strike-slip faults. The steep zone also shows evidence of intrafolial folds (F_1) that show shallow north-northeast plunges (030/05°) (Fig. 5.1.A), indicating higher strain in these zones. A set of moderately dipping (calculated dip of 45°) D_2 reverse faults cross-cuts the central steep belt (Fig. 5.21.B). In the east, the three reverse faults dip towards the east and record top-to-the-west sense of displacement (calculated orientation: 110/49°) (Fig. 5.22.A). The two western reverse faults dip towards the west and record top-to-the-east kinematics (Fig. 5.22.B). These reverse faults converge above a relatively fresh graphitic, sulphide-bearing pelitic-schist unit.

The central domain is bordered by equally steeply dipping rocks, but dip directions rotate to more northwesterly trends. Steeply plunging and tight F_2 folds are suggested for the eastern and western domains of Sintroko, indicated by variations in the dip and dip direction (Fig 5.21.A). The western fold is better defined than the eastern fold, plunging towards 345/71°. In the eastern domain of the open pit, bedding describes a somewhat sigmoidal, S-shaped pattern, defined by the consistently clockwise rotation of bedding against north-south trending zones of subvertical bedding. This geometry of gently-folded, steeply dipping, sigmoidal bedding suggests a dextral strike-slip component along the north-south steep belts separating the sigmoidally folded domains (Figs. 5.22.C and D). The S_{2a} foliation is subtle, but still well developed in Sintroko, showing mainly east-southeast dips, but also west-northwest dips. On average, S_{2a} has an orientation of 115/77°.

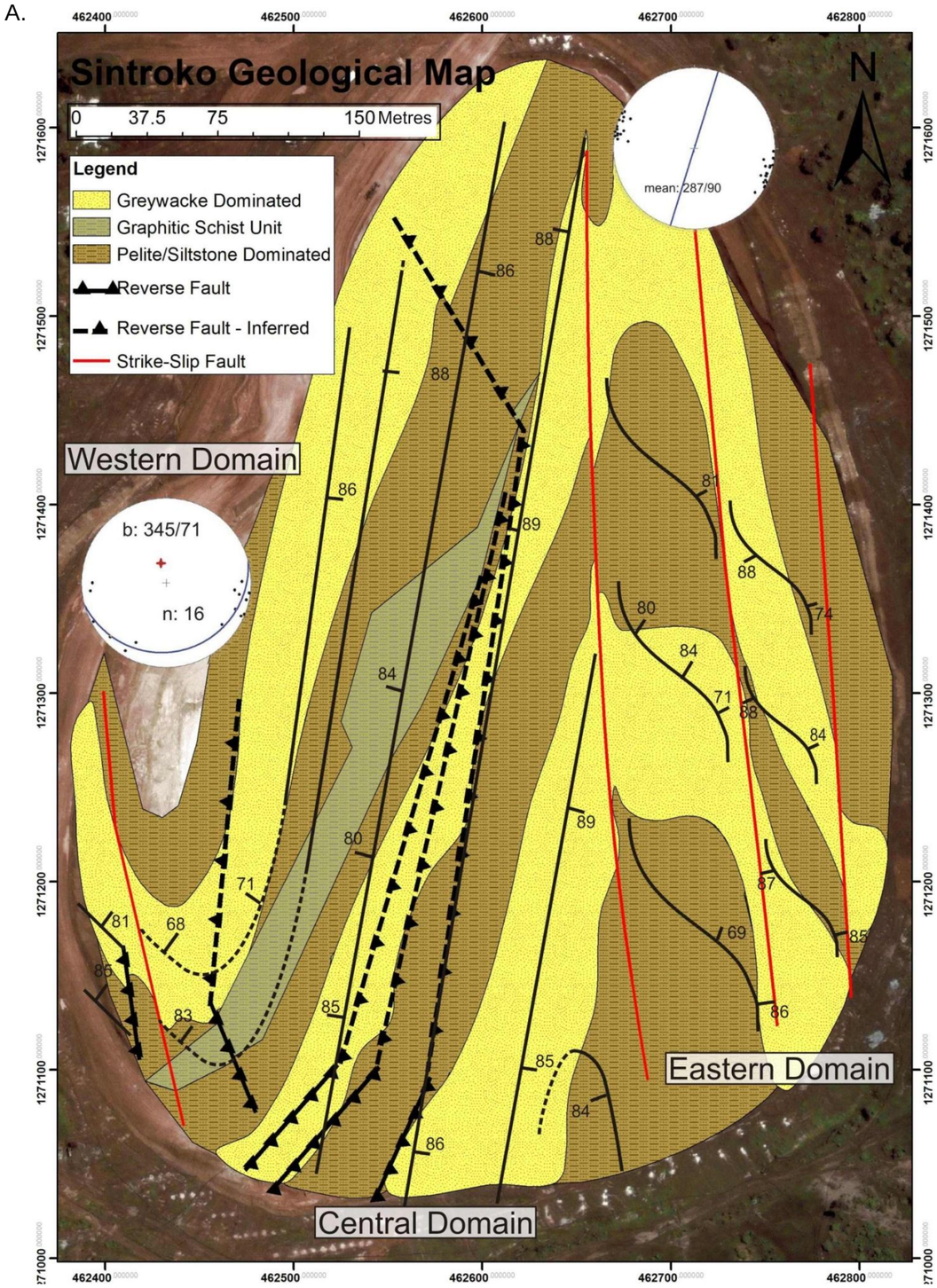

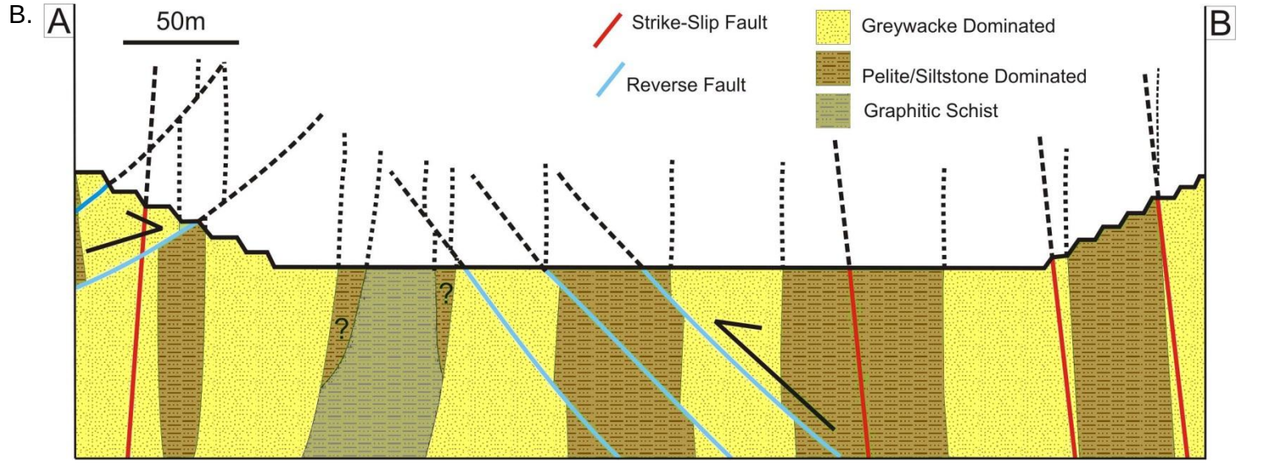

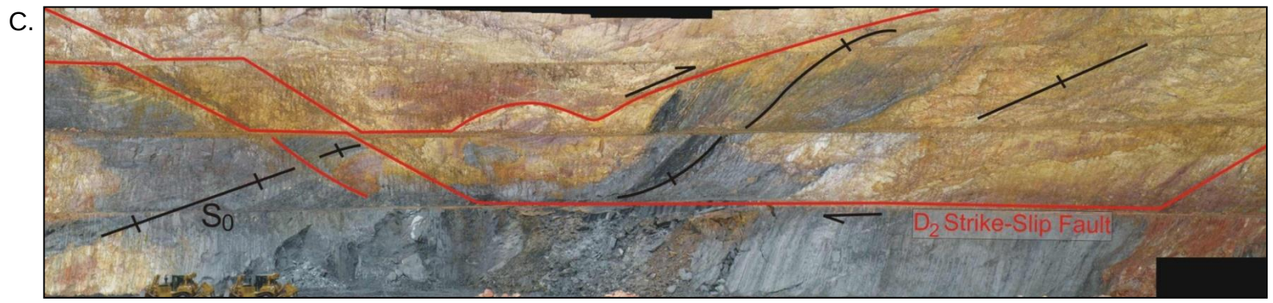

Figure 5.21: **A.** Structural formline map of Sintroko. Stereographic projections show the plunge direction and plunge of the synform underlying the western domain of the pit and the orientation of the steeply dipping bedding located in the central domain of the pit (poles to bedding are plotted). The map shows the steeply plunging, tight F_2 fold-pair underlying the eastern and western domains, with steep NNE-trending bedding in the central domain. The map also indicates the location of the sigmoidally folded bedding, between the NNW-trending strike-slip faults. See text for further details (Chapter 5.2.9). **B**. Cross-section through the southern parts of Sintroko, from west to east, along the line A-B (Fig. 5.21.A). The cross-section shows the subvertical- to vertical bedding of the rocks in the Sintroko pit. The central- and western domains are underlain by a series of oppositely dipping reverse faults. The reverse faults converge in the vicinity of the central graphitic schist layer. The pit is also truncated by a series of D_2 NNW-trending strike-slip faults. **C.** Photo panel of the eastern wall of the Sintroko pit. The photo depicts a series of north-south trending D_2 strike-slip faults (red lines). Bedding between the faults describes a sigmoidal S-shaped pattern and the drag along the faults suggests a component of dextral slip. The strike-slip faults are planar and the undulating fault traces on the photo are a result of the intersection of the faults with the pit topography. The darker lithotype forms part of the central graphite-schist.

A.

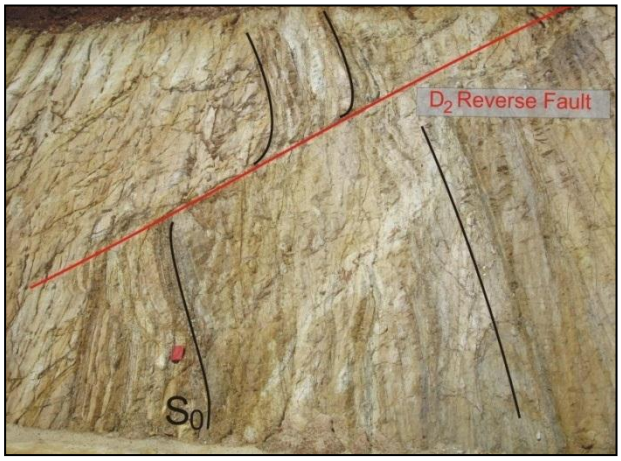

D.

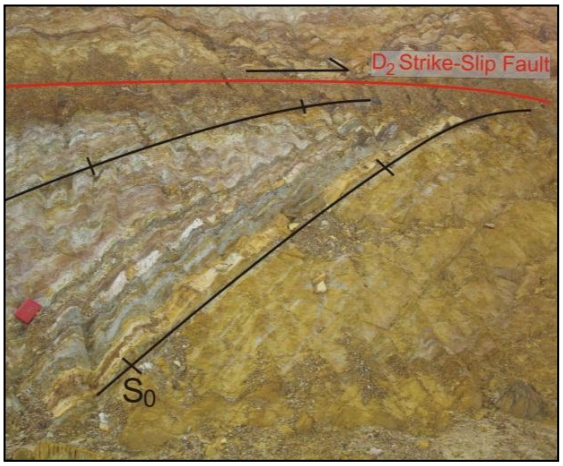

B.

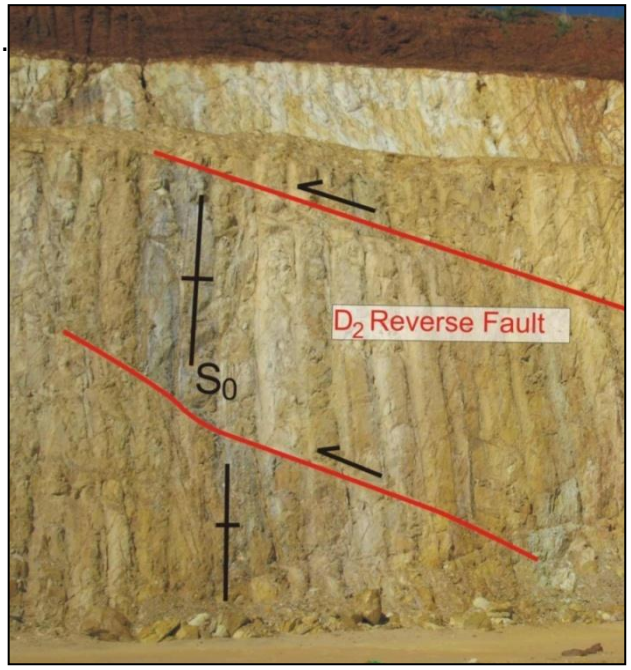

C.

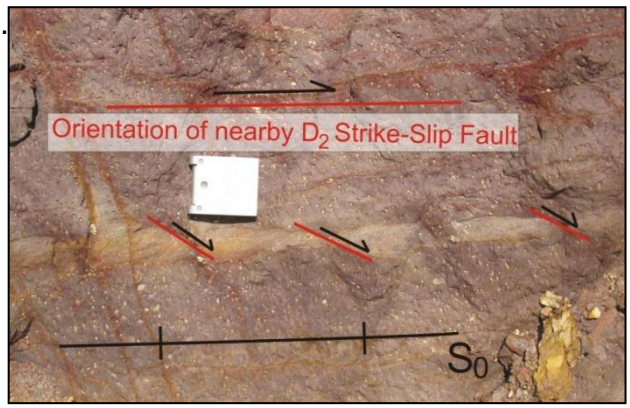

Figure 5.22: **A.** Field photograph (looking south) of an east-dipping reverse fault offsetting the steep dipping bedding by ca. 7 m. The bedding is dragged into the fault plane. The reverse fault forms part of a set of NNE-trending reverse faults in the central- and eastern domains. **B.** Photo showing closely-spaced reverse faults in the southern parts of the western domain, looking southwest. The faults dip to the west and record a top-to-the-east sense of displacement. **C.** Photograph (plan view) taken close to a north-south trending, bedding-parallel D_2 strike-slip fault in the eastern domain of Sintroko, showing small-scale subsidiary (R1 Riedel) shears displacing a thin greywacke layer (light) within a thick pelite layer (red).The offset of the greywacke bed along NNE-trending Riedel-shears suggest a dextral offset for the main strike-slip fault. North is to the left hand side of the photo. **D.** Field photograph of the drag of subvertical bedding into a subvertical, north-trending D_2 strike-slip fault (southern part of the eastern domain, oblique view, looking east). The sense of rotation of bedding into the fault suggests a dextral component of shear.

5.2.10 Eureka North

The structural geology of the Eureka North pit (the northernmost open pit of the Siguiri Mining Complex) deviates from the north-south trending geology of the other open pits. Rocks rather show north-westerly trends and shallow dips. Recent exploration carried out by AngloGold Ashanti geologists during the field mapping indicate that northwesterly trends seem to dominate these northern extents of the Siguiri Mining Complex, possibly marking a more regional swing in the trends of rocks and structures. However, information on this remained too sporadic and these results await further confirmation and tighter field constraints.

The structure of Eureka North is largely determined by the two moderately (40° to 60°) SW-dipping, NW-trending D_3 normal faults that divide the pit into a southwestern, central and northeastern domain (Fig. 5.23.A). The normal sense of displacement is inferred from the rotation of wall-rock strata into the fault planes (Figs. 5.24.B and C). The southwestern fault, with an orientation of ca. 220/55°, outcrops in the northwestern part of the pit. Here it is identified by the brecciation of wall rocks along the fault plane, and the abrupt change of bedding orientations as bedding is rotated into the fault plane (Fig. 5.24.B) The northeastern fault (ca. 230/40°) is well exposed in the central-eastern part of the pit, where it truncates the wall of the pit (Fig. 5.24.C). Here, the fault plane is intruded by thin (< 20 cm wide) mafic dykes.

In the southwestern domain, bedding along the western fault plane trends subparallel to the fault with moderate (30° to 40°) dips to the southwest. Towards the west and southwest, away from the faults, bedding shows slightly shallower dips and dip directions to the south, progressively rotating to more southeasterly dips further to the west. In the northwestern corner of Eureka North, bedding shows shallow (20° to 35°) southwesterly dips near the fault planes, which possibly indicates the drag of bedding into the fault plane. The central domain of Eureka North outcrops in the northwestern corner of the pit sandwiched between the two faults. Here, bedding assumes shallow (ca. 20°) northwestern dips away from the fault traces, with NW-trending bedding closer to the fault planes (Fig. 5.23.B).

The northwestern extent of the north-eastern domain of Eureka North is underlain by very shallow to shallow (2° to 35°) SW-dipping strata which trends

A.

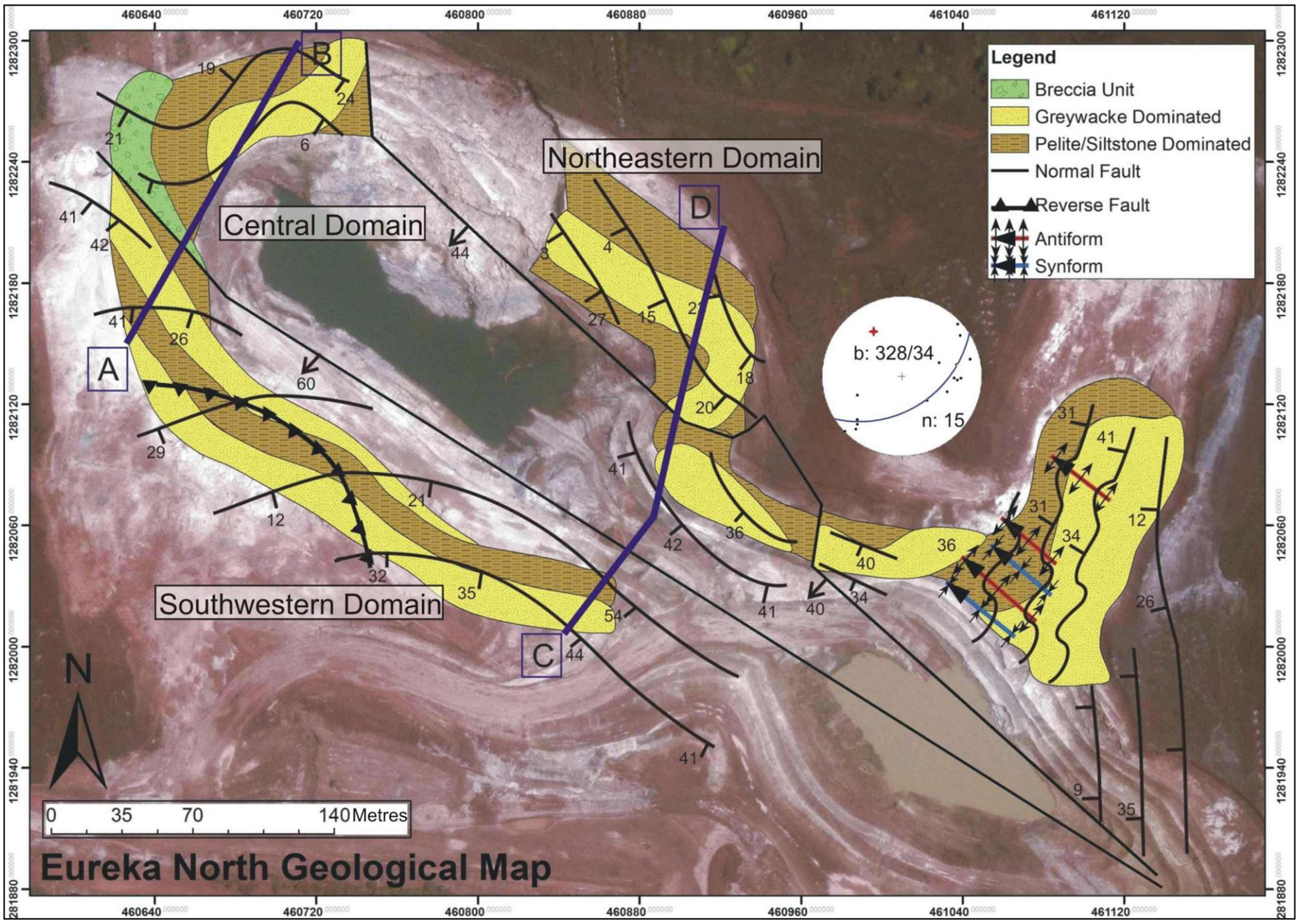

B.

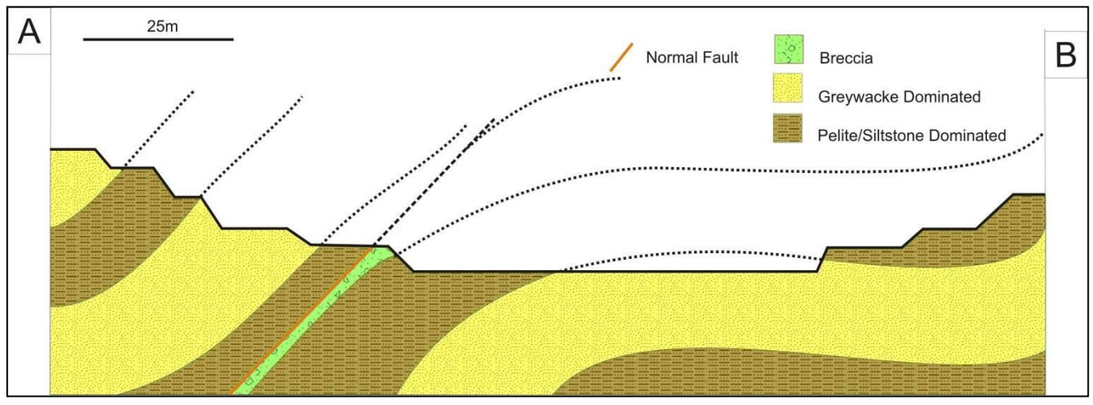

C.

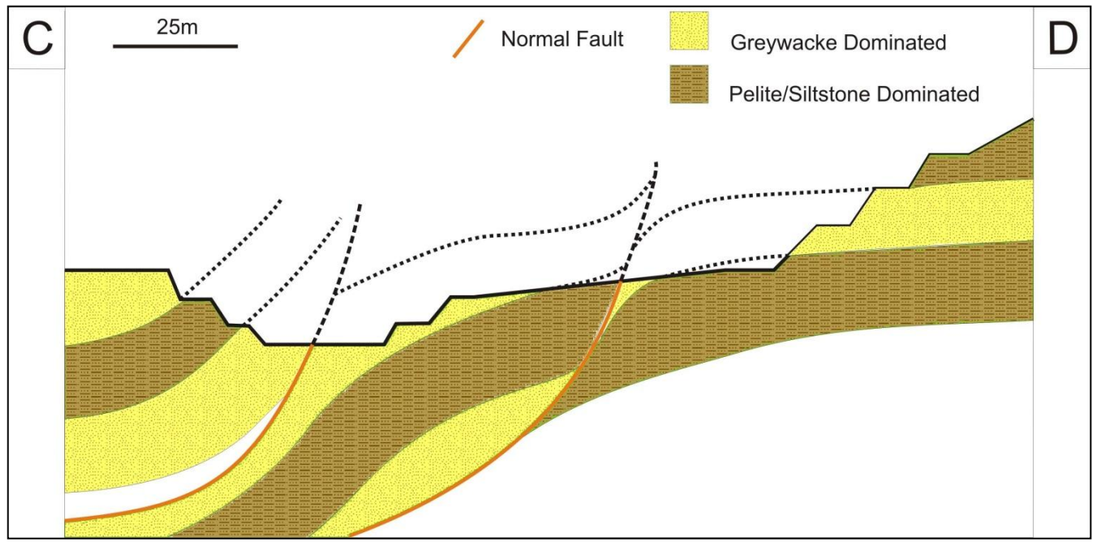

Figure 5.23: **A.** Structural formline map of Eureka North. The lithologies consist of greywacke- and pelite/siltstone-dominated packages, together with intraformational breccias. The stereographic projections show plunge direction and plunge of the small-scale folds in the vicinity of the cutback, in the eastern part of Eureka North. **B**. Cross-section along the northwestern wall of Eureka North, from southwest to northeast, along line A-B indicated in figure 5.23.A. The cross-section shows the western NW-SE trending normal fault, with the breccia unit observed along the fault plane. Bedding describes a southwest facing monoclinal warp between the western- and eastern normal faults, with bedding only becoming steeper close to the fault traces. **C.** Cross-section through the south-central parts of the pit, from southwest to the northeast, along line C-D, included in figure 5.23.A. The cross-section shows the two NW-SE trending normal faults that truncate bedding in Eureka North. A monoclinal structure is suggested to be developed between the two faults. The bedding assumes shallower dips away from the faults.

A.

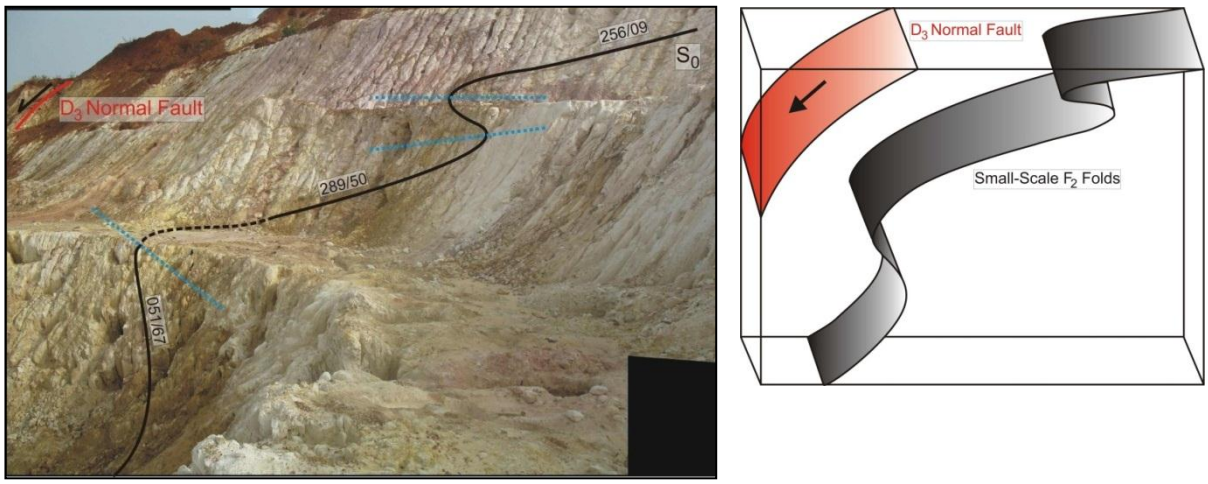

B.

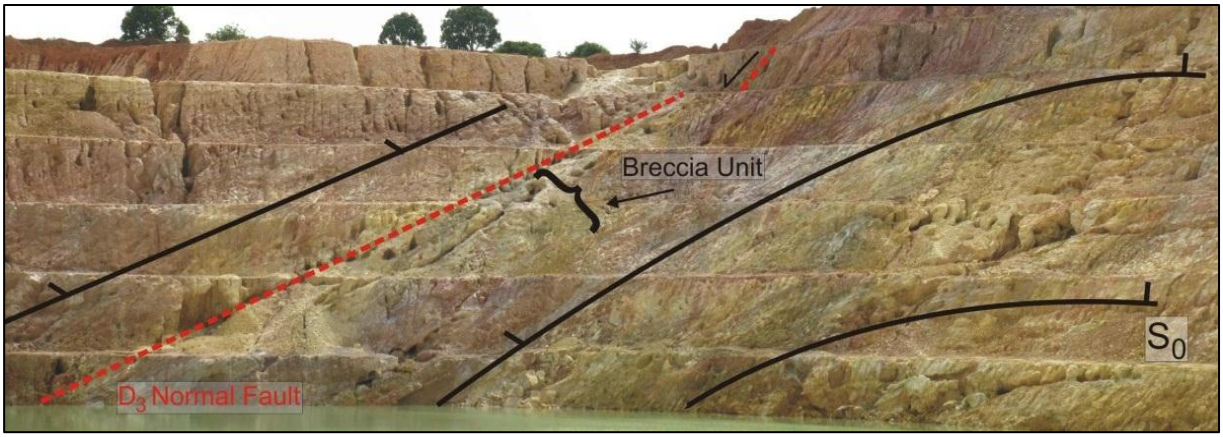

C.

Figure 5.24: **A.** Field photograph and schematic sketch of a series of small-scale folds developed in close proximity to the normal fault to the southwest, i.e. the hanging wall of the folds (eastern domain of Eureka North, in the vicinity of the cutback, looking northwest).The northeastern fold is overturned and tightly folded. The folds to the southwest become more open, with the axial planes (blue dashed lines) assuming more upright positions (see sketch). These folds plunge subparallel to the nearby normal fault at moderate angles. Pit benches have a height of 6 m. **B.** Cross-sectional view, facing northwest, of the southwestern normal fault. Close to the normal fault, bedding trends subparallel to the fault. Away from the fault planes, bedding traces assumes northeasterly trends to the north and westerly trends to the south. The breccia unit found in the pit is located in the hanging wall along the fault plane. **C.** Oblique view of the northeastern domain, looking southeast. Bedding is dragged into parallelism with the fault plane. To the northeast of the fault, bedding dips shallow- to moderately to the west-southwest, whereas bedding to the southwest of the fault dips subparallel to the normal fault.

subparallel to the adjacent normal fault but undulates somewhat along strike. The southeastern extent of the northeastern domain shows shallowly (10 to 35°) dipping, north-south trending strata. A series of smaller-scale folds (F_2) is located in the areas surrounding the major normal faults. These folds have an average fold plunge of 320/40°. Two fold pairs are well exposed in a prominent embayment in the north-eastern domain of the pit (Fig. 5.24.A). The wavelengths of these folds range from 10 to 20 m. The northeastern antiform is tight and overturned to the southwest, with a subhorizontal axial plane, whereas the folds to the southwest are more open and upright (Fig. 5.24.A). An open, upright antiformal fold occurs towards the northeast of the embayment, with a wavelength of 20 m and with a similar northwesterly plunge direction compared to the other smaller-scale folds. A secondary foliation observed in the Eureka North, is developed as a transecting foliation (S_{2b}) with respect to the F_2 folds and shows moderate (40 to 50°) dips to the south. This also differs from S_{2b} foliation trends observed in the rest of the Siguiri Mining Complex.

A minor, NW-SE trending reverse fault (D_2) is located in the southwestern domain of the pit, dipping 45° towards the southwest (Fig. 5.23.A).

Chapter 6 Quartz veining in the Siguiri Mining Complex

6.1 Introduction

Quartz veins are ubiquitous in the Siguiri Mining Complex testifying to the structurally-controlled fluid-flow. Moreover, the regionally widespread carbonate alteration spots point to a more pervasive fluid-flow in addition to the fracture-controlled flow.

Based on quartz-vein orientation and cross-cutting relationships with respect to regional structures, a number of different quartz-vein sets can be distinguished, namely: Steep-S-dippers (Fig. 6.1.A); shallowly dipping veins (Fig. 6.1.B); Bedding-parallel veins (Fig. 6.1.C); en-echelon veins (Fig. 6.1.D).

6.1.1 Steep-S-dippers

Geometry, morphology and orientation

The steep-S-dippers are omnipresent in the Siguiri Mining Complex and are considered to be the main auriferous vein set in the mine complex. Veins contain sulphides (pyrite and arsenopyrite), but these are only preserved in fresh samples (Fig. 6.2.A), whereas sulphides in the saprolite zone are completely oxidized to Fe-hydroxides. This may also explain why veins in the saprolite zone are commonly bordered by an up to several centimetre-wide margin of Fe-hydroxides (Fig. 6.2.B). In fresh rock, the quartz veins are not surrounded by any macroscopically visible alteration and the ferruginous halos seem to be related to the saprolitization event and oxidation of primary sulphides rather than the initial veining. It is also important to note that not all Fe-hydroxide rims are related to quartz veining and there are numerous locations where Fe-hydroxide crusts are developed without a quartz vein.

Carbonates, mainly siderite and ankerite, may constitute up to 50 vol.% of the auriferous quartz-carbonate veins, but pure milky quartz veins are more abundant (Fig. 6.2.C). Carbonates typically form a blocky to needle-like phase that has grown at right angles from the margin of the vein towards the centre (Fig. 6.2.D). This is also

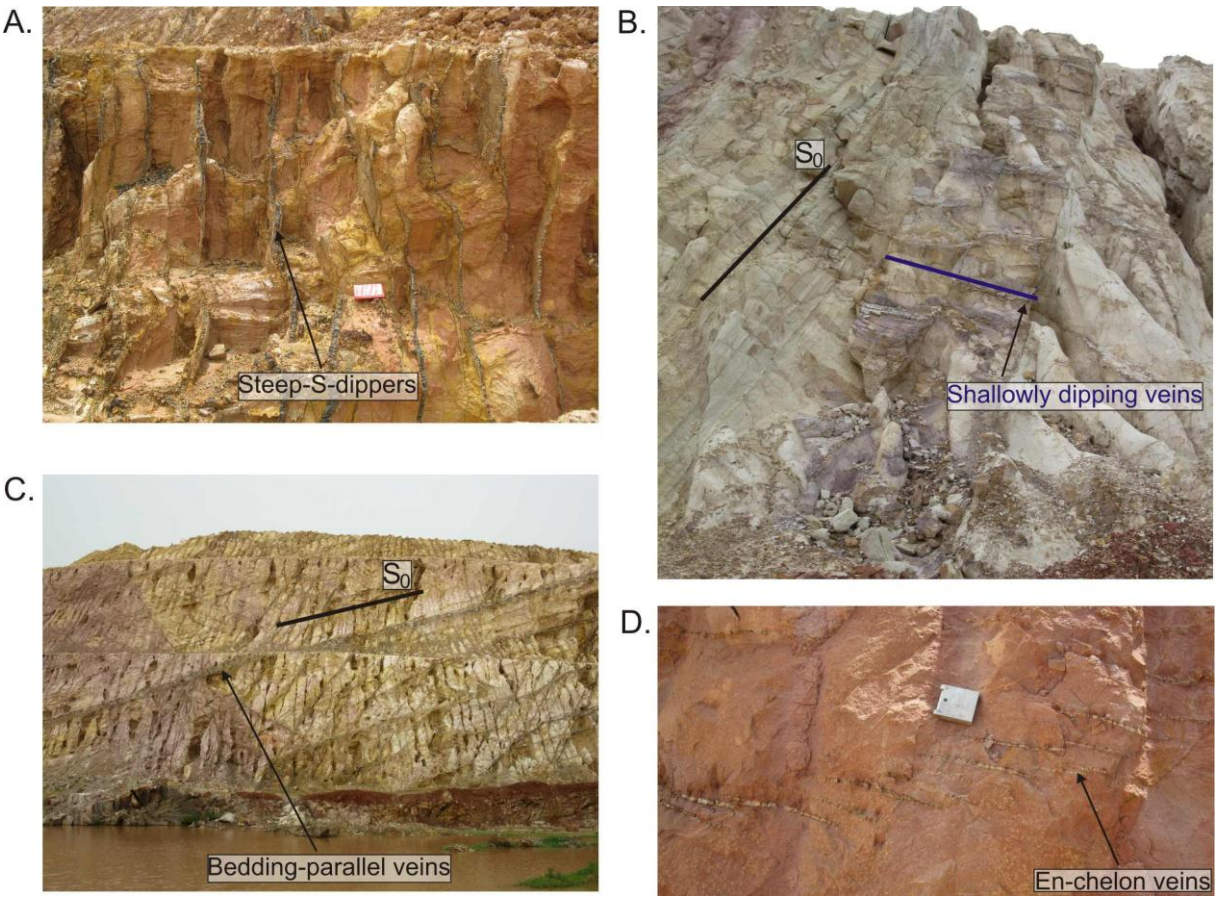

Figure 6.1: **A.** Cross-sectional view of the steep-S-dipper set showing a close spacing in a competent greywacke unit. The photo was taken in the eastern domain of Toubani, looking east-southeast. **B.** Shallowly dipping veins, developed as ladder veins in a greywacke unit. Photo was taken in the steeply dipping eastern domain of Kossise, looking south. Note how veins are sigmoidally folded in some places **C.** Bedding-parallel veins are the thickest veins in the Siguiri Mining Complex, reaching a thickness of commonly 5 to 20 cm (northeastern extent of Kami South, looking west). **D.** En-echelon veins developed in the steep dipping strata in Toubani. The veins record a left-stepping geometry and are developed in a siltstone unit. This set shows very thin and short veins and is relatively rare.

a good indication that veins were formed as mode I fractures and that they are syntaxial veins (e.g. Ramsay and Huber, 1983).

The steep-S-dippers show steep- to subvertical dips (65-90°), with predominantly southerly and southeasterly dip directions. More easterly dip directions are recorded in the northern parts of the Siguiri Mining Complex in the Eureka North pit (Fig. 6.3.A). Vein walls are sharp and the veins incorporate no wall-rock slivers. The veins are commonly between 0.4 and 6 cm wide, although up to 13 cm thick veins were observed, and individual veins can be traced for metres and up to tens of metres

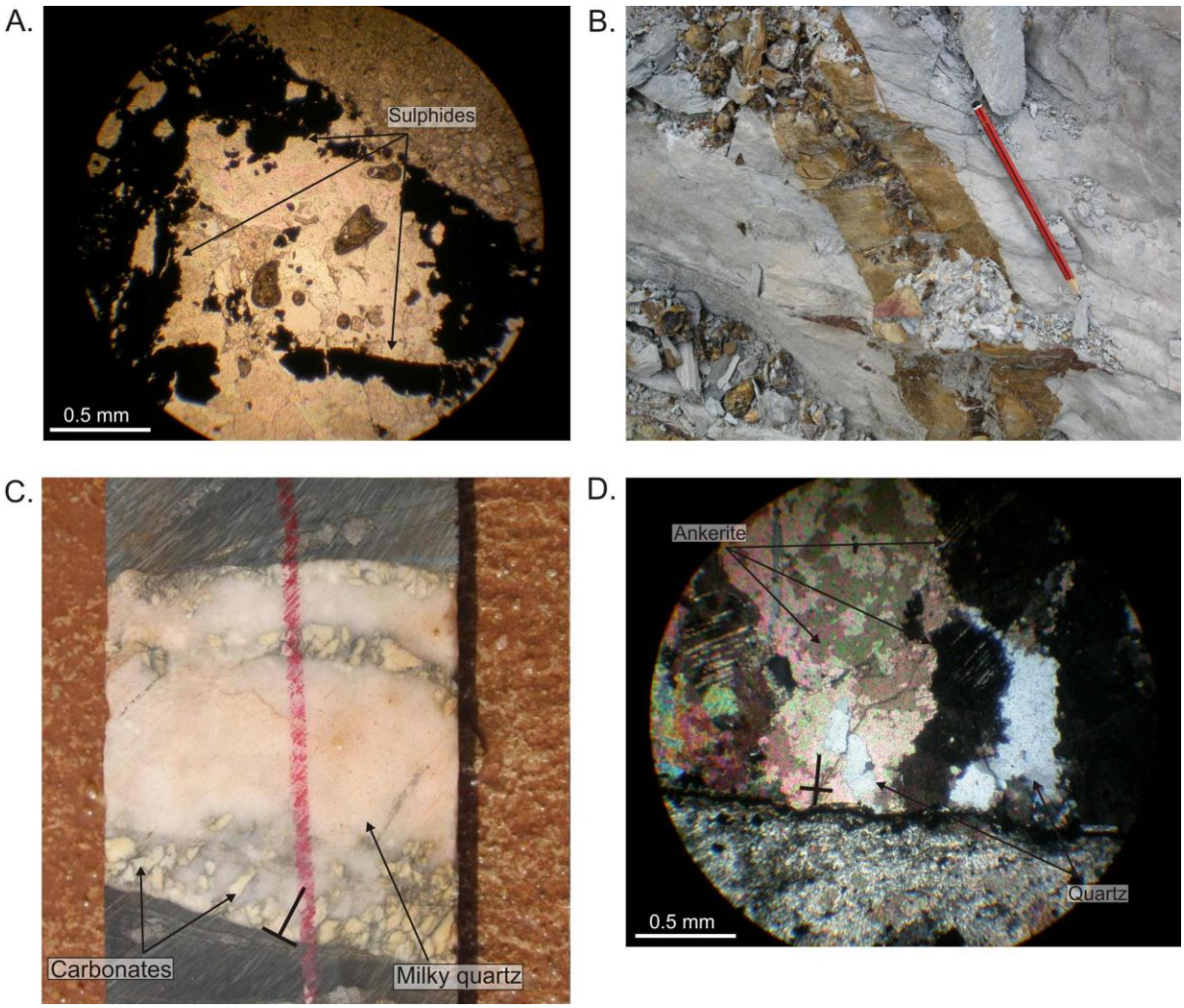

Figure 6.2: **A.** Thin-section photograph of a quartz vein containing abundant amounts of sulphides (plane polarized light). **B.** A quartz vein developed close to the fresh rock-saprolite transition zone. The vein is surrounded by a cm-wide Fe-hydroxide rim. **C.** Quartz-carbonate vein in core sample. Note the growth of carbonate (ankerite) along or close to the vein walls and at high angle to the vein (see 6.2.D) **D.** A thin section photo of a prominent quartz-carbonate vein, truncating a greywacke unit (cross-polarised light). Here, quartz and ankerite also grow perpendicular to the vein wall, suggesting veins developed as mode I extension veins.

along strike. The veins are developed as parallel-sided, planar veins that taper towards their lateral terminations (Fig. 6.3.B). Veining shows a clear lithological control, being most prominent in greywacke units. Shale- and silt-dominated units may, in contrast, show thinner and fewer veins (Fig. 6.3.C). Where veins cross-cut a lithological sequence, the veins are commonly refracted at bedding planes, between beds of differing competence (Fig. 6.3.D). Lithological controls also influence the spacing of the steep-S-dippers. Veins show a spacing of between 0.5 to 3 m and tend to be closer in greywacke units, with rare stockworks located in some sites, in the Kami Complex (Fig. 6.4.A). There are numerous localities where the

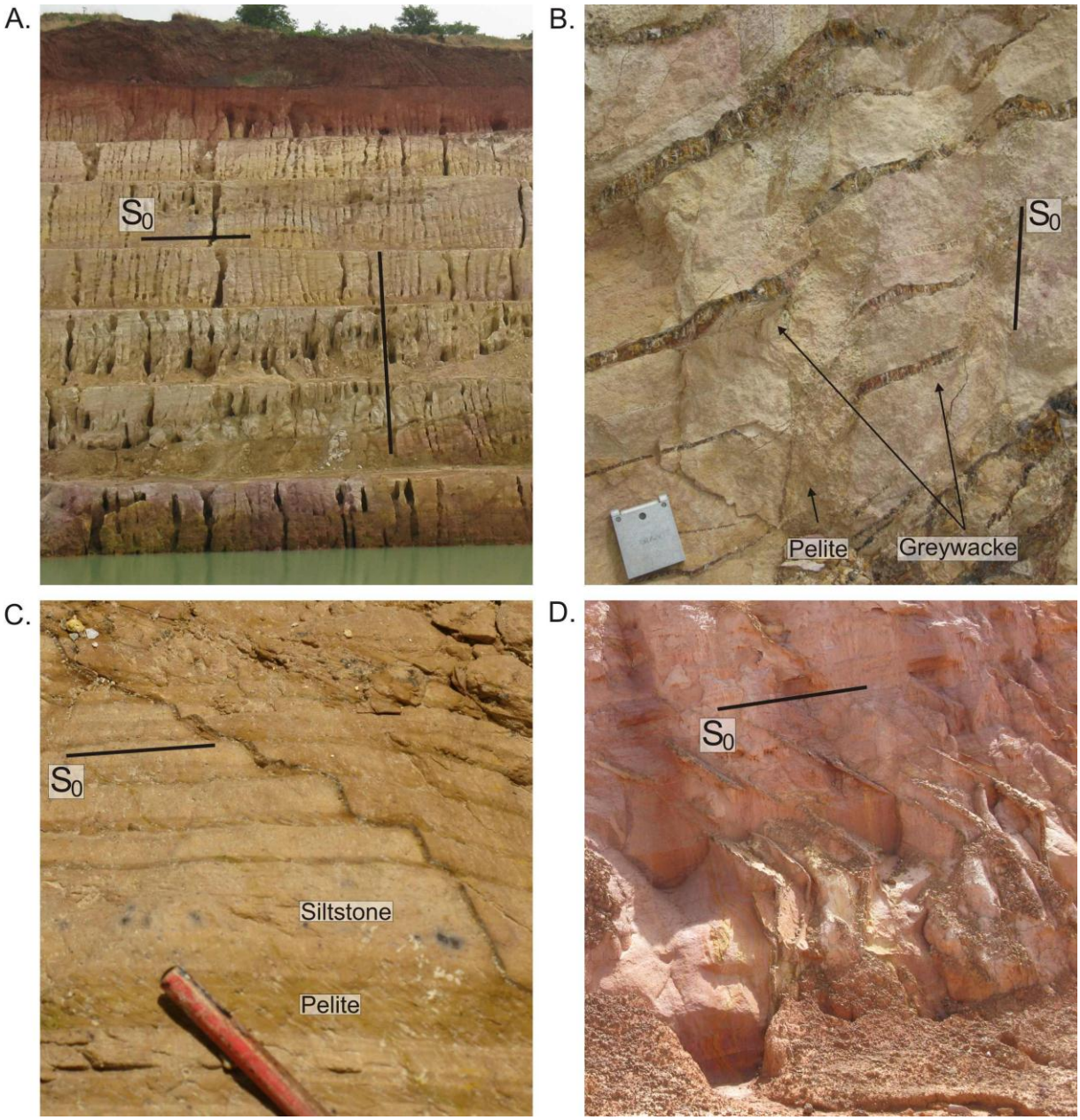

Figure 6.3: **A.** Cross-sectional view of a set of steep-S-dippers developed along the northern wall of Eureka North. The photo was taken looking southeast. The vein set represents the set preferably mined by the local miners. Veins are more abundant in the shallowly dipping greywacke-dominated unit, in the lower parts of the pit wall, compared to the pelite-rich upper parts. **B.** Steep-S-dippers developed in the steep strata in Sintroko. Here, veins are predominantly developed in the greywacke unit. Veins commonly terminate at the boundary between the greywacke and pelitic units, with only a few veins truncating the pelite. Note the tapered ends of the veins**. C.** A thin steep-S-dipper developed in thinner laminated beds of siltstones and pelites. Note the bedding-parallel deflection of the otherwise high-angle vein. **D.** A photo showing the refraction of steep S-dippers, here in Kossise, between units of different competencies. This refraction may also account for the scatter of vein orientations shown by the steep S-dippers.

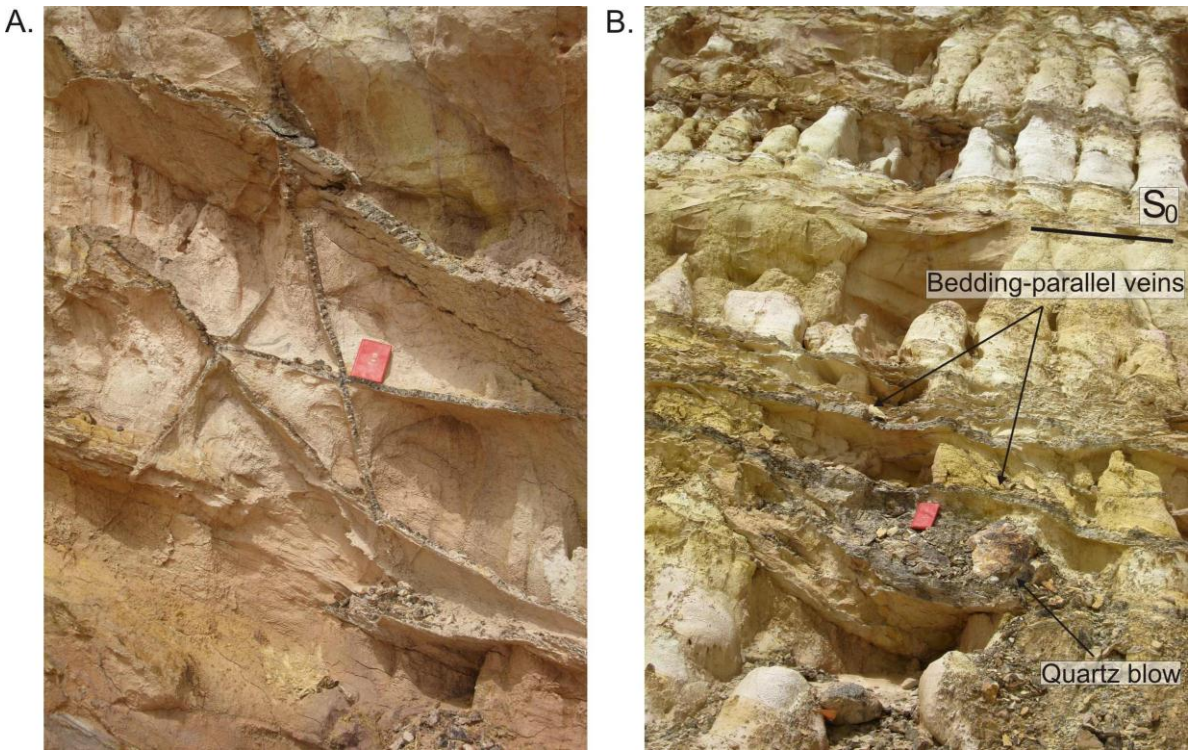

Figure 6.4: **A.** Cross-sectional view of cross-cutting sets of quartz veins in the thicker greywacke unit recorded in the eastern and western walls of Kami North. Here veins develop a wide range of vein orientations, almost stockwork-like. **B.** A quartz blow developed close to where a steep-S-dipper, intersects bedding-parallel veins. The photo was taken in the vicinity of the Kami Old Pit, looking east.

mineralization seems to follow the intersection between the steep-S-dippers and bedding-parallel veins, or, in places, also bedding planes without bedding-parallel veins. This is prominent in the Kami Complex and in Eureka North. Distinct quartz blows form where the steep-S-dippers intersect prominent bedding-parallel veins (Fig. 6.4.B). The development of the blows along these intersections of steep S-dippers with bedding-parallel veins seems to be restricted to shallowly dipping strata. This gives the mineralization a pronounced plunge that is preferentially followed by the local miners. The quartz blows are not encountered in subvertical or vertical strata (see below).

6.1.2 Shallowly dipping veins

Geometry, morphology and orientation

Shallowly dipping veins are common in the Siguiri Mining Complex, particularly in steeply dipping strata (Fig. 6.1.B). They are spatially closely associated with the

steep-S-dippers (see above) with which they appear to form a conjugate set in Kossise and Kami North. Cross-cutting relationships between the two sets (steep and shallow) are inconsistent and point to their largely contemporaneous formation (Figs. 6.5.A and B). The veins are commonly confined to particularly sandy, more competent (greywacke) units where they form short, ladder-type vein arrays in Kossise (Fig. 6.1.B).

The shallowly dipping veins are more prominent in the southern pits of the Siguiri Mining Complex in the Kami complex, Kossise and Sintroko, but shallowly dipping veins are also recorded in Eureka North. The veins are commonly shallow dipping (< 50°), with dip directions varying from south- to east- to north. The width of individual veins rarely exceeds 5 cm. Veins can be closely spaced (0.5-1 m), particularly where

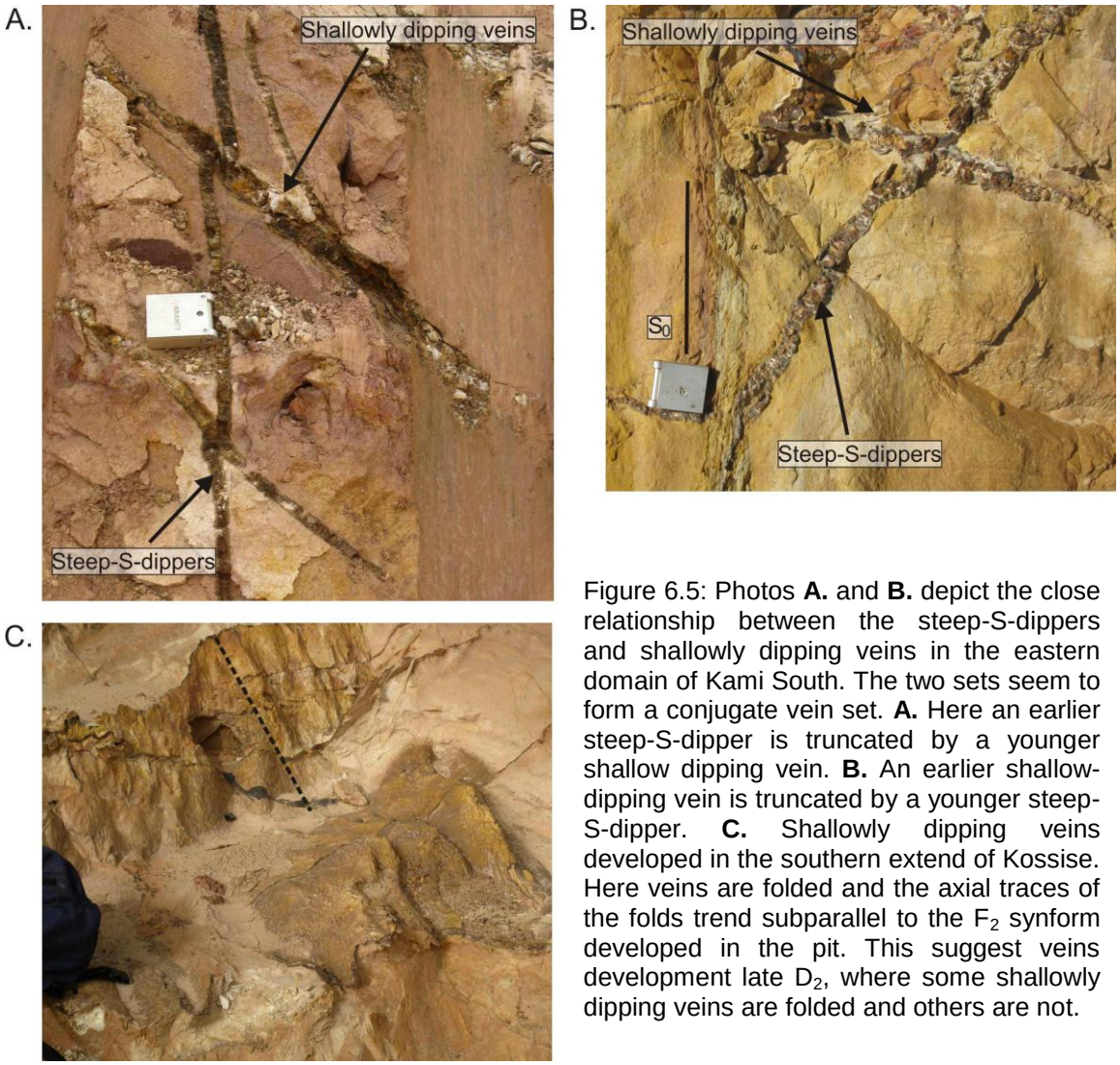

Figure 6.5: Photos **A.** and **B.** depict the close relationship between the steep-S-dippers and shallowly dipping veins in the eastern domain of Kami South. The two sets seem to form a conjugate vein set. **A.** Here an earlier steep-S-dipper is truncated by a younger shallow dipping vein. **B.** An earlier shallow-dipping vein is truncated by a younger steep-S-dipper. **C.** Shallowly dipping veins developed in the southern extend of Kossise. Here veins are folded and the axial traces of the folds trend subparallel to the F_2 synform developed in the pit. This suggest veins development late D_2, where some shallowly dipping veins are folded and others are not.

they occur in more competent greywacke units. Their extent along strike is limited and largely confined to the competent bed in which they occur. In places, shallowly dipping veins are folded into upright, northerly-trending folds with shallow plunges, parallel to F_2 folds (Fig. 6.5.C). Folded veins may occur in the same units and adjacent to undeformed veins suggesting veining during the regional deformation (D_2).

6.1.3 Bedding-parallel veins

Geometry, morphology and orientation

Bedding-parallel quartz veins are not that widespread in the Siguiri Mining Complex, but appear to be particularly abundant in relatively shallowly dipping strata (dips < 20 to 40°) such as in Eureka North and Kami South (Figs. 6.6.A and B). Bedding-parallel quartz veins at Sintroko and Bidini form exceptions to this. Here, bedding-parallel veins are contained within the subvertical bedding of the wall-rock strata. These veins show steep south-southeasterly dips and are regarded as steep-S-dippers.

Bedding-parallel veins show large strike- and down-dip extents, which can reach several tens of metres. They also include the thickest quartz veins mapped in the mining complex, with veins in the northern parts of Kami South, in the vicinity of Kami

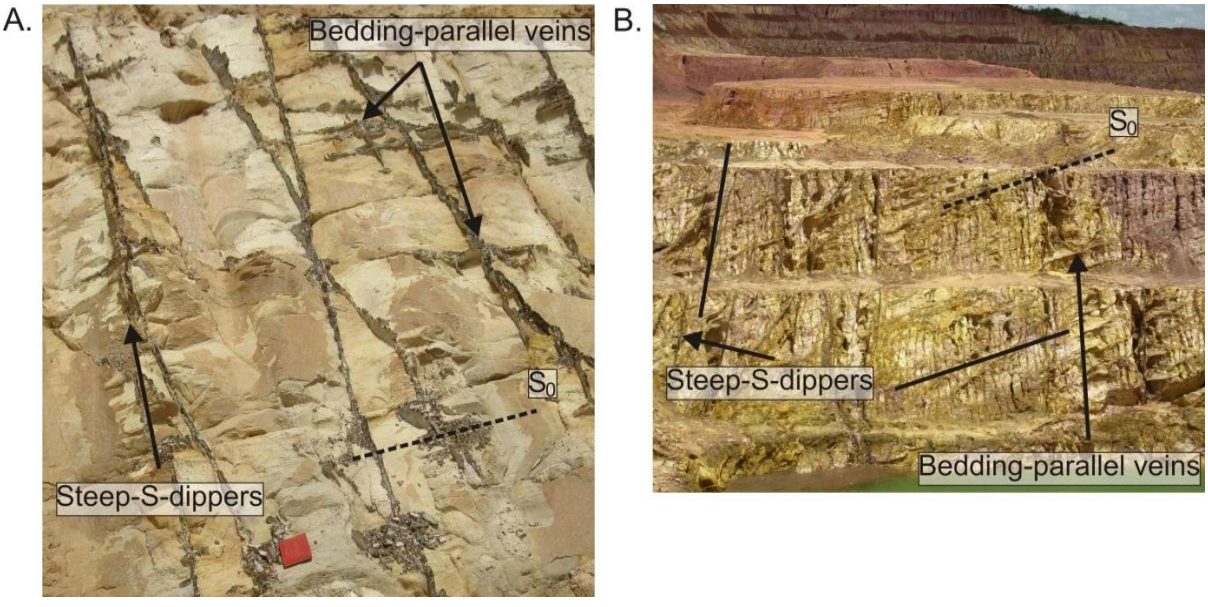

Figure 6.6: **A.** Bedding-parallel veins developed along bedding planes and closely associated with the steep-S-dippers. Photo was taken along the southern wall of Eureka North. **B.** Photo taken in Kami-South. Here, bedding-parallel veins occur in shallowly dipping strata. They also cross-cut the steep-S-dippers and develop intense veining complexes.

Old Pit, frequently attaining widths of > 20 cm and up to 40 cm (Fig. 6.1.C). Individual veins show irregular shapes with variations in vein thickness. Dips of these veins rarely exceed 40°, except for veins at Sintroko and Bidini, where the quartz veins are subvertical.

Judging from the mining activities of the local miners, bedding-parallel veins are, in places, mineralized. Mineralization is particularly well developed at intersections with steep-S-dippers (see above).

6.1.4 En-echelon veins

Geometry, morphology and orientation

En-echelon veins are common in the Siguiri Mining Complex. These veins are well developed in subvertical bedding in Sintroko, Kossise and Toubani, but are also found in bedding with shallower dips at Kami South. The veins tend to be thin and rarely thicker than 4 cm. En-echelon veins form sets of closely spaced, straight, overlapping veins and seldom show sigmoidally folded veins (Fig. 6.7.A). Strike extents are confined to individual lithological beds and rarely exceed 1-2 m and veins commonly only measure 0.5 m in strike extent (Fig. 6.7.B). Due to the confined extent of these veins, terminations of veins are commonly observed, with adjacent veins overlapping by as much as 75% of the total length of the veins.

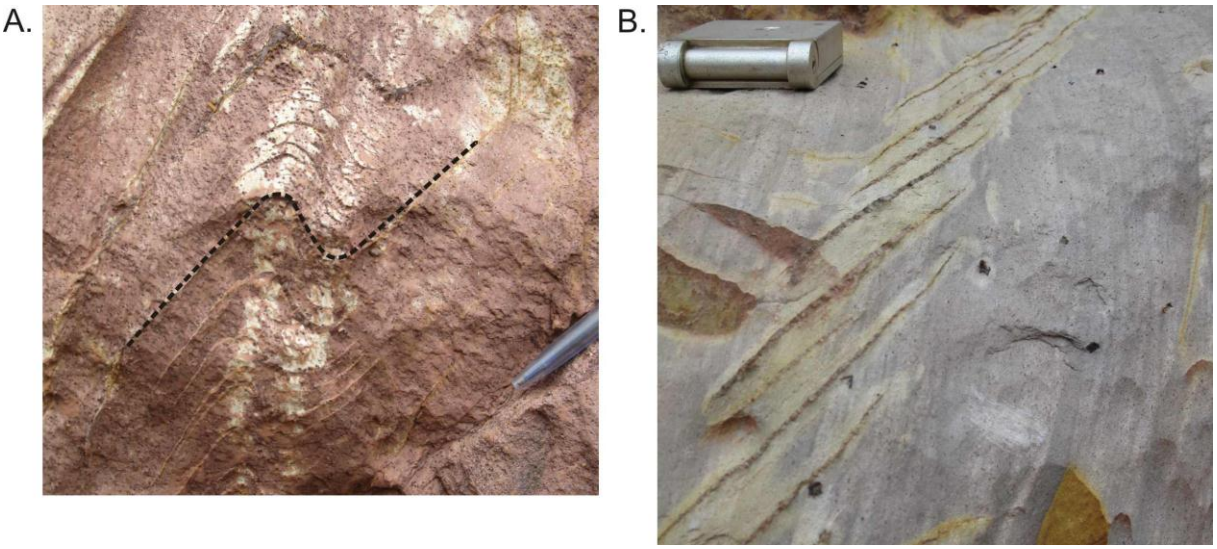

Figure 6.7**: A.** Cross-sectional view of a sigmoidally folded en-echelon vein set. The photo was taken along the limb of the easternmost fold in Kozan, looking south. This folded vein set is indicative of the flexural-slip component along the limbs of the folds during progressive fold amplification**. B**. Left-stepping en-echelon vein set developed in the steep strata in the eastern extent of the Kozan pit, in a greywacke unit.

6.2 Quartz vein sets in the open pits of the Siguiri Mining Complex

6.2.1 Sanu Tinti

Quartz-vein orientations for Sanu Tinti are shown in figure 6.8.A-C. In the western domain of Sanu Tinti (Fig. 6.8.A), two sets of quartz veins were identified, namely: a steep (80°) NNW-dipping set; and a moderate (60°) SE-dipping set. The steep NNW-dipping set, trends at an angle to the steep zone in the central domain of the pit. The moderately dipping vein set trends subparallel to the steep zone and the axial trace of the prominent fold developed in the eastern domain, as well as the axial traces of the small-scale folds in the northern extent of the pit. The eastern domain (Fig. 6.8.B) shows a wide scatter of quartz-vein orientations. Here, veins show steep- to moderate dips (55-90°), with dip directions toward the south, northwest and north-northeast to east-northeast. The understanding of quartz-vein orientations in Sanu Tinti was hampered by the high degree of weathering of the pit. Due to this no definitive sets of veins could be clearly identified in Sanu Tinti. However, veins clearly show a higher abundance in the more competent greywacke-dominated units in the eastern domain of Sanu Tinti (Fig. 6.8).

6.2.2 Bidini

In Bidini, the steep-S-dippers (red set, Fig. 6.9) are the predominant vein set (Figs. 6.9.A-D). Vein orientations are very consistent in the central and eastern domains (Figs. 6.9.B-D), with steep (70 to 90°) dips and dip directions towards the NNW to NW and SSE to SE. The veins are developed at ca. 45° to the approximately north-south trending steep belts that constitute the eastern and western walls of Bidini. The steep-S-dippers show orientations subnormal to the axial planes of the steeply plunging fold in the western domain and the moderately plunging fold pair in the eastern domain (ac-orientation). In the western domain (Figs. 6.9.A and D), the orientation of the steep-S-dippers shows a larger degree of scatter. Veins show steep (70 to 90°) dips, but trends may vary by as much as 45° from northeast to easterly trends. Here, veins are mainly bedding-parallel veins along the steep E-W to NE-trending bedding in the southern extent of the western domain.

Again, veins show higher concentrations in the greywacke-dominated units and in particular, in the steep strata (Fig. 6.9). However, in the shallow dipping strata in the

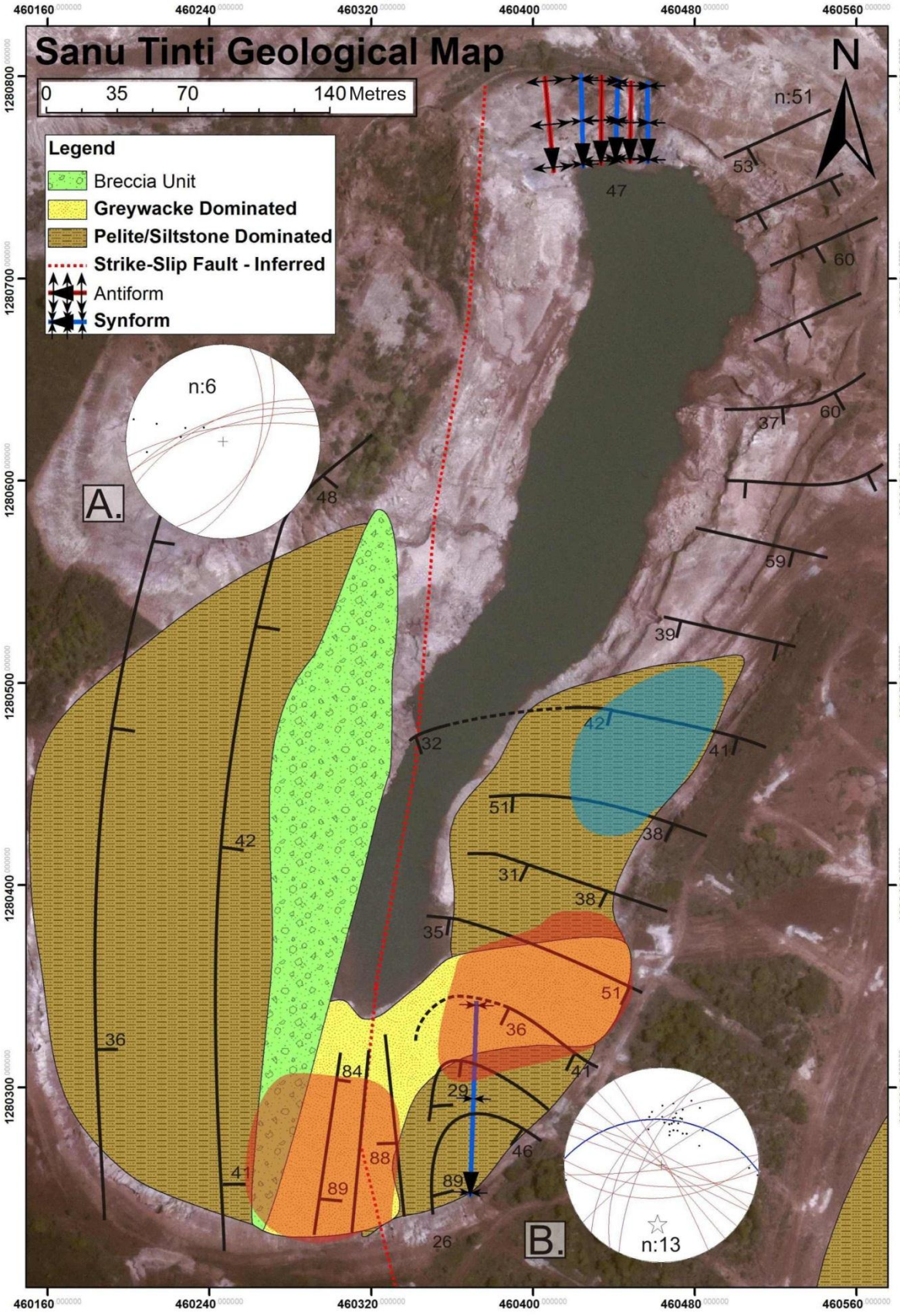

Figure 6.8: Geological map of Sanu Tinti. Red areas indicate a high density of veins, whereas blue areas indicate a lower than average abundance of veining. The stereographic projections indicate 1) poles to bedding orientations – black dots; 2) π-girdle to poles of bedding - thick blue line ; 2) quartz vein orientations: all veins– red great circles.

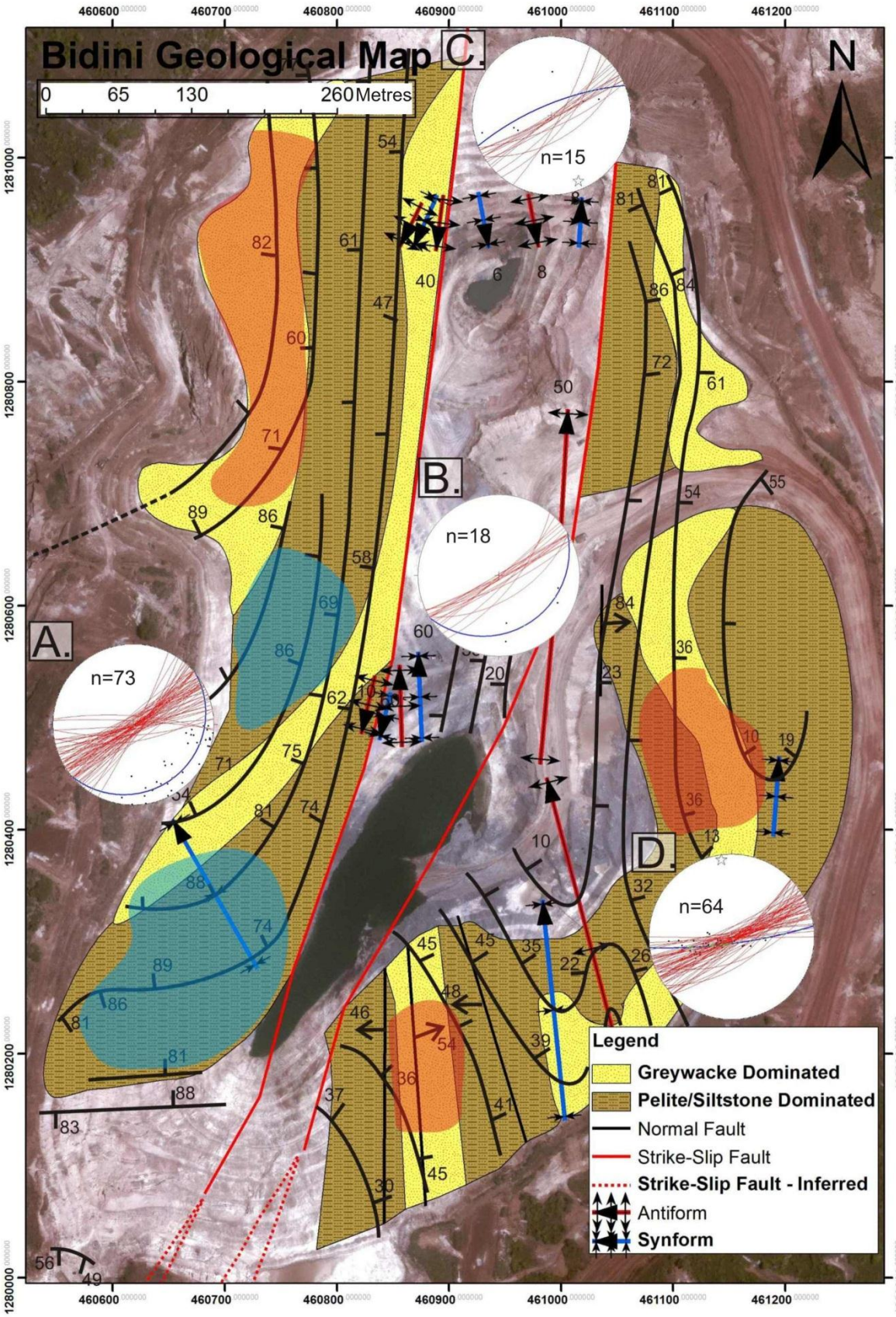

Figure 6.9: Geological map of Bidini. Red areas indicate a higher than average density of quartz veins; blue areas indicate a low abundance of veining. The stereographic projections indicate 1) poles to bedding orientations – black dots; 2) π-girdle to poles of bedding planes - thick blue line; 3) quartz vein orientations: steep-south dippers – red great circles.

central parts of the eastern domain (vicinity of dome structure), veins are abundant in the greywacke units, as well as in the pelitic and siltstone units.

6.2.3 Toubani

Quartz-vein orientations in the three structural domains of Toubani are shown in figure 6.11. The steep-S-dippers (red set) stay consistent throughout the pit, with steep (70-90°) dips and strike of veins showing northeast- to east- to southeasterly trends (Figs. 6.11.A-C). Trends of the steep S-dippers are east-southeast- to northeast, in the subvertical southwestern domain where the veins commonly occur as evenly spaced, subvertical veins, largely confined to individual competent beds (Figs. 6.10 and 6.11.A). The central-northern domain (Fig. 6.11.B) shows similar orientations of the steep-S-dippers. Here, the veins trend east-southeast- to northeast, subparallel to the dominant vein orientations in the steep southwestern domain of Toubani, as well as to the dominant vein orientations found in Bidini to the north-northeast (Fig. 6.9). A steep (70°-85°), N- to NNE-trending vein set (black set), is situated in the gently folded eastern domain of Toubani (Fig. 6.11.C). This vein set is developed with approximately an ac-orientation with respect to the moderately east-plunging fold observed in the eastern domain of Toubani. Here, the steep-S-dippers are subparallel to the steep-S-dippers in Bidini.

Abundant quartz veins are commonly situated in greywacke- dominated units of the steep, north-south trending southwestern domain, shown in figure 6.11. This again emphasizes the important control of competent units on vein spacing in the steep,

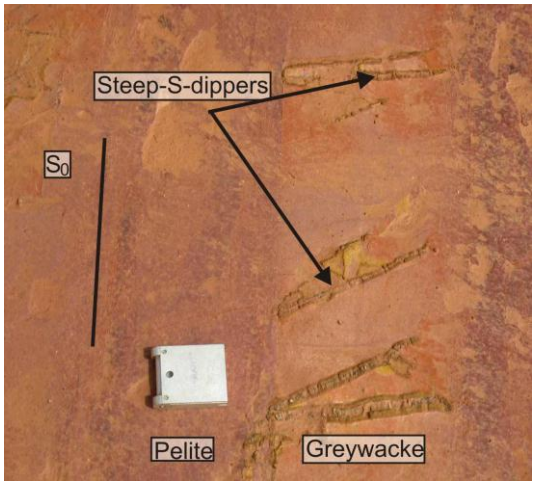

Figure 6.10: Photo of steep-S-dippers in Toubani. Here veins develop as subvertical planar veins in a subvertical, north-south trending greywacke unit. Notice how veins terminate against the pelitic unit.

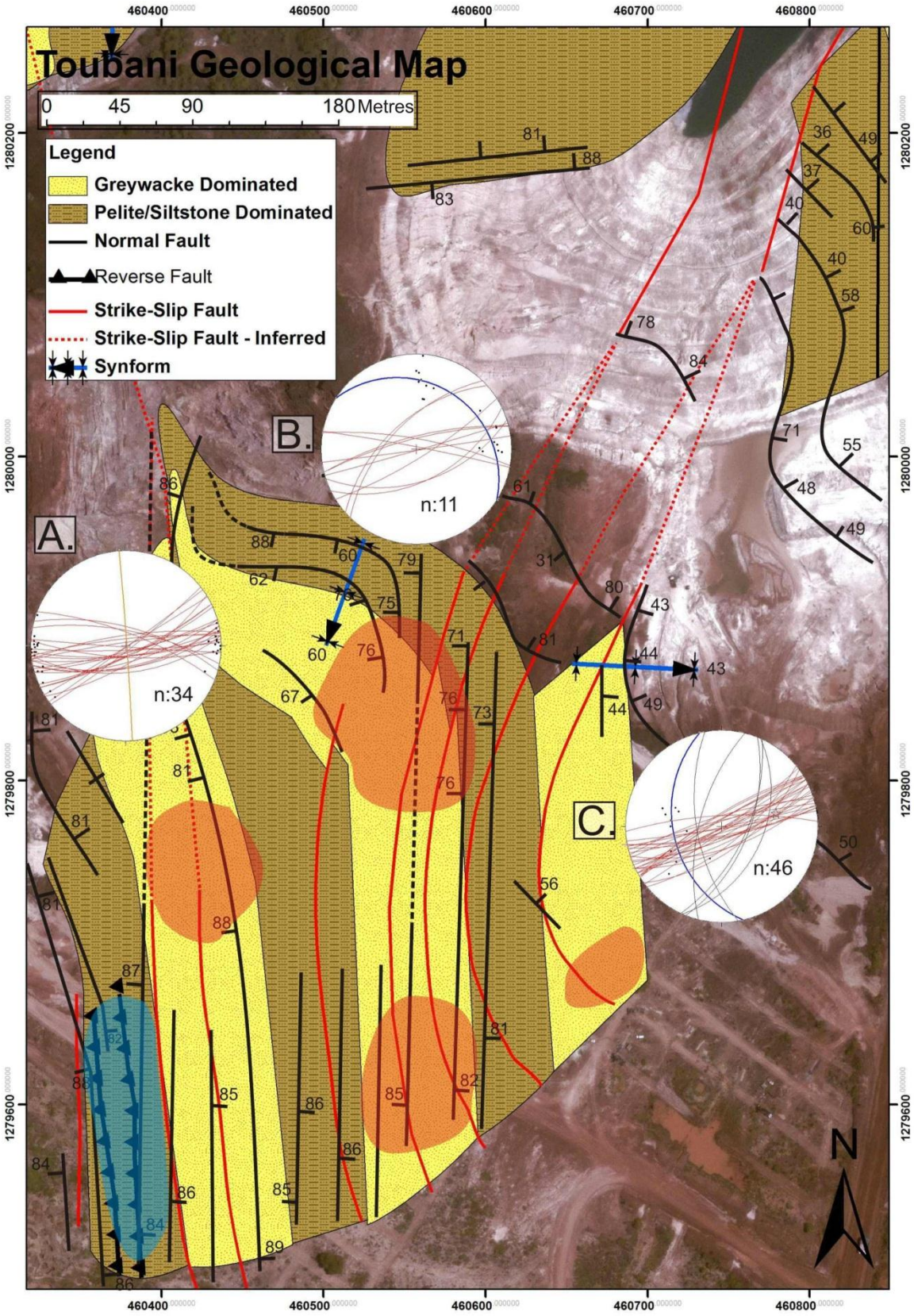

Figure 6.11. Geological map of Toubani. Red areas indicate a high abundance of veining and blue areas indicate a low abundance of veining. The stereographic projections indicate 1) poles to bedding orientations – black dots; 2) π-girdle to poles of bedding planes – thick blue line; 3) average bedding orientation – orange line; 4) quartz vein orientations: steep-south-dippers – red great circles; shallower veins – black great circles.

north-south trending zones of the Siguiri Mining Complex. Vein abundances also increase to the northeast, close to where bedding is sigmoidally folded by the structure underlying the Toubani Old Pit (Fig. 6.11).

6.2.4 Kami North

Figure 6.12 shows quartz-vein orientations in the northeastern and western domains of Kami North. Steep-S-dippers (red set) show steep (65-90°) south-southeasterly dip directions throughout Kami North, as well as steep north-northeasterly dip directions in the western domain (Fig. 6.12.A). The steep-S-dippers show an ac-orientation with respect to the antiform underlying the western domain of Kami North. This vein orientation also trends subparallel to the localized ENE-trending axial culmination, underlying most of the Kami North pit, again suggesting a close relationship between regional deformation and quartz veining. The moderately to shallow (10-50°) dipping sets (black sets) have dip directions to the east and west in the western domain (Figs. 6.12.A-B), with only westerly dips in the eastern domain (Fig. 6.12.B). The easterly-dipping, shallow vein set is developed as bedding-parallel veins, and is limited to the shallowly dipping strata recorded in the south-eastern extent of Kami North, in the vicinity of Kami Old Pit. The north-south trending, bedding-parallel veins represent the thickest veins observed in the Siguiri Mining Complex.

Competent, greywacke-dominated units developed higher abundance of quartz veins. This is evident in the thicker competent unit developed in the eastern and western extents of Kami North, which commonly records quartz-vein stockworks and thus high amounts of veining (Fig. 6.12). The main Kami North pit is orientated subparallel to the ENE-trending axial culmination, which underlies most of the pit. In the western domain of the pit, the pit is extended towards the south, along the axial trace of the NNW-trending antiform. Vein abundance decreases away from the antiform and axial culmination (Fig. 6.12).

6.2.5 Kami South

The central domain of Kami South (Fig. 6.13.A) shows steep-S-dippers that dip steeply (80-90°) to the south-southeast (red set in Fig. 6.13). Two other sets are also developed, including a moderate- to steeply (70-90°) west-dipping set (green set) and a moderately shallow (30-45°) SE-dipping set (black set). The eastern domain of Kami South, as seen in figure 6.13.B, shows two types of quartz-vein sets. A shallow

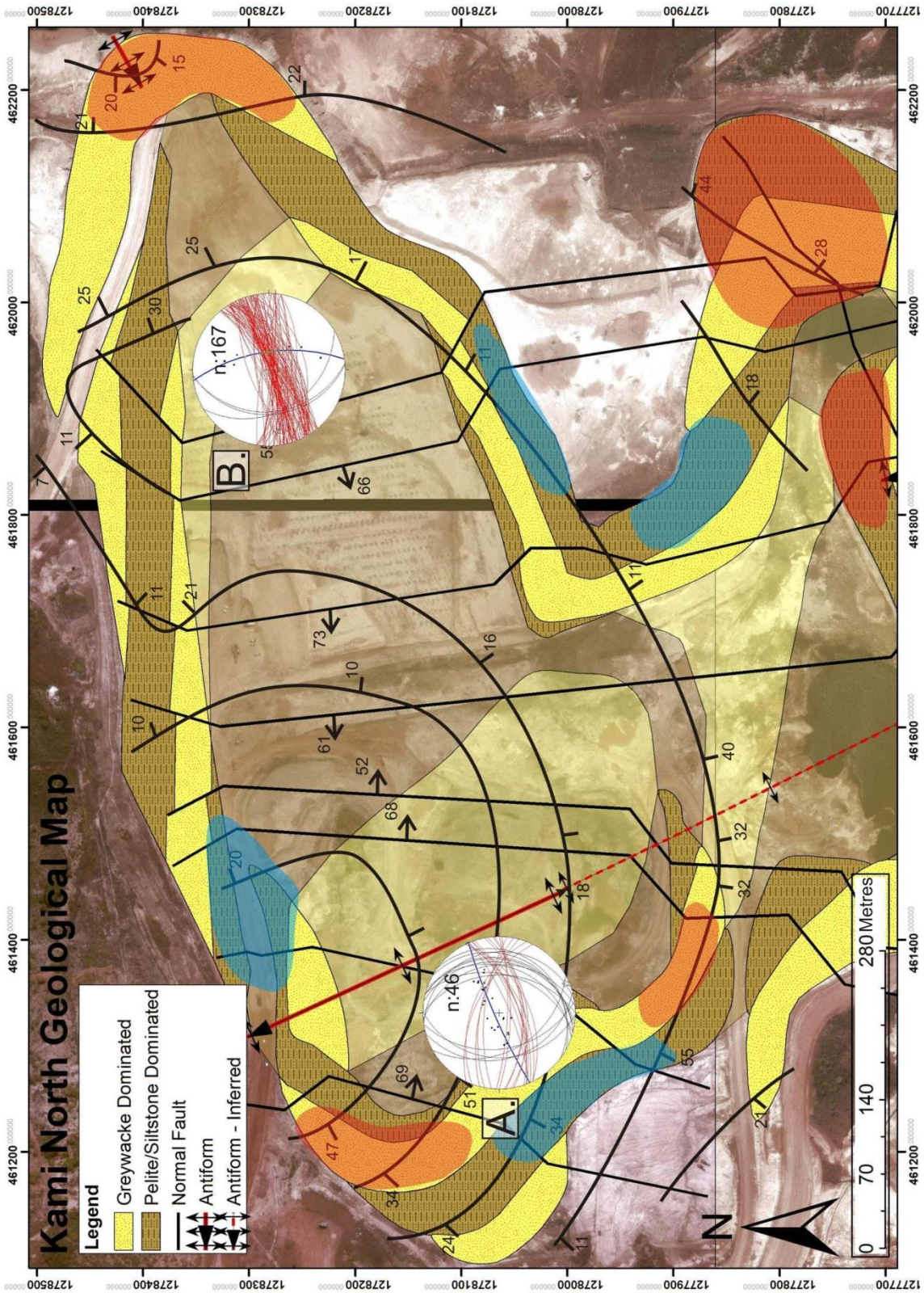

Figure 6.12: Geological map of Kami North. Red areas indicate a high abundance of veining and blue areas indicate a below average abundance of veining. The stereographic projections indicate 1) poles to bedding orientations – black dots; 2) π-girdle to poles of bedding planes – thick blue line 3) quartz vein orientations: steep-S-dippers – red great circles; shallowly dipping veins and bedding-parallel veins – black great circles.

E- to SE-dipping vein set (black set), as well as the regional steep-S-dipping vein set (red set) which dips steeply to the south-southeast to southeast. The steep-S-dippers show a relatively constant orientation throughout the pit, with a slight variation in dip directions for the eastern domain of Kami South (Fig. 6.13.B). The SE-dipping steep-S-dippers of the central- and eastern domains is subnormal to the axial trace of the NNW-trending antiform, which underlies most of the Kami South pit. These trends are also subparallel to the ENE-trending set of D_2 normal faults. The relationship between veins and D_2 normal faults will be developed in Chapter 7. The more SSE-dipping set, which is only recorded along the eastern wall of Kami South, trends subparallel to the orientations of the steep-S-dippers located in Kossise to the southeast (see below; Fig 6.14). The north-south trending, steeply dipping vein set, located in the central domain, record orientations subparallel to the axial plane of the NNW-trending antiform. This indicates a bc-orientation of the vein set, with respect to the antiformal structure in which it is developed. The shallowest dipping veins recorded in the central- and eastern domains are most commonly developed as bedding-parallel veins in the northern extent of each domain, respectively (Fig. 6.1.C). These veins are chiefly developed in the vicinity of the Kami Old Pit. Where these veins are not developed as bedding-parallel veins, the moderately dipping veins form a conjugate set with respect to the steep-S-dippers (Figs. 6.5.A-B).

Vein abundances are higher where they are developed in the thicker greywacke-dominated units along the eastern- and western domains. Less competent lithologies tend to show lower vein development (eastern domain in figure 6.13.). Very low quartz-vein abundances are recorded in the northern extent of the central domain. This is, spatially, closely related to an ENE-trending axial depression in this area. This area also corresponds to particularly well developed, thick, bedding-parallel veins, which may suggest that fluid flow was rather accommodated by bedding-parallel veins compared to the thinner, steep-S-dippers. The bedding-parallel veins are, in places, mineralized, judging from the mining activities of the local miners. The largest part of Kami South is underlain by the NNW-trending antiform, with the exception of Kami Old Pit, which is located in the shallowly dipping eastern limb of the antiform in the north-eastern extent of the pit (Fig. 6.13).

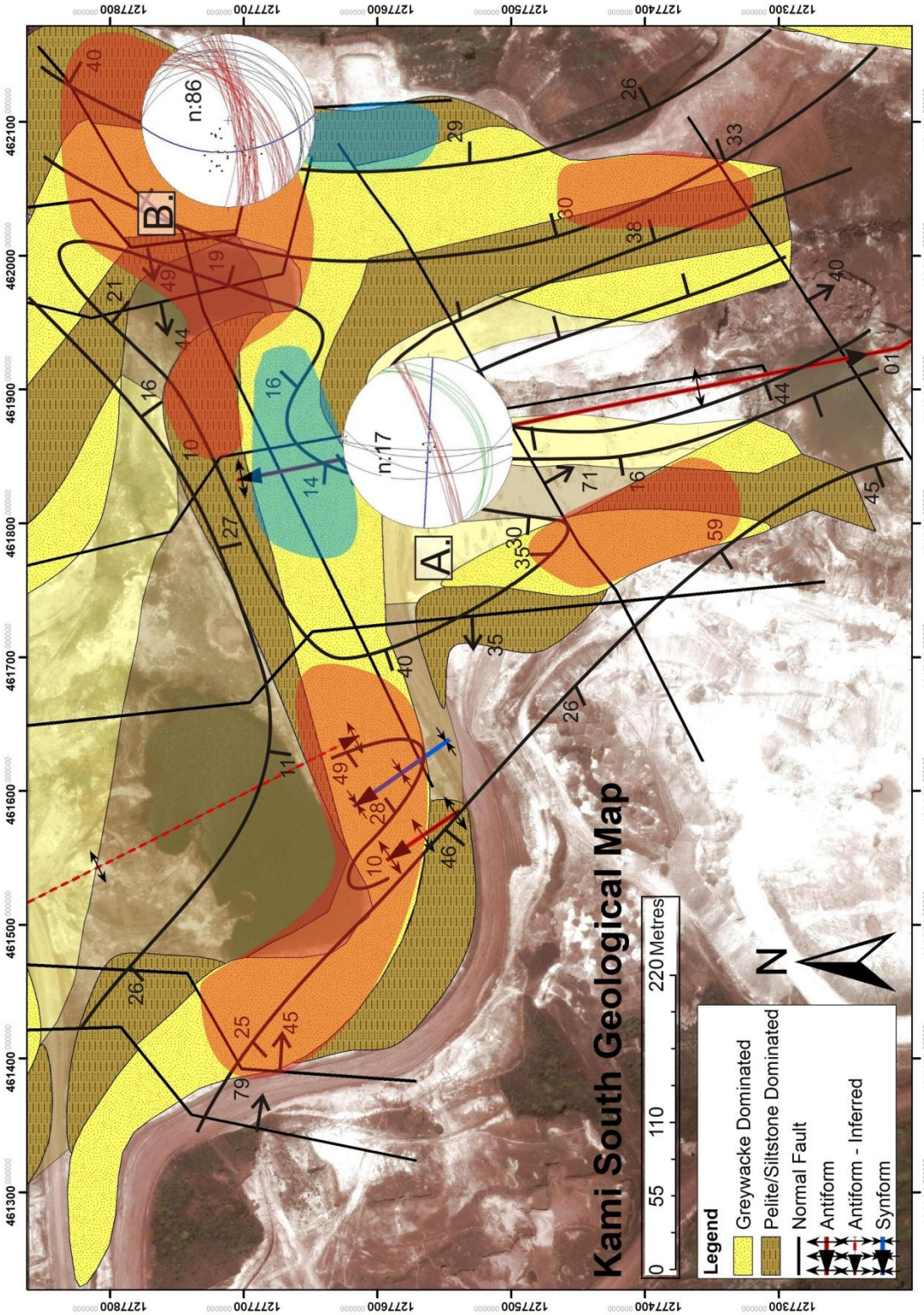

Figure 6.13: Geological map of Kami South. Red areas indicate a high abundance of veining and blue areas indicate a below average abundance of veining. The stereographic projections indicate 1) poles to bedding orientations – black dots; 2) π-girdle to poles of bedding planes – thick blue line 3) quartz vein orientations: steep-south dippers – red great circles; **A.** bc-veins, **B.** Bedding-parallel- and shallowly dipping veins – black great circles; bedding-parallel veins – green great circles.

6.2.6 Kossise

Quartz-vein sets present in Kossise are shown in figure 6.14.A-B. Steep-S-dippers (red set in Fig. 6.14.A-B) are prominent throughout the pit, with dips commonly varying between 70 and 90° and south to south-southeast dip directions. Notably, the more southerly-dipping, steep-S-dippers are developed subnormal to the fold axis of the Kossise synform (ac-orientation), whereas the SE-dipping steep-S-dippers record orientations developed at ca. 45° to the north-south trending steep belt in the eastern extent of the pit. The steeply dipping strata in the eastern parts of the pit (Fig. 6.14.B) includes two more vein sets, which are absent from the western part of the pit. This includes a moderately (50-60°) northwest (black set in Fig. 6.14.B) and a shallow (10-35°) SE-dipping set (green set in Fig. 6.14.B). The shallowly dipping set is commonly gently folded in Kossise, with plunges of these small-scale folds subparallel to that of the larger synformal F_2 structure which underlies the pit (Fig. 6.5.C). The shallowly dipping veins are predominantly developed as short ladder veins, confined to individual competent units (Fig. 6.1.2). The moderately NW-dipping vein set (Fig. 6.14.B) is developed as a conjugate set, with respect to the steep-S-dippers and, thus, suggests a close relationship between the two. The moderately dipping veins show no buckling along the traces of individual veins.

Veining is more closely spaced in the greywacke-dominated units recorded in Kossise, especially in the thicker competent unit observed in the central- and western domains of the pit (Figs. 6.14. and 4.8 in Chapter 4). Stockwork vein-development is recorded in the thicker greywacke-dominated unit in the southwestern extent of the pit. Siltstone- and pelitic-dominated units record lower degrees of vein development across the pit, with very low amounts of veins where the less competent rocks occur along the hinge of the synformal structure (Fig. 6.14).

6.2.7 Kozan

Only one quartz-vein set is recognized in Kozan, as shown in figure 6.15.A. This vein set forms part of the regional steep-S-dippers (red set in Fig. 6.15.A) with steep- to moderate (45-90°) dips. Along strike, this vein set shows north-northeast to easterly trends. The steep-S-dippers show similar orientations to the set recorded in Kossise (see above, Chapter 6.2.6). This points to vein development subnormal to the

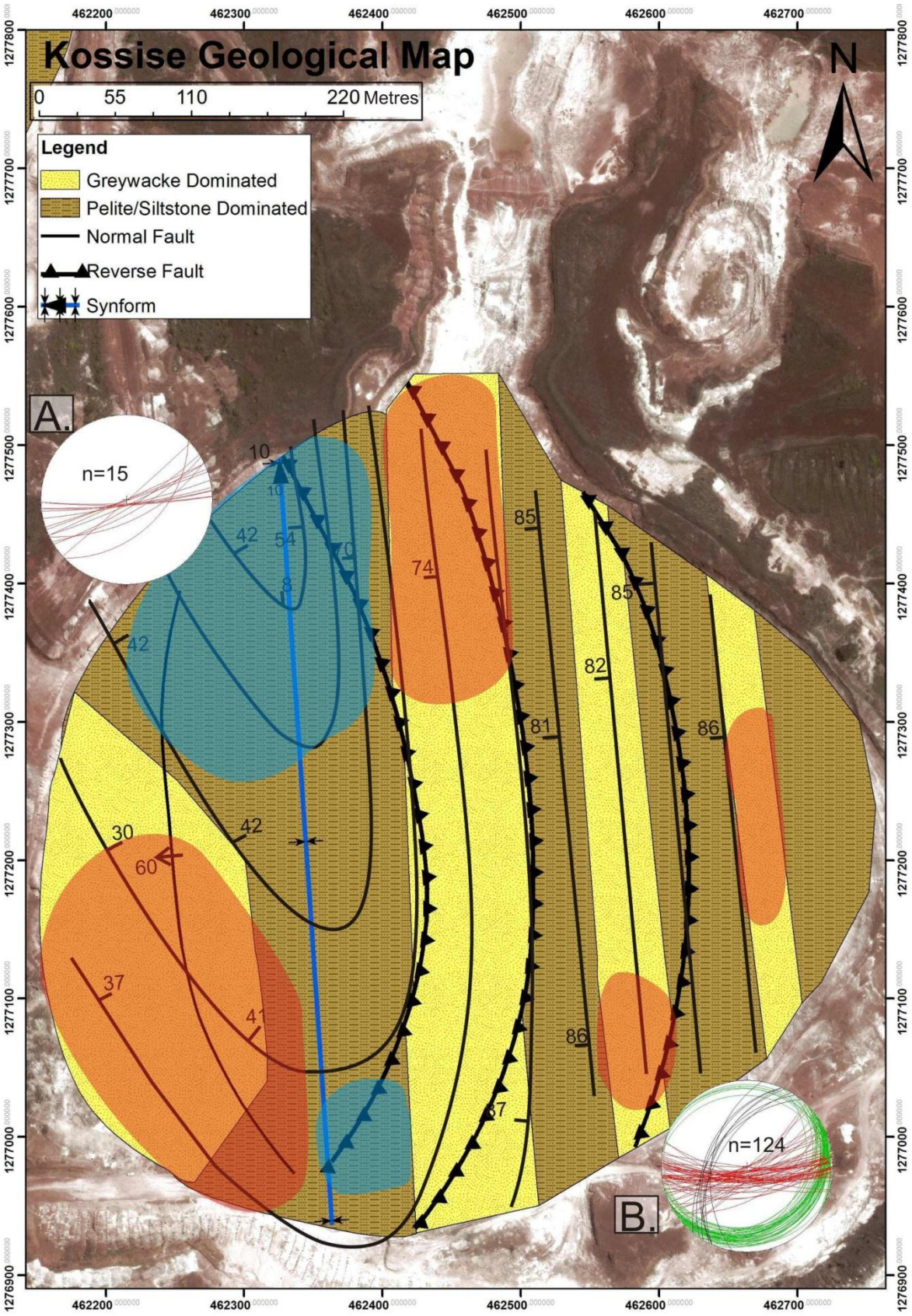

Figure 6.14: Geological map of Kossise. Red areas indicate a high abundance of veining and blue areas indicate a low abundance of veining. The stereographic projections indicate 1) poles to bedding orientations – black dots; 2) π-girdle to poles of bedding planes – thick blue line; 3) quartz vein orientations: steep-S-dippers – red great circles; conjugate set to steep-S-dippers – black great circles; shallowly dipping veins – green great circles.

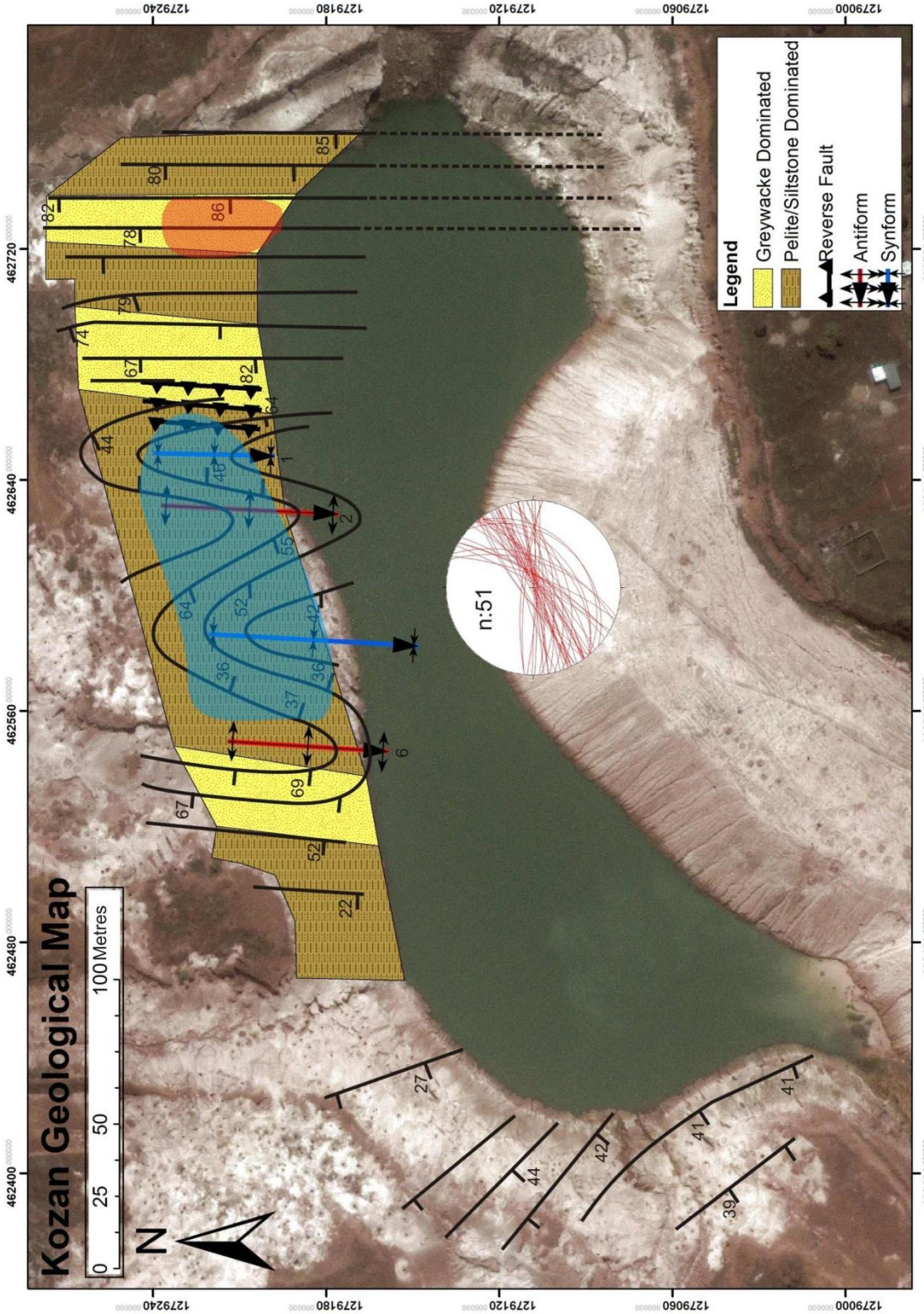

Figure 6.15: Geological map of Kozan. Red areas indicate a high abundance of veining and blue areas indicate a low abundance of veining. The stereographic projections indicate 1) poles to bedding orientations – black dots; 2) π-girdle to poles of bedding planes – thick blue line; 3) quartz vein orientations: steep-S-dippers – red great circles.

north-south trending F_2 folds, for the more south-dipping veins, and at ca. 45° to the north-south trending steep belts, for the more SE-dipping veins.

In Kozan, vein abundances are higher in the more competent greywacke-dominated units, recorded in the eastern domain of the pit, whereas the siltstone- and shale dominated rocks found in the gentler folded central domain show minor vein development (Fig. 6.15). The documentation of quartz-vein abundances in Kozan remains rather patchy due to the deep weathering of the pit.

6.2.8 Sintroko

As shown in figure 6.16, the vein sets present in the pit records subtle changes in vein orientation between different structural domains in Sintroko. Steep-S-dippers (red set in figure 6.16.A-C) remain mostly consistent in orientation throughout the pit. This vein set record steep dips (65-90°), with dip directions varying between southeast to south-southeast. The steep-S-dippers show quartz veins developed at ca. 45° to the bounding steep belts and D_2 faults in the eastern and western extent of Sintroko and also obliquely truncate the steeply plunging F_2 folds in the eastern- and western domains of the pit (Fig. 6.16). The steep-S-dippers developed in the central domain (Fig. 6.16.B) show more northeasterly trends, whereas the same set in the eastern- and western domains rather records more east to east-northeasterly trends (Fig. 6.16.A and C). This suggests a slight anti-clockwise rotation for the veins developed in the central domain, with respect to the eastern- and western domains. A steep subvertical NW to NNW-dipping vein set (black set in figure 6.16.A-C) has approximately the same strike as the steep-S-dippers and shows similar crosscutting relationships with the structures recorded in Sintroko and is suggested to represent a conjugate set with the latter. The shallowly dipping vein set (green set), record dips between 10 and 45°, with dip directions varying from SSW to SSE for the central domain to south-southeastern dips for the eastern and western domains. The shallow vein set is orientated subnormal to the axial traces of the steeply plunging folds, underlying the eastern- and western domain of Sintroko (ac-orientation) (Fig. 6.16). The shallowly dipping veins show a wide scatter in dip directions in the central domain and are spatially closely associated with the reverse faults truncating the central domain of Sintroko (Fig. 6.16.B).

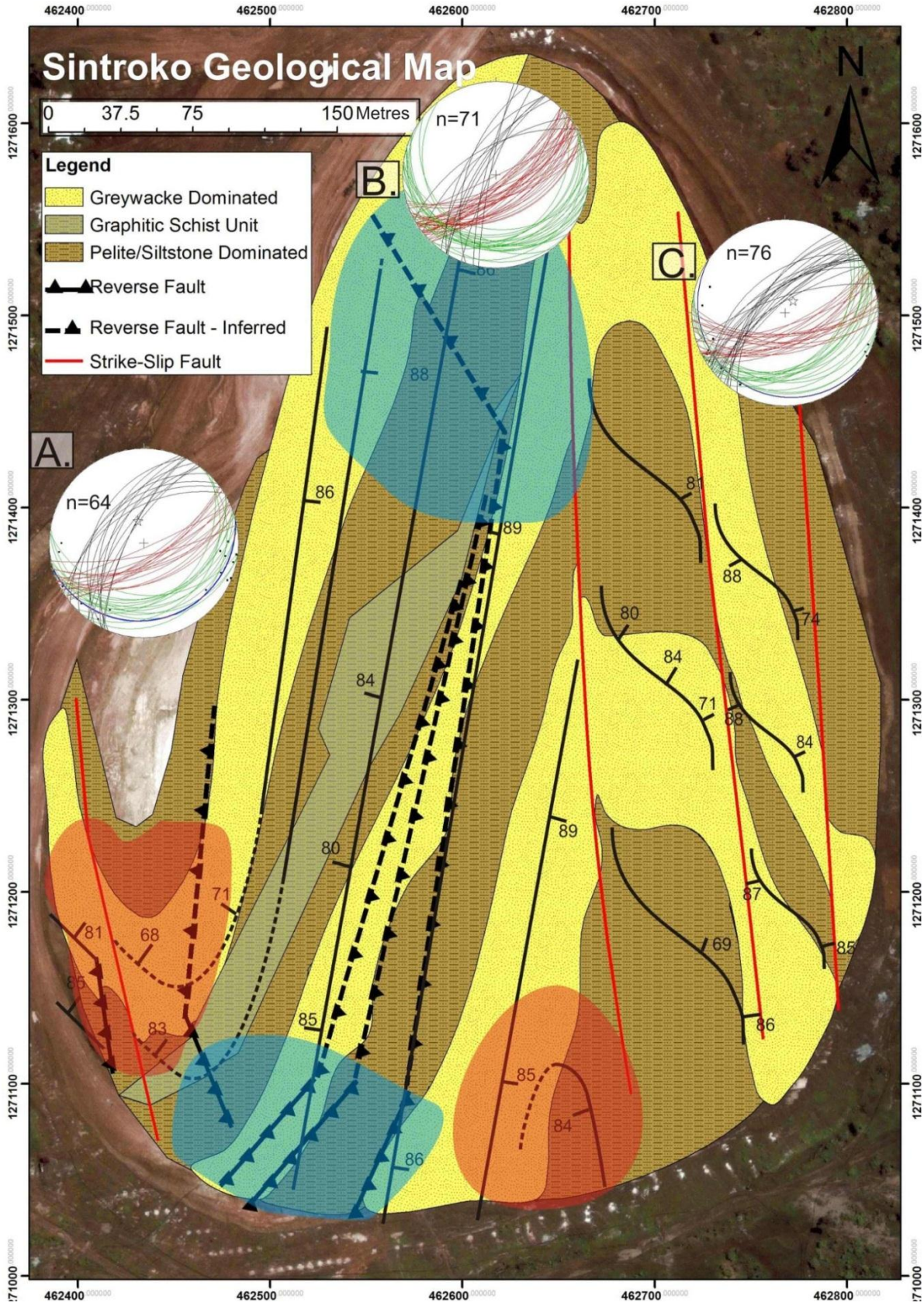

Figure 6.16: Geological map of Sintroko. Red areas indicate a high abundance of veining and blue areas indicate a below average abundance of veining. The stereographic projections indicate 1) poles to bedding orientations – black dots; 2) π-girdles to poles of bedding planes – thick blue line; 3) quartz-vein orientations: steep-S-dippers – red great circles; conjugate set with steep-S-dippers – black great circles; shallowly dipping veins – green great circles.

Quartz veins developed higher abundances in the vicinity of the hinges of the steeply plunging F_2 fold pair, irrespective of the lithologies present in the areas. Lower quartz-vein abundances are recorded in the northern and southern extents of the central domain, where lithological controls seem to have little influence on veining (Fig. 6.16).

6.2.9 Eureka North

Quartz-vein sets in Eureka North are shown in figure 6.17.A-D. In the northwestern corner of the central domain, the steep-S-dippers (red set in Fig. 6.17.A) show steep (80°-90°) dips, trending N-S to NE-SW along strike. In the northeastern domain, the dip of this vein set remains steep, with more northeast-southwest to east-west trends (Fig. 6.17.B). Here, the orientations for the steep-S-dippers vary considerably, and are interpreted to be a result of vein refraction between the shallowly dipping units with different competencies. In the central domain, the more north-south trending orientation of the steep-S-dippers is attributed to a change in the structural grain to the northern extent of the Siguiri Mining Complex. In the southeastern and southwestern domains (Fig. 6.17.C-D), the steep-S-dippers trend northeast-southwest along strike, recording steep dips (65°-90°). In the southeastern extent of the northeastern domain, the vein orientation truncates the small-scale folds developed here at subnormal angles and suggests an ac-orientation of the veins with respect to the folds (Fig. 6.17.D). This also points to a change in the structural trend in the pit, compared to the rest of the Siguiri Mining Complex. A steep- to moderately-steep (40°-80°) vein set (black set) occurs throughout the pit, but most commonly in the southeastern domain (Fig. 6.17.D). This vein set dips west to west-southwest in the southeastern, southwestern and northeastern domains, but changes to east-northeast dips in the northwestern domain. The black set developed subparallel to the axial planes of the small-scale folds in the southeastern extent of the northeastern domain (bc-orientation). This vein set also trends subparallel to the normal faults. In the southwestern domain (Fig. 6.17.C), the shallowly (20°-45°) dipping vein set (green set) is present, with dip directions to the south-southeast. This set developed as bedding-parallel veins.

The central part of the central domain records lower vein abundance, and coincides with areas where mining operations mined to shallower depths, compared to the rest of the pit. Higher degrees of veining coincide with the breccia unit developed in the

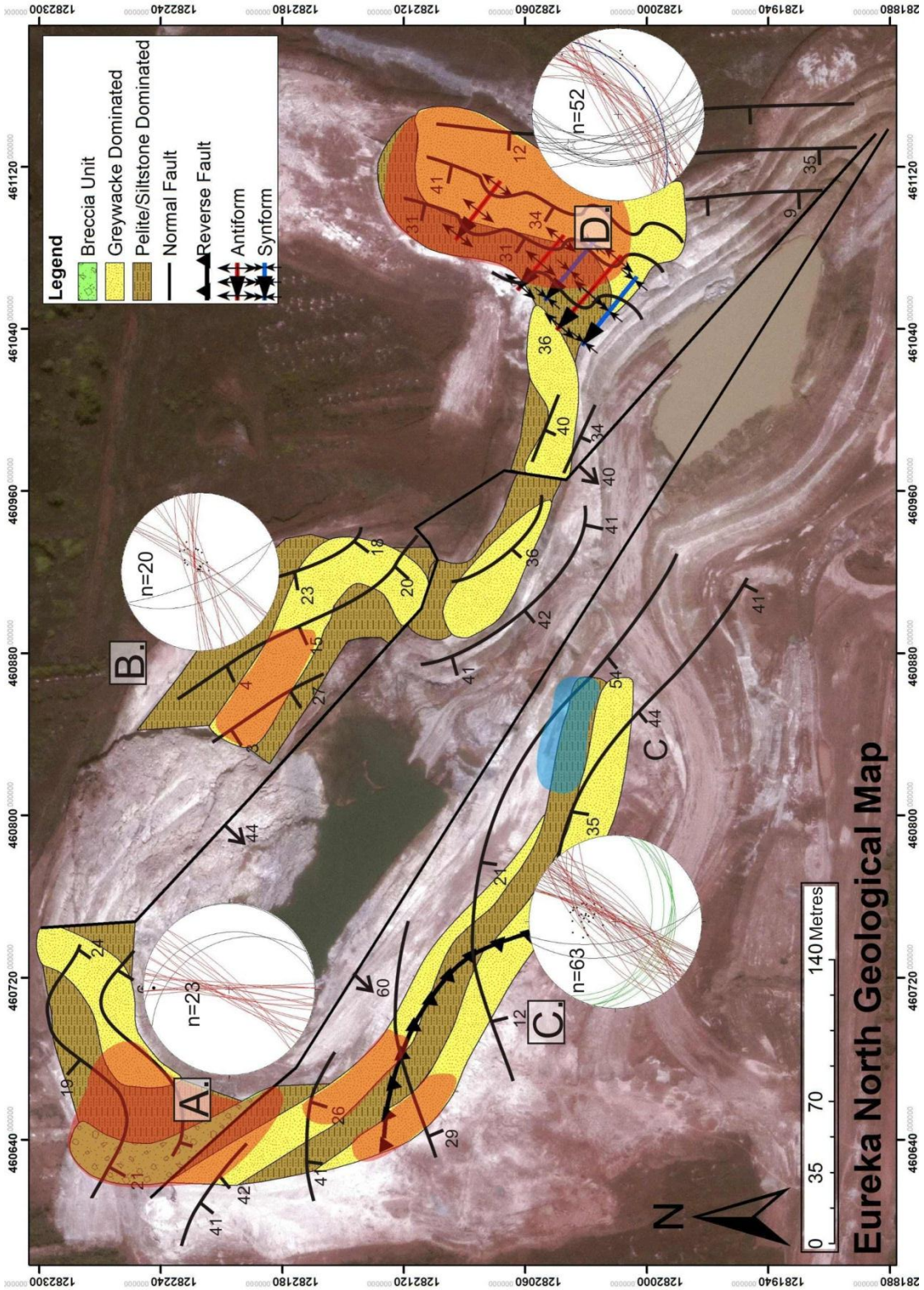

Figure 6.17: Geological map of Eureka North. Red areas indicate a high abundance of veining and blue areas indicate a below average abundance of veining. The stereographic projections indicate 1) poles to bedding orientations – black dots; 2) π-girdle to poles of bedding planes – thick blue line; 3) quartz vein orientations: steep-S-dippers – red great circles; bc-orientated veins black great circles; bedding-parallel veins – green great circles

northwestern corner of the pit (Fig. 6.17). Veins are more pronounced in greywacke-dominated packages, evident by the activities of the local miners (Fig. 6.3.A). The folded domain located in the cutback in the northeastern extent also shows higher degrees of vein development.

Chapter 7 Discussion

The Siguiri Mining Complex forms a window into the Palaeoproterozoic Birimian Supergroup that was accreted during the Eburnean event onto the Archaean basement to the southwest to form part of the West African Craton (e.g. Ledru et al., 1991). The lode-gold deposits of the West African Shield form an integral part of this tectonic evolution having formed during the terminal stages of terrane accretion and collisional tectonics (Milési et al., 1991; Feybesse et al., 2006). Vein-type gold deposits are spatially and temporally associated with shear zones, related to the regional accretionary history (e.g. Kerrich and Cassidy, 1994). Regional structural patterns are, thus, directly linked to the development of fluid-flow patterns and mineralization (e.g. Ridely, 1992; Vearncombe, 1993; Oliver, 2001).

A discussion of the regional structural evolution and tectonic setting of the Siguiri Mining Complex is beyond the scope of this study. Moreover, regional structural studies are sparse and outcrop conditions that would allow for a better correlation with adjacent areas are very poor. However, an attempt will be made to place the Siguiri Mining Complex geology into the broader geological framework established by other workers (e.g. Ledru et al., 1991; Feybesse and Milési, 1994; Lahondère et al., 2002; Egal et al., 2002; Feybesse et al., 2006; Lompo, 2010). In detail, the discussion is aimed at (1) summarizing and interpreting the lithological and structural inventory of the Siguiri Mining Complex; (2) integrating the lithological-, structural- and quartz-vein inventory, in order to understand the controls of veining and, thus, gold mineralization; and (3) developing an overall mineralization model, from a structural perspective, also considering the broader tectonic framework as far as possible.

7.1 Lithologies

The host rocks of the Siguiri Mining Complex consist primarily of low-grade metamorphic, medium- to very fine-grained clastic metasediments that form part of the larger Siguiri Basin of the Boualé-Mossi domain (Egal et al., 2002). The clastic sediments of the Siguiri Basin have been suggested by previous authors (e.g. Egal et al., 2002) to represent part of a metaturbiditic succession. This agrees with the results of the present study. The greywacke-dominated units typically show upward-

fining trends (Fig. 4.8), interlayered and/or capped by finer siltstones and pelites, reminiscent of Bouma-type sequences. The psammitic lithotypes of the Siguiri Mining Complex are broadly classified as greywacke due to the abundance of mica, mainly sericite, feldspar and notable amounts of lithic fragments observed in fresh samples (Fig. 4.7). The abundance and the angularity of feldspar point to the low maturity of the greywackes being derived from a proximal source. The feldspar is almost exclusively plagioclase, which may indicate a TTG- rather than granite- (*sensu stricto*) dominated hinterland. The abundance of lithic fragments and rip-up clasts at the bottom of greywacke of siltstone beds, and the presence of intraformational breccias, point to a relatively energetic depositional environment. This possibly represents channel fills along a basin slope rather than the basin plains.

Mafic intrusives constitute very minor, but lithologically distinct rock types. The mafic dykes tend to follow the D_3 normal fault zones, at Eureka North (Figs. 4.14 and 4.15). This may indicate an origin of the mafic magmatism during crustal stretching and associated D_3 normal faulting.

The metamorphic grade of rocks in the Siguiri Mining Complex is low. The predominance of muscovite, chlorite and albite, together with siderite/ankerite in the alteration assemblage and pyrite/arsenopyrite as the main sulphides is consistent with lower- to mid-greenschist facies grades of metamorphism. This also agrees with the commonly brittle-ductile style of deformation.

7.2 Structure

The Siguiri Mining Complex underwent three phases of brittle-ductile and brittle deformation, namely D_1, D_2 and D_3.

D_1 deformation

An S_1 foliation is developed axial planar to small-scale F_1 folds and is commonly bedding- (S_0) parallel. However, the occurrence of D_1-related structures is too sporadic to conclude on the actual nature and significance of this event and further research is needed on fresh bedrock during the advanced stages of the mining operation.

D_2 deformation

The geology of the Siguiri Mining Complex is dominated by structures assigned to the D_2 phase of deformation. D_2 structures include two main structural elements or components, namely (1) northerly-trending domains of steep bedding (steep belts) anastomosing around (2) openly folded domains.

The steep and folded domains are interpreted to have formed during D_2. The temporal relationship between the two domains is suggested by:

(1) their similar orientation. Both steep and folded domains show northerly trends, although gently undulating (Figs. 7.1 and 7.2).

(2) F_2 fold trends, vergence directions and interlimb angles show characteristic variations across the steep belts. In general, fold axial traces and steep belts are parallel to each other where they are in direct contact. Fold axial traces tend to diverge from these trends with increasing distance from the steep domains. This divergence is caused by the anticlockwise rotation of fold axial traces, resulting in overall sigmoidal, S-shaped axial traces (Figs. 7.2 and 7.3). Similarly, folds show either an east- or west-vergence adjacent to steep belts, but become more upright away from the steep domains. Lastly, interlimb angles of F_2 folds are commonly tighter adjacent to steep belt, becoming open- to gentle away from the steep domains (Fig. 5.19.A).

(3) F_2 folds contained within steep belts are commonly tight and the foliation/bedding in the steep domains has an axial planar orientation with respect to the folds (Fig 7.2). Fold tightening is associated with a steepening of folds and, in contrast to the shallowly plunging F_2 folds in folded domains, plunges of F_2 folds in steep belts are mostly steep.

In summary, these spatial relationships indicate that steep belts envelope F_2 folded domains, rather than truncating them, suggesting the coeval development of the two domains.

The folded domains record a component of approximately E-W to ENE-WSW shortening, also indicated by the orientation of the S_{2a} foliation that accompanies folding (see below).

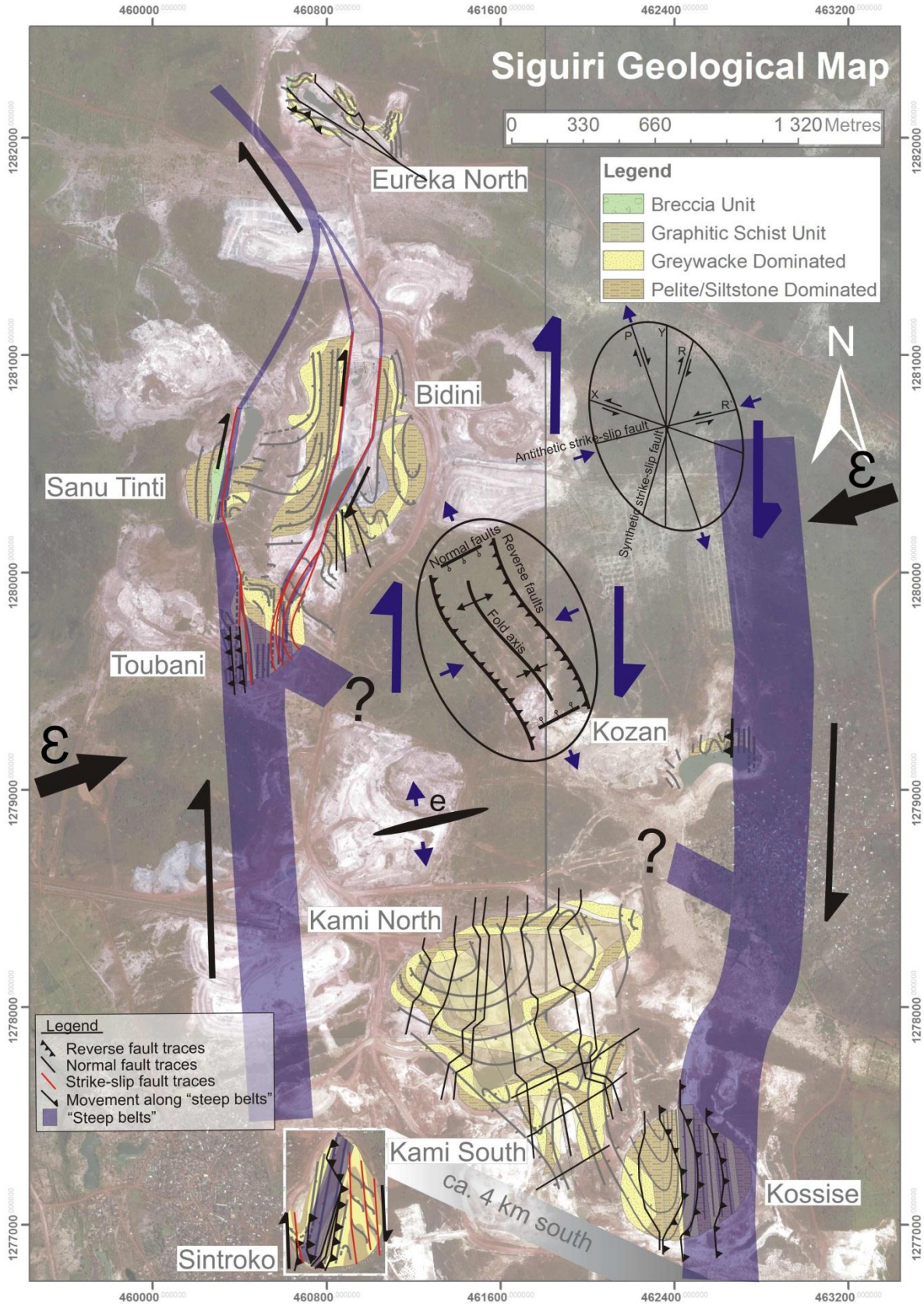

Figure 7.1: Formline map of bedding, and D_2 and D_3 faults in the Siguiri Mining Complex. The location of the main steep belts and significant D_2 faults is highlighted in purple. The symbol ε is the principle shortening direction, with the letter e indicating the principle extension direction. Strain ellipses indicate the orientation of sigmoidal shaped reverse faults, within a dextral transpressional environment, as well as the orientation of shears development. Shear orientation of the Siguiri Mining Complex suggests shears developed as Y-, P- and synthetic Riedel shears (R`).

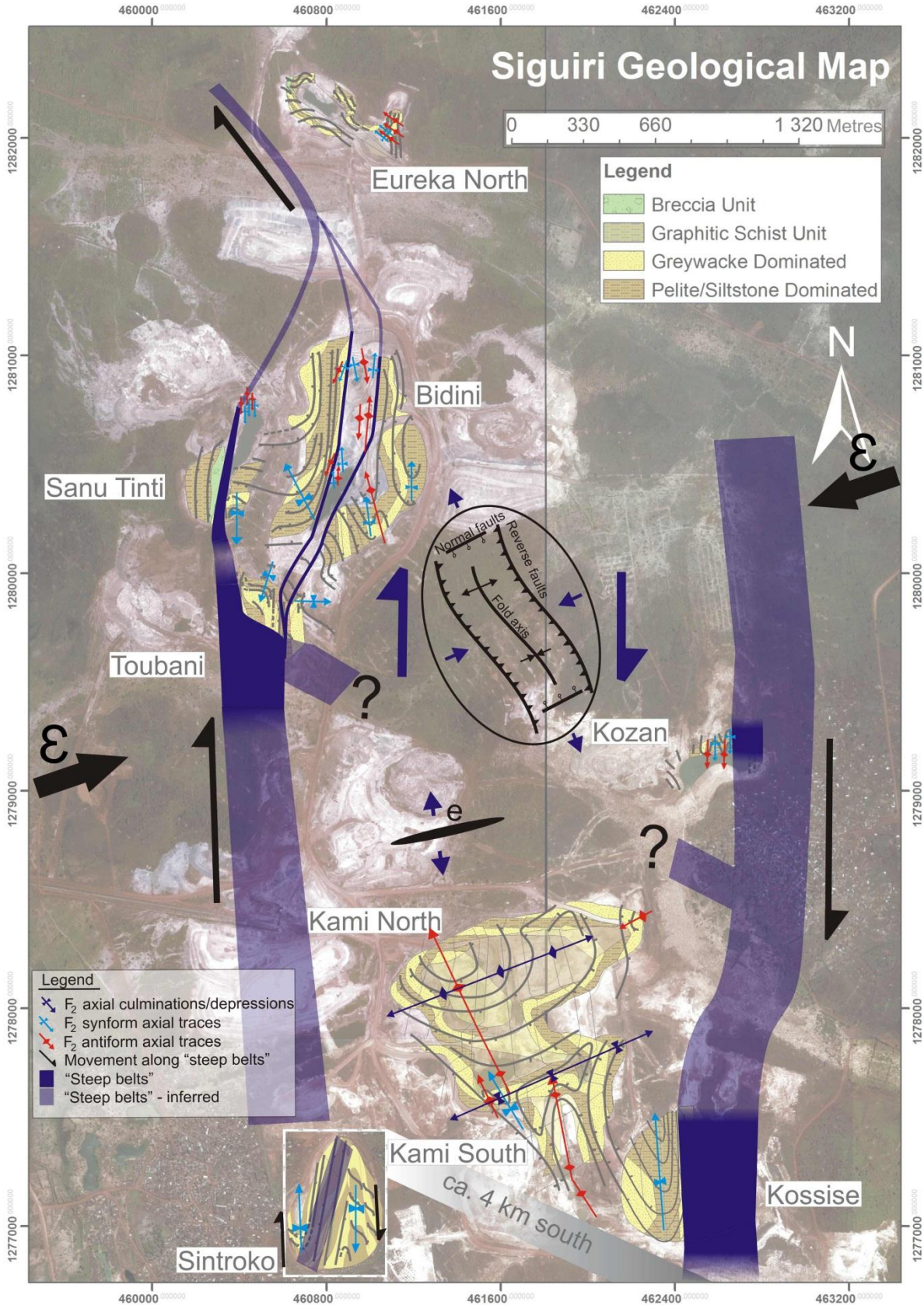

Figure 7.2: Formline map of the Siguiri Mining Complex emphasizing the presence and orientation of prominent F_2 folds. The symbol ε is the principle shortening direction, with the letter e indicating the principle extension direction. The strain ellipse indicates the development of sigmoidally shaped D_2 fold traces during a dextral transpressional event. D_2 folds are progressively rotated to north-south trends closer to the bounding shear zones.

The northerly-trending steep belts also record this component of approximately east-west shortening, but an additional non-coaxial component of strain is suggested by the occurrence and close spatial association of smaller-scale, metre-wide strike-slip and reverse faults confined to or directly adjacent to the steep domains (Figs. 5.12.A-B, 5.17.A-D, 5.21A-C, 5.22.A-B and D).

Reverse faults show both a top-to-the-east and -west sense of displacement and both westerly and easterly dips, respectively, even within individual pits and in a single steep belt (Sintroko; Fig. 5.21.B; or reverse faults in Kozan and Kossise; Figs, 5.17.B and 5.20.B). Hence, reverse faults show a conjugate arrangement centred about the steep bedding. The faults clearly post-date the steepening of bedding (Fig. 5.17.D; Kossise). The displacement, conjugate arrangement and relatively late timing suggest that the reverse faults have accommodated progressive east-west shortening in response to the geometric hardening associated with the steepening of bedding. The sporadically developed S_{2b} fracture cleavage is particularly prominent in areas of D_2 reverse faulting and its moderate easterly and westerly dips also correspond to the orientation of the reverse faults. Hence, the formation of S_{2b} is tentatively related to D_2 reverse faulting.

Strike-slip faults occur in close spatial relation to reverse faults in the steep belts (Figs. 5.12.B; 5.21.B.). The commonly subvertical, north to NNE-trending strike-slip faults may have a bedding-parallel orientation or they may cross-cut bedding (Figs. 5.9.B and D; 5.12.B). Shear-sense indicators are rare, but numerous strike-slip faults show a consistent drag of wall rocks adjacent to them pointing to a dextral sense of displacement (Figs. 5.12.A; 5.21.A and C).

Small-scale thrusts and the vergence of F_2 folds led, for example Holcombe (2007) to suggest the Siguiri Mining Complex was underlain by fold-and-thrust belt geology. This is not supported by the results of the present study. The spatial association of D_2 steep belts and folded domains and the coexistence of D_2 reverse and dextral strike-slip faults rather suggest that the Siguiri Mining Complex forms part of dextral transpression zone. Transpression describes deformation along a shear or fault zone. This is characterized by a component of shear-zone parallel simple shear and a component of shear-zone normal pure shear (shortening in the case of transpression zones; extension in case of transtension zones) (e.g. Harland, 1971; Sanderson and Marchini, 1984; Tikoff and Fossen, 1993). As a result of this,

transpression zones are commonly characterized by a pronounced strain partitioning. The simple-shear component is resolved along strike- or oblique-slip faults. The shear-zone normal pure-shear component is accommodated by a combination of folding and/or reverse faulting and/or uplift (Casas et al., 2001; Viola et al., 2004). The predominance of simple shear over pure-shear structures in transpression zones is mainly related to the convergence angle, i.e. the angle of shortening with respect to the shear-zone boundary. During high-angle, pure-shear dominated transpression (convergence angle is > ca. 30° to the shear zone boundary), deformation is dominated by folding and reverse faulting. Fold axial traces originate at an angle to the shear zone boundary, but will be rotated into parallelism at higher strains (Tikoff and Peterson, 1998). Analogue models of folding during transpression also highlight the often en-echelon arrangement of fold trains and the commonly doubly-plunging nature of folds and/or opposite plunge directions of adjacent fold pairs (e.g. Merle, 1997). At lower convergence angles (< ca. 30°), deformation will be strike-slip dominated (e.g. Tikoff and Peterson, 1998; Casas et al., 2001). Strike-slip faults either show a shear-zone parallel orientation (Y-shears) or trend at low- and high angles with respect to the bounding shear zones, corresponding to synthetic and or compressional P-shears (Fig. 7.1).

The observations made above are illustrated in the following discussion of the geology of the open pits. Based on the fabric intensity, and the position of the open pits in either steep or gently-folded D_2 fabric domains, three different cases can be distinguished that may illustrate the structural evolution of the Siguiri Mining Complex. This includes (1) the Kami-Kossise Complex, where gently-folded domains are bounded by a major steep belt; (2) the Bidini-Toubani-Sanu Tinti Complex, where folded domains are transected by closely-spaced steep zones and D_2 faults; and (3) Sintroko, which is entirely situated in a steep domain, containing steeply plunging, tight F_2 folds and a number of D_2 reverse and strike-slip faults.

Kami-Kossise Complex (-Kozan)

The Kami-Kossise Complex and the Kozan pit in the far north are bounded by a steep-belt in the east (Kossise) and an inferred steep belt in the far west, some 500 m from the westernmost open pit workings (Fig. 7.1). The eastern belt can be

connected with the steep domain of Kozan to the north, whereas the western belt can be connected to the steep domain in Toubani in the north (Fig. 7.1). The folded domain measures ca. 2 km across strike and is dominated by only openly folded, shallowly dipping strata with no evidence for D_2 strike-slip or reverse faults. Fold axial traces are north-south in the Kossise and Kozan pits, located directly adjacent to the bounding eastern steep belt (Fig. 7.2). Fold trends change to more north-westerly trends into the Kami Complex and with increasing distance from the steep belt (Fig. 7.3). This progressive re-orientation of fold axial traces in the Kami-Kossise Complex corresponds to folds formed in transpression zones (e.g. Tikoff and Peterson, 1998). The anticlockwise rotation of fold-axial traces and overall resulting S-shaped geometries defined by F_2 fold hinges correspond to a dextral transpression (Fig. 7.3). Similarly, analogue models of transpression zones show that folds developed at some distance from the bounding strike-slip shear zones show more open geometries, lower fold amplitudes and subvertical axial planes (Tikoff and Peterson, 1998; Casas et al., 2001). This also corresponds to the fold profiles developed in the Kami-Kossise Complex from east to west and away from the bounding steep belt.

The doubly-plunging, non-cylindrical geometry of folds results in axial depressions and culminations that resemble gentle cross-folds trending at high angles to the northerly-trending F_2 folds. The central dome-like structure that underlies Kami North is the result of an axial culmination. The southern limb of the dome forms part of an axial depression caused by the southerly plunge of F_2 folds in the north and northerly plunge of folds in Kami South (Figs. 5.13.A and 5.15.A). Doubly-plunging, en-echelon folds resulting in basin- and dome-like fold geometries structures are commonly observed in transpressional environments (Sanderson and Marchini, 1984; Tikoff and Peterson, 1998). Opposite plunges in adjacent fold pairs is explained by the rotation of folds at different rates during wrench kinematics, as a result of differing degrees of strain partitioning (Tikoff and Peterson, 1998). This results in dome- and basin-structures that are not the result of superimposed fold phases, but rather represent the axial culminations or depressions of the doubly-plunging folds. Trending subparallel to these cross-folds is a set of subvertical D_2 normal faults. In contrast to the northerly-trending D_3 faults, these easterly-trending faults are interpreted to have developed syn-F_2 folding. A component of fold-hinge-parallel stretch in folds formed during transpressional shearing is common (e.g. Jamison, 1991). This stretch is interpreted to be responsible for the formation of the easterly-trending D_2 normal

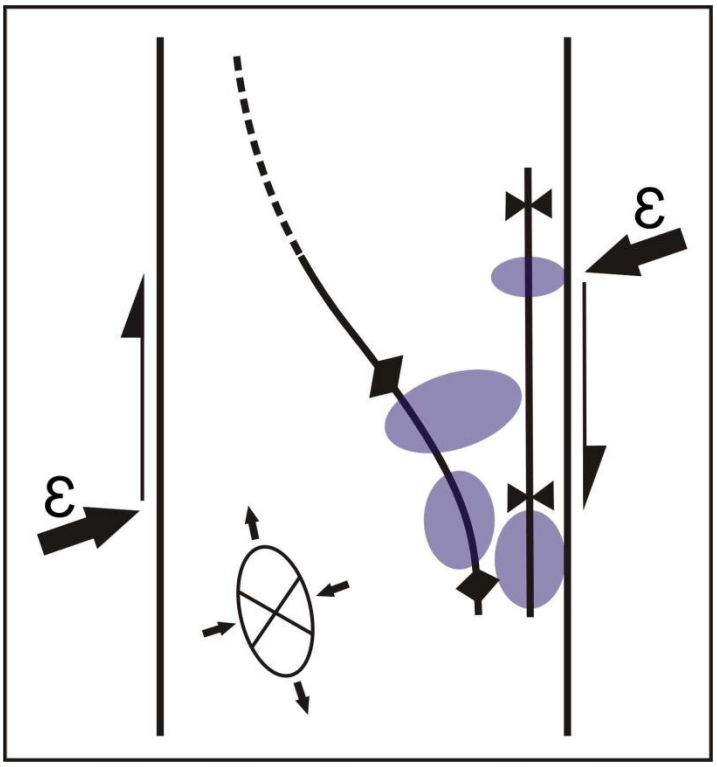

Figure 7.3: Simplified line drawing, showing the sigmoidal shape of the axial traces of the main F_2 folds, with respect to the north-south trending D_2 shear zones. The strain ellipse indicates an ENE-shortening direction (ε: principal direction of shortening), with extension to the north-northwest. The purple ellipses indicate the relative position of the pits of the Kami-Kossise Complex and Kozan.

faults at high-angles to the fold trace, as is the case in Kami South where the central antiform (Fig. 5.15.A) is truncated by the ENE-trending normal faults. Notably, the normal faults are parallel to the main set of steep S- to SE-dipping quartz veins (steep-S-dippers) in the Siguiri Mining Complex (see Chapter 6).

Bidini-Toubani-Sanu Tinti Complex

The Bidini-Toubani-Sanu Tinti Complex contains significantly more D_2 reverse and strike-slip faults than the Kami-Kossise Complex, but openly folded F_2 domains are still present. The western steep belt is prominent in the Toubani pit, but branches into three narrower belts, i.e. subvertical D_2 strike-slip faults that transect the pits of Bidini and Sanu Tinti with a spacing of ca. 50 to 400 m (Fig. 7.1). To the north of Bidini and Sanu Tinti, the steep belts are interpreted to merge again into a single NW-trending steep belt that follows the structural grain of Eureka North. To the southeast of Toubani, D_2 strike-slip faults rotate from northerly to northwesterly trends. This is sketched in figure 7.4, where the belt connects to the eastern belt, just south of Kozan. This is interpreted to find its manifestation in the rotation of bedding to more northwesterly trends in the western parts of Kozan. Taken in conjunction, the

geometry and kinematics of structures in the Bidini-Toubani-Sanu Tinti Complex describe a dilational jog in an overall dextral transpressional environment (Fig 7.4). The D_2 strike-slip faults contain a dip-slip component, indicated by the drag of the bedding along the fault traces (compare east-west cross-sections through Bidini, Fig 5.9.B and D). The overall structure underlying Bidini and Sanu Tinti, thus, resembles a positive flower structure, caused by local (pit-scale) dilatancy in the overall transpressive system.

The small-scale F_2 folds between and adjacent to the central D_2 fault zones in Bidini show shallow, but opposite plunges in adjacent fold pairs typical for transpressional environments (Merle, 1997; Tikoff and Peterson, 1998). In the eastern domain of Bidini (Fig. 5.9.A), a doubly-plunging synform forms a basin-like structure, similar to the dome-structure in Kami North (see above). Drag along the shears can be seen between Bidini and Sanu Tinti and in Toubani, where bedding forms S-shape and Z-shape structures (Figs. 7.2 and 7.4). In zones of dextral transpression, original bedding or earlier foliation should be deformed into S-shaped folds (e.g. Curtis et al., 2010). From a study on transpression environment by Curtis et al., (2010), fold symmetry is dominated by S-folds. Here the plunges of S-folds range from gently plunging to being subvertical. The S-folds observed in the Siguiri Mining Complex most commonly show steep plunges and can be seen in the pits of Sintroko and Toubani. Between Sanu Tinti and Bidini a subvertical plunging Z-fold is inferred in order to explain the synformal-structures developed along the eastern wall of Sanu Tinti and the western wall of Bidini respectively. The S-fold in the vicinity of Toubani Old Pit suggests a dextral-orientated displacement along the shear zones, whereas the Z-fold between Sanu Tinti and Bidini suggests a contradictory sinistral shear sense. This can be explained and interpreted by opposite shear senses that may develop in a system that is pure-shear dominated. Here rocks extrude laterally and steep belts may envelop structures indicating opposite shear senses (Fig 7 .4). However displacement along shears are small and shearing cannot explain the structures developed here. These folds may be inherited from the original F_2 folding and overprinted during later transpressional shearing, i.e. D_2 strike-slip shear zones may preferentially develop on the steep limbs of folds (bedding-parallel) and further tighten the folds. The folds thus seem to imply sinistral/dextral displacement, but the geometry is inherited from an earlier fold pair.

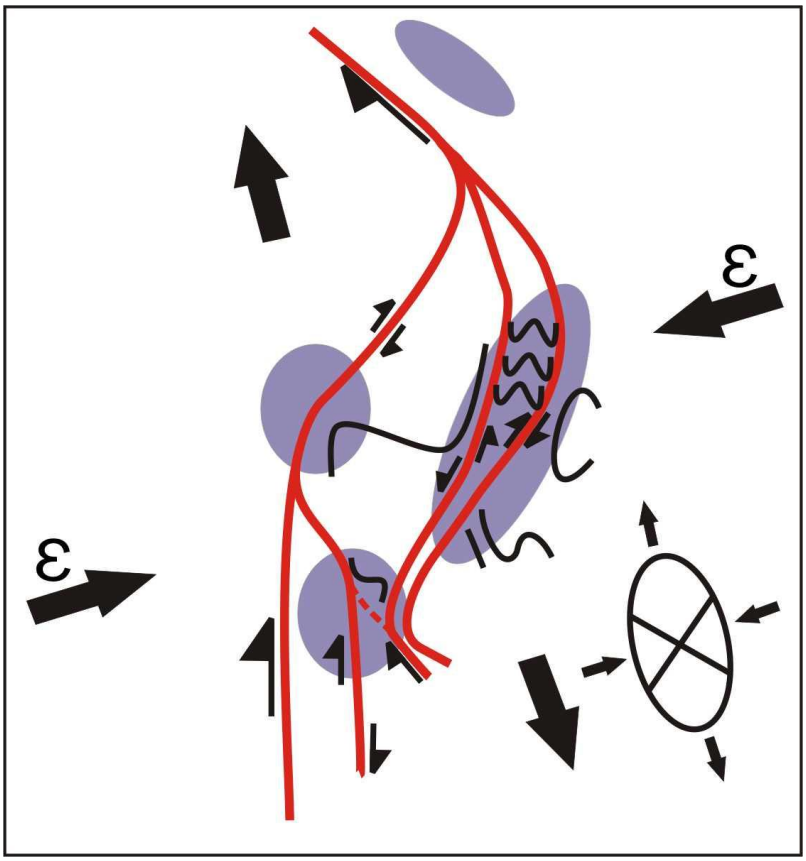

Figure 7.4: Simplified line drawing of the geometry of D_2 shear zones and folded domains interpreted to define a dilational jog geometry developed in the Bidini-Toubani-Sanu Tinti Complex. D_2 strike-slip shear zones represent anastomosing subsidiary shears. The strain ellipse indicates an ENE-shortening direction (ε), with extension to the north-northwest, corresponding to the orientation of the steep-S-dippers. Structural formlines are indicated by the black lines. The purple ellipses indicate the relative position of the pits of the Bidini-Toubani-Sanu Tinti Complex and Eureka North.

Sintroko

Sintroko is the only open-pit operation entirely located in subvertical strata and in a steep belt (Fig. 5.21.A). The Sintroko pit is also underlain by a steeply plunging synform-antiform pair, developed as an S-fold (Fig. 5.21.A). The eastern- and westernmost limbs of this S-fold structure are truncated by north-south trending D_2 strike- or oblique slip zones (Figs. 5.21.A and C). The closely-spaced oblique-slip shear zones enclose highly deformed rocks. The wall-rock drag along the faults results in sigmoidally folded bedding indicating a dextral sense of displacement (Fig. 5.22.D). In contrast, rocks in the central domain of the pit contain D_2 reverse faults. The reverse faults dip in opposite directions and record a top-to-the-east and -west displacement, respectively (Figs. 5.22.A-B). The opposite dips and displacements along the D_2 reverse faults, together with the eastern and western bounding strike-slip belts, describe an overall positive flower structure (Fig. 7.5).

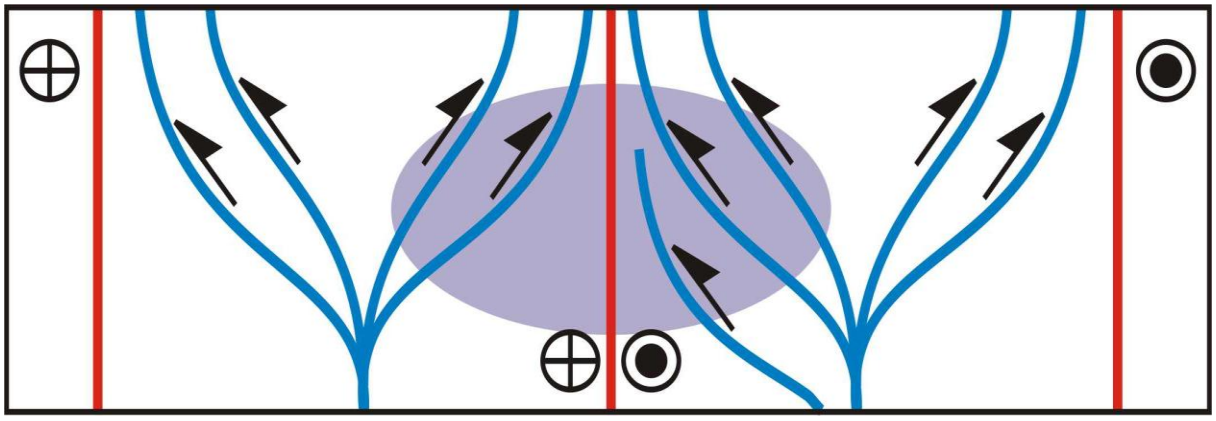

Figure 7.5: A cross-sectional view of Sintroko (pit location indicated by the purple ellipse). Here the central reverse faults (blue lines) are bounded by the steep strike-slip faults (red lines) in the east and west. A central strike-slip fault is inferred in central part of the sketch, to explain the convergence of the reverse faults located in the central parts of Sintroko. This resembles two adjacent positive flower structures, with an overall dextral shear sense.

The structural inventory of the Sintroko pit illustrates the close spatial and temporal relationship between strike-slip and reverse faults in transpression zones (e.g. Harland, 1971; Tikoff and Peterson; 1998; Dewey et al., 1998; Viola, 2004). The lateral displacement along D_2 strike- or oblique-slip faults is dextral, highlighting the significance of right-lateral kinematics in the Siguiri Mining Complex in addition to the east-west shortening component. The tight interlimb angles and steep plunges of the F_2 folds are interpreted to indicate the progressive tightening and rotation of initially shallow plunging open F_2 folds during non-coaxial dextral shear in the steep belts.

Progressive D_2 deformation

The three cases sketched above are interpreted to represent different stages in the evolution of the Siguiri Mining Complex, illustrating the development from low- to high-strain domains during progressive dextral transpressive shearing. The Sintroko geology represents the high-strain end-member of the Siguiri Mining Complex geology, characterized by an abundance of D_2 strike-slip and reverse faults in the steep strata in which F_2 folds appear tightly folded and even partly transposed. In contrast, the only gently folded strata, low fabric intensities and the lack of D_2 faults suggest the Kami-Kossise Complex (-Kozan) to represent the low-strain end member of the mineralized zones. Here, the early stages of D_2 strains have been preserved,

possibly through strain partitioning around the complex, i.e. in the eastern and far western steep belt. The geology of the Bidini-Toubani-Sanu Tinti represents a transitional type in which folded F_2 domains may still preserve open fold shapes and shallow plunges, but in which D_2 strains have led to the attenuation of fabrics and, in places, rotation of folds.

The S_{2a} foliation

In this study, the S_{2a} foliation recorded throughout the Siguiri Mining Complex has so far been regarded as being approximately axial planar to F_2 folds. In fresh samples, S_{2a} is defined by the preferred orientation of muscovite- or sericite (Fig. 5.2.A) and the preferred alignment of siderite alteration spots (Fig 5.2.B), suggesting an origin during the low-grade metamorphic deformation of the rocks. In detail, however, S_{2a} consistently describes a clockwise rotation in its orientation compared to F_2 folds by an angle of about 15-20°. It is, strictly speaking, a transecting cleavage to F_2 folds. The north-northeasterly trends of S_{2a} and, hence, slight angle of the foliation with respect to F_2 fold axial planes is consistent with sinistral transpression (e.g. Merle, 1997).

On a regional scale, Egal et al. (2002) recorded shear zones with sinistral displacement, although with west-northwest trends, along the north-western edge of the Kenema-Man shield, located some 50 km south of the Siguiri Mining Complex. Previous authors also recognized NNE-trending, sinistral strike-slip faults along the western edge of the Kenema-Man shield that is interpreted to have accommodated shortening from the southeast (Feybesse et al., 1994; Feybesse et al., 2006; Lompo, 2010). While sinistral strike-slip faults with broadly northerly, but also westerly trends are a regionally recorded feature, the significance of this deformation for the evolution of the Siguiri Mining Complex is not clear. As detailed above, F_2 folded domains and steep belts overwhelmingly record structures and kinematics pointing to dextral transpressive kinematics. The actual kinematic significance of S_{2a} for the evolution of the Siguiri Mining Complex still needs to be resolved at this stage.

D_3 deformation

The final D_3 deformation in the Siguiri Mining Complex is characterized by moderate- to steeply dipping, north-south trending normal faults (Fig. 7.1). The normal faults are particularly common in the pits of the Kami Complex, Kossise and Bidini. In Kami North these normal faults show opposite dip directions from east to west and develop prominent half-graben structures on either side of a central graben structure in the central domain of the pit. The orientation and displacement along the normal faults indicate east-west extension. The absolute timing of normal faulting is not constrained, but the presence of chlorite in the brittle fault rocks indicate that the rocks were still at greenschist-facies metamorphic grades.

7.3 Quartz veins

Mineralization of the Siguiri Mining Complex is associated with prominent quartz-veining in the Palaeoproterozoic rocks of the Birimian Supergroup. The presence of albite, chlorite and muscovite/sericite as well as siderite/ankerite alteration spots is consistent with lower-greenschist facies conditions of metamorphism during fluid-flow. Tourmaline as an alteration mineral is also consistent with the low-grades of metamorphism of the marine pelitic sediments enriched in boron.

The identification of the fluid source is beyond the scope of this study, but the abundance of quartz veins points to elevated fluid pressures in the relatively low-grade metamorphic wall rocks. A more pervasive fluid-flow in the Siguiri Mining Complex is evidenced by the omnipresent siderite alteration spots, particularly in the coarser-grained greywacke units, but also siltstones. In addition to the more pervasive fluid-flow, a structurally and fracture-controlled fluid-flow is evidenced by the presence of quartz veins that are developed throughout the Siguiri Mining Complex. It is the auriferous quartz vein sets that are the main source of the gold mineralization in the Siguiri Mining Complex.

Fracturing and veining during deformation are promoted by elevated fluid pressures (e.g. Etherdige, 1983; Sibson and Scott., 1998) and veining most likely occurred in the presence of suprahydrostatic and transiently lithostatic fluid pressures, resulting in the embrittlement of the rocks. This has potentially important consequence for an

understanding of the mineralization processes. For example, regional deformation processes such as faulting or folding that may occur with no, or only limited, fracturing and veining at low (hydrostatic to slightly suprahydrostatic) fluid pressures are accompanied by abundant fracturing and veining under suprahydrostatic and lithostatic fluid pressures. The latter is suggested to have been the case during deformation at the Siguiri Mining Complex and may explain (1) the abundance of veins, and (2) their relationship to regional and localized deformation structures.

Steep-S-dippers

Mining activities by the local “opailleurs” are a good indication as to whether vein sets are mineralized or barren and it is the set of steep-S-dippers that are particularly targeted by the local miners (Chapter 6, Fig. 6.3.A). The steep south-dipping vein set is present in all pits of the Siguiri Mining Complex only showing slight variations in dip direction from south to southeast between different open pits (Fig. 7.6). A significant change in orientation is, however, recorded in the Eureka North open pit, which correlates with the overall rotation of wall-rock structures in Eureka North compared to the southern pits.

The steep-S-dippers trend at high-angles (45 to 90°) to the north-south trending shear zones. They are developed throughout the Siguiri Mining Complex in gently folded domains as well as steep belts and in greywacke units as well as pelites, albeit with varying abundances. This suggests that the first-order control of the auriferous veins is the regional strain developed during dextral transpressional tectonics (Fig. 7.6). The veins are extension veins trending parallel- to subparallel to the regional ENE-WSW shortening direction and the northwest-southeast stretch, i.e. normal to the principal stretching direction (Fig. 7.6). Their easterly and northeasterly trend and steep- to subvertical dips are consistent with an origin as tension veins during dextral shear. Moreover, in individual pits, steep-S-dippers commonly show an orientation normal to the hinges of underlying F_2 folds, having an ac-orientation (Fig. 6.13). This is particularly well illustrated in the Kossise and Kami open pits (Fig. 7.6 and 7.7). The orientation of the steep-S-dippers normal to F_2 fold hinges (ac-orientation), and subparallel to steep ENE-trending late-D_2 normal faults (see structural discussion), indicate to a hinge-zone parallel and subhorizontal stretch in

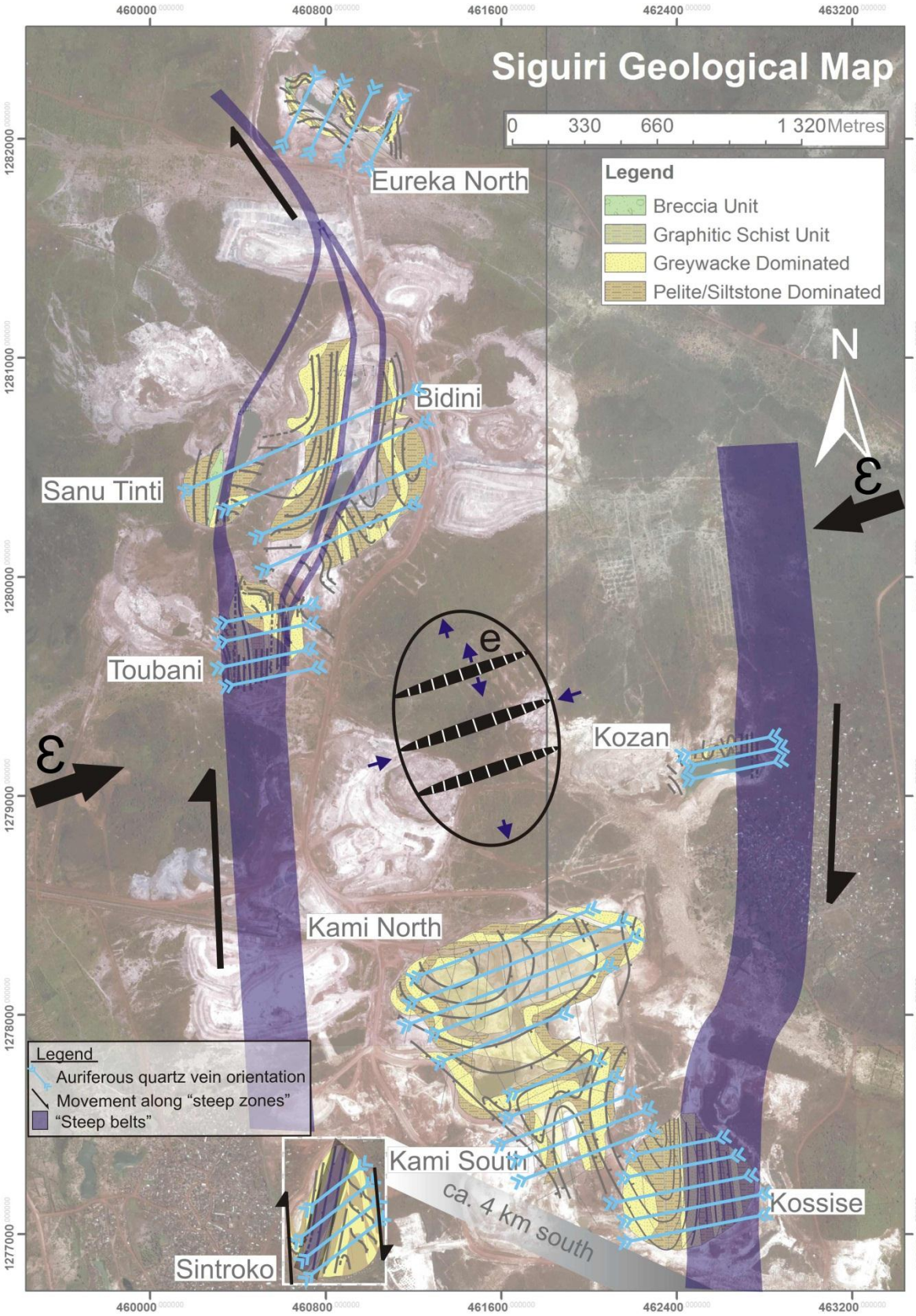

Figure 7.6: A schematic line drawing, overlaying the map of the Siguiri Mining Complex. This drawing shows the orientation of the main auriferous vein set (steep-S-dippers) recorded in the Siguiri Mining Complex. This orientation is subparallel to the principle shortening direction (ε) and subnormal to the principle extension direction (e). Vein orientation is consistent with vein development along extensional fractures (extensional veins). Note the significant change in the orientation of the main vein set to the far north (Eureka North).

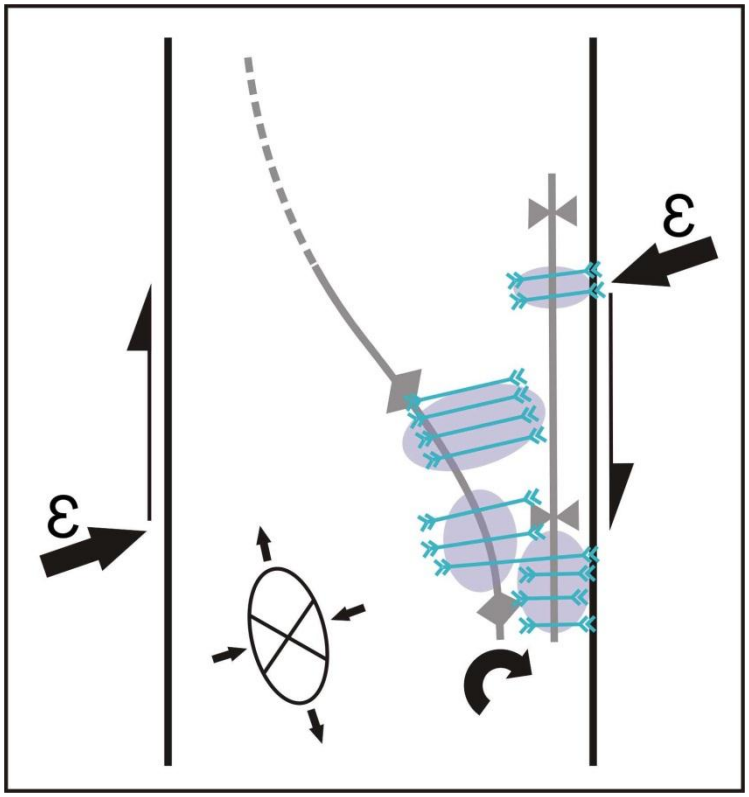

Figure 7.7: Simplified sketch, showing variations in the orientation of the steep-S-dippers between the pits of the Kami-Kossise Complex. In the gently folded domains, the vein set trends normal to subnormal to the F_2 fold hinges. The orientation of the vein set shows a clockwise rotation from west to east as veins are closer to the bounding steep belt. (ε: principal direction of shortening)

the Siguiri Mining Complex during D_2 transpressional tectonics. Steep-S- dippers in the Kami Complex are particularly well developed in areas of axial culminations and depressions that trend at high-angles to F_2 folds, caused by the doubly-plunging geometry of the folds (Figs. 7.6, 7.7 and 7.8). Fold plunges in these areas are only shallow (< 15°), but the gentle warp of the fold hinges has evidently resulted in a larger stretch and, as a result, higher vein densities. This component of hinge-parallel stretch particularly in axial culminations and depressions is underlined by the occurrence of ENE-trending normal faults (D_2) folds restricted to these areas and parallel to the steep S-dippers. Both the D_2 normal faulting as well as formation of the extensional steep south-dipping veins are interpreted to have accommodated the hinge-parallel stretch in these zones.

In many transpression zones, the maximum stretch is vertical, recording the extrusion and material flow of the rocks towards a free surface, commonly represented by the Earth's surface (e.g. Sanderson and Marchini, 1984). However, transpression zones may also record an oblique or horizontal stretch (e.g. Kuiper and Jiang, 2010). A principal component of horizontal stretch in transpression zones is particularly common in escape-type structures that record the lateral extrusion or flow of rocks in

response to indentor-type tectonics and accretion (e.g. Fossen and Tikoff, 1998). The transpression zone of the Siguiri Mining Complex may, thus, form part of a larger system of fault and shear zones recording the accretion of the Birimian onto the Archaean craton.

The spatial and geometric relationship between steep zones, folding and veining suggests that the steep south-dipping veins are temporally related to the D_2 deformation. However, veining must have occurred at a relatively late stage in the structural evolution of the Siguiri Mining Complex. The steep-S-dippers cross-cut F_2 fold structures and steep belts, and the majority of veins have not experienced any post-emplacement deformation.

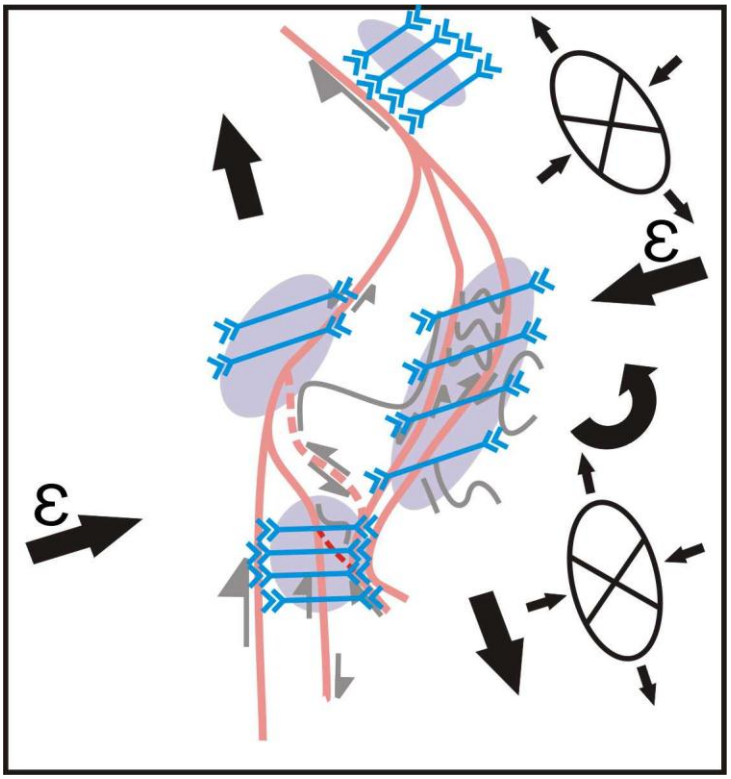

Figure 7.8: Line drawing of the orientations of the steep-S-dippers found in the pits of the Bidini-Toubani-Sanu Tinti Complex and Eureka North where the main steep-S-dippers also trends at an angle to the axial traces of folds, albeit small (< 20°). Veins developed in the steep belts of Toubani shows a more east-west orientation for the steep-S-dippers. The orientation of the vein set in Eureka North is consistent with a change in the direction of the steep belt, and veins trend normal to the axial traces of the F_2 folds found here. Veins show an anticlockwise rotation of their orientation from south to north. (ε: principal direction of shortening)

Shallowly dipping veins

Shallowly dipping veins are abundant in steeply dipping strata on the steep eastern limb of the Kossise synform (Fig. 6.1.B). In contrast, this vein set is almost absent from the shallowly dipping western limb of the first-order fold (Fig. 6.14). The subhorizontal dips and restriction of the veins to steep strata most likely indicates a

component of vertical extension of the steeply dipping strata during subhorizontal shortening. This is the result of a geometric hardening, i.e. subhorizontal layer-normal shortening after rotation of the bedding to vertical attitudes. In this orientation, further shortening can no longer be accommodated by folding and flexural-slip, but the rocks will rather undergo internal deformation and stretch in the bedding plane. The very shallow attitude of the veins suggests a subvertical component of stretch during the D_2 deformation. The western limb of the synform, in contrast, can accommodate progressive D_2 shortening by further steepening of bedding before shallowly dipping extension factures (ladder veins) start to form (Fig. 7.9). The presence of both shallowly dipping veins and steep-S-dippers in Kossise indicates a subvertical and subhorizontal stretch. This may indicate either (1) very low differential stresses and the fact that the principal directions of stretch were very similar, or (2) that the principal directions of stretch swapped during progressive deformation (Fig. 7.9). Both shallowly dipping veins and the steep-S-dippers have formed during the later stages of D_2. Cross-cutting relationships are uniform and the two sets seem to have formed at the same time. This would suggest the first scenario, although the ubiquitous presence of steep S-dippers would argue for a dominant component of horizontal stretch (Fig. 7.9).

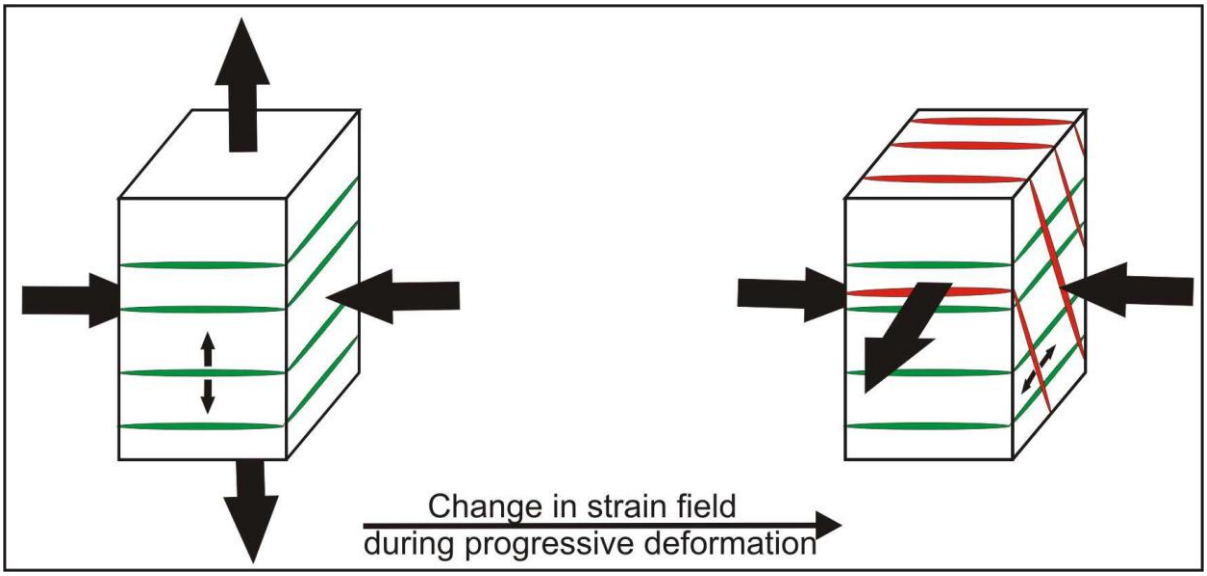

Figure 7.9: Schematic sketch illustrating the formation of both shallow and steep veins in Kossise during horizontal D_2 shortening. The presence of horizontal- and steep veins suggest a swop of the main extension direction, from vertical (shallowly dipping veins) to subhorizontal (steep-S-dippers) during progressive D_2 shortening. View to the south.

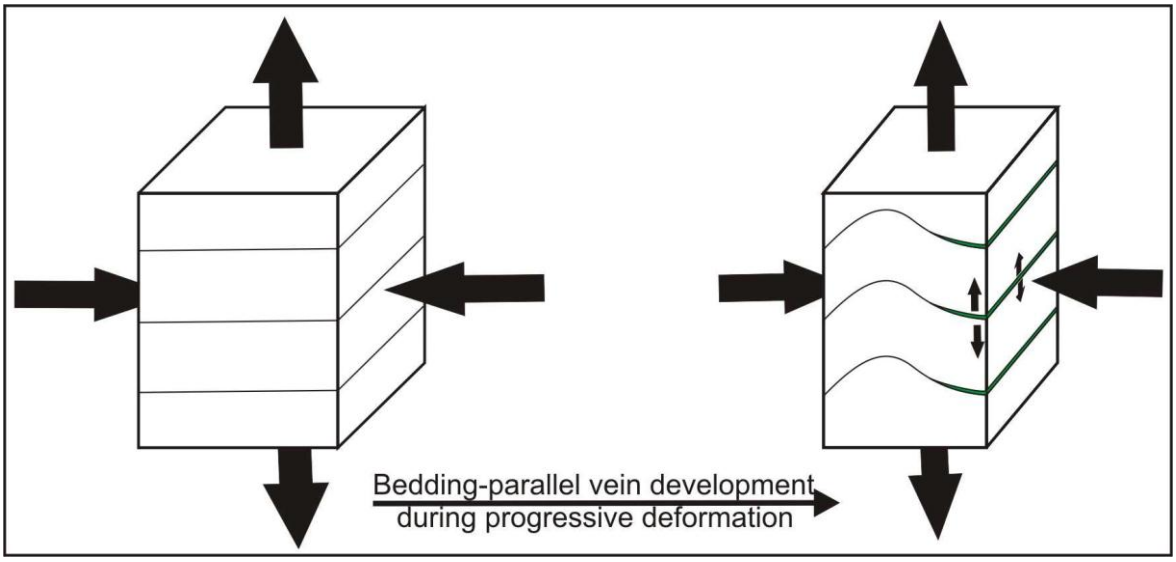

Figure 7.10: Schematic sketch illustrating the formation of bedding-parallel veins during progressive deformation.

Bedding-parallel veins

Bedding-parallel veins are mostly recorded in shallowly dipping (< 30°) strata and veins tend to be thick and laterally continuous along the bedding planes (Fig. 6.3). Bedding-parallel veins are here interpreted to record veining during the initial buckling of the strata and the tendency for bedding to delaminate during horizontal shortening due to the profile section of folds increasing in area as the fold develops (e.g. Hodgson, 1987) (Fig. 7.10). The intersection between bedding-parallel veins and steep-S-dipping veins is commonly the locus for small-scale blows and ore-shoots within the bedding plane. This suggests some degree of hydraulic connectivity between the two veins sets and the contemporaneous, at least in parts, formation of the two sets.

Lithological controls on veining

Lithologies exert an important additional control on quartz veining in the Siguiri Mining Complex (Fig. 6.1.C). There is a clear correlation between quartz-vein spacing and, hence, the abundance of quartz veins in different rock types. Psammitic, greywacke-dominated units commonly show a closer spacing of veins

compared to adjacent pelitic units (see quartz vein abundance maps; Chapter 6). This is a reflection of the different competencies (Young's moduli) of different lithological units. Extensional and oblique-extension veins develop preferably in competent units and given a constant stretch of a layered sequence, the units with lower tensile strengths (competent units) will develop closely spaced fractures and veins compared to less competent rocks (e.g. Sibson, 1996; Robert and Poulsen, 2001). Higher vein densities most likely result in higher Au-grade. For instance, the cutback in the northern parts of the Kossise pit is underlain by a thick greywacke package (Fig. 4.8).

The role of competency contrasts for veining can also be seen where veins may be refracted by as much as 20° (Fig. 6.3.D) or by the termination of veins along bedding contacts between different units (Fig. 6.3.B). This is particularly pronounced for shallowly dipping veins (Kossise, Fig. 6.1.B) that are confined to psammitic beds.

7.4 Tectonic correlations

The present study suggests the Siguiri Mining Complex to be located in a north-south trending dextral transpressive corridor. Regional work in West Africa identified an initial D_1 collisional event followed by D_2 and D_3 transcurrent and accretionary tectonics between the Archaean craton and the Palaeoproterozoic basins and volcanic arcs (e.g. Feybesse and Milési, 1994; Feybesse et al., 2006; Lompo, 2010). Evidence for the D_2 transpressional event is regionally widespread in form of north-south trending, sinistral shear zones along the eastern margin of the Kenema-Man Shield (e.g. Feybesse et al., 2006) and ENE-trending sinistral shear zones along its northeastern margin (Egal et al., 2002). These kinematics are not observed in the rocks of the Siguiri Mining Complex, where the structures mainly record dextral transpressive kinematics. Hence, a correlation of structures of the Siguiri Mining Complex with regional tectonic patterns is not straightforward given the, in particular, only very sporadic and patchy outcrop. However, given the sheer size of the mineralized system, presently exposed over an area of 12 by 3 km, the underlying structure that controlled fluid-flow is likely to be much larger or form part of a larger and regional system. Regional studies commonly propose that the shear zones in the Palaeoproterozoic are invariably associated with the accretionary history of the

Palaeoproterozoic domains, volcanic arcs and intervening basins, onto the Archaean Craton. The actual correlation of the evolution of the Siguiri Mining Complex with regional events seems only possible if a better and tighter constrained regional framework can be established, through more and better constrained field- as well as geochronological data.

Chapter 8 Conclusions

Gold mineralization in the Siguiri Mining Complex is the result of a combination of structural and lithological controls. From this study, the following main conclusions can be drawn.

- The Siguiri Mining Complex is hosted by a clastic turbidite sequence that forms part of the larger Palaeoproterozoic Siguiri basin, correlated with the lower (B1) parts of the Birimian Supergroup. Mineralogical and textural characteristics point to relatively proximal source of the sediments. The sequence has undergone lower- to mid-greenschist facies metamorphism, but at the present level of exposure, the rocks are deeply weathered and situated in an up to 80 m deep saprolite profile so that the primary mineralogy and many textural features have been obliterated.

- Based on the dominance of, pelitic over psammitic units in the turbiditic succession, 10 to 40 m thick lithological packages can be distinguished in the Siguiri Mining Complex. These packages can be correlated within and between adjacent open pits, but a mine-scale correlation must remain tentative due to the lack of marker horizons, the monotonous nature of the wall rocks and the deep weathering.

- All rocks have been affected by a pervasive hydrothermal alteration and fluid flow, evidenced by the development of near-pervasive carbonate alteration spots. Alteration and regional mineral parageneses are dominated by quartz, siderite and/or ankerite, chlorite, muscovite and albite, whereas the sulphide parageneses in the primary ore is dominated by pyrite and arsenopyrite, consistent with the greenschist-facies grades of the wall rocks.

- The main structural features underlying the Siguiri Mining Complex can be assigned to a D_2 deformational event. D_2 structures are interpreted to form part of a north-south trending system of strike-slip and reverse faults and shear zones anastomosing around folded domains. The geometry, orientation

and kinematics of faults and folds suggest that D_2 structures formed during progressive deformation in an overall dextral transpressive brittle-ductile shear zone. Structures within the D_2 corridor record east-northeast subhorizontal shortening and north-northwest subhorizontal extension. The Siguiri Mining Complex only exposes an area of 12 by 3 km, but the D_2 transpressive corridor is assumed to have a significantly larger along-strike continuation.

- Gold mineralization is associated with one main and, at least, three minor sets of auriferous quartz veins. The main quartz-vein set shows remarkably consistent easterly to northeasterly trends and steep southerly to subvertical dips throughout the Siguiri Mining Complex. This orientation is consistent with the dextral transpressive kinematics and strain (northerly to northwesterly stretch) within the D_2 host structure. It also illustrates that D_2 strains are the main control of quartz veining in the Siguiri Mining Complex. The volumetrically minor vein sets can be shown to be related to different stages of folding and fold amplification during progressive deformation.

- Lithologies exert a second important control on quartz veining. The spacing of quartz veins is, in many places, controlled by wall-rock lithologies. Competent, greywacke-dominated psammitic units tend to show closer quartz veining compared to metapelite-rich packages. Significant variations in quartz- vein abundance occur even within individual, lithologically heterogeneous packages.

- Zones of increased mineralization occur in areas where thick psammitic units coincide with specific structural sites of increased dilatancy. Areas of dilatancy are represented by either dilational jog geometries within the overall transpressive structure or zones of pronounced shear-zone subparallel stretch. Jog geometries could be identified in the larger Bidini-Toubani-Sanu Tinti Complex, due to the anastomosing geometry of bounding D_2 shear zones. In the large Kami Complex, F_2 axial culminations and depressions correspond to zones of increased stretch within the D_2 transpression zone, delineated by closer vein spacing and the formation of D_2 normal faults parallel to the main vein set and normal to F_2 fold hinges.

- The entire area has been affected by later D_3 normal faults that segment the Siguiri Mining Complex into graben and half-graben structures. The throws on individual faults is minor (<5 m), but the cumulative throw on the half-graben systems and displacement of well-mineralized packages is likely to have an influence on mining.

Reference List

Butt, C.R.M., Lintern, M.J. and Anand, R.R. (2000) Evolution of regoliths and landscapes in deeply weathered terrain – Implications for geochemical exploration, *Ore Geology Reviews 16*, pp. 167-183

Casas, A.M., Gapais, D., Nalpas, T., Besnard, K., Román-Berdiel T. (2001) Analogue models of transpressive systems, *Journal of Structural Geology 23*, pp. 733-743

Cohen, H.A. and Gibbs, A.K. (1988) Is the equatorial Atlantic discordant, *Precambrian Research 42*, pp. 353-369

Curtis, M.L., Flowerdew, M.J., Riley, T.R., Whitehouse, M.J., Daly, J.S. (2010) Andean sinistral transpression and kinematic partitioning in South Georgia, *Journal of Structural Geology 32*, pp. 464-477

Dewey, J.F., Holdsworth, R.E., Strachan, R.A. (1998). In: Holdsworth, R.E., Strachran, R.A., Dewey, J.F. (Eds.), Continental Transpressional and Transtensional Tectonics. Geological Society of London, *Special Publications 135*, pp. 1-14

Egal, E., Thiéblemont, D., Lahondère, D., Guerrot, C., Costea, C.A., Iliescu, D., Delor, C., Goujou, J.C., Lafon, J.M., Tegyey, M., Diaby, S. and Kolié,´ P. (2002) Late Eburnean granitization and tectonics along the western and northwestern margin of the Archean Kénéma–Man domain (Guinea, West African Craton), *Precambrian Research 117,* pp. 57-84

Etheridge, M.A. (1983) Differential stress magnitudes during regional deformation and metamorphism: Upper bound imposed tensile fracturing, *Geology*, Vol. 11, pp. 231-234

Ferry, J.M. (1994) A historical review of metamorphic fluid flow, Journal of Geophysical Research, Vol. 99, pp. 487-497

Feybesse, J.L. and Milési, J.P. (1994) The Archaean/Proterozoic contact zone in West Africa: a mountain belt of décollement thrusting and folding on a continental margin related to 2.1 Ga convergence of Archaean cratons?, *Precambrian Research 69*, pp. 199-227

Feybesse, J.L., Billa, B., Guerrot, C., Duguey, E., Lescuyer, J.L., Milési J.P. and Bouchot, V. (2006) The paleoproterozoic Ghanaian province: Geodynamic model and ore controls, including regional stress modelling, *Precambrian Research 149*, pp. 149-196

Fossen, H., and Tikoff, B. (1998) Extended models of transpression/transtension and application to tectonic settings, Holdsworth, R.E., Strachan, R.A., Dewey, J.F., Eds. Continental Transpressional and Transtensional Tectonics*, Special Publications 135, Geological Society of London*, pp. 15–33

Goldfarb, R.J., Groves, D.I. and Gardoll, S. (2001) Orogenic gold and geologic time: a global synthesis*, Ore Geology Reviews 18,* pp. 1-75

Goldfarb, R.J., Baker, T., Dube, B., Groves, D.I., Hart, C.J.R., Craig, J.R., Gosselin, P. (2005) Distribution, character and genesis of gold deposits in metamorphic terranes, *Economic Geology 100th Anniversary Volume*, pp. 407-250

Groves, D.I., 1993. The crustal continuum model for late-Archean lode-gold deposits of the Yilgarn Block, Western Australia, *Mineralium Deposita*, Vol. 28, pp. 366-374

Groves, D.I., Goldfarb, R.J., Gebre-Mariam, M., Hagemann S.G. and Robert, F. (1998) Orogenic gold deposits: A proposed classification in the context of their crustal distribution and relationship to other gold deposit types, *Ore Geology* Reviews 13, pp. 7–27

Groves, D.I., Goldfarb, R.J., Knox-Robinson, C.M., Ojala, J., Gardoll, S., Yun, G., Holyland, P. (2000) Late-kinematic timing of orogenic gold deposits and significance for computer-based exploration techniques with emphasis on the Yilgarn block, Western Australia, *Ore Geology Reviews*, Vol. 17, pp. 1-38

Harland, W.B. (1971) Tectonic transpression in the Caledonian Spitzbergen, *Geological Magazine 108*, pp. 27-42

Hirdes. W., Davis, D.W., Eisenlohr, B.N. (1992) Reassessment of Proterozoic granitoid ages in Ghana on the basis of U/Pb zircon and monazite dating, *Precambrian Research 56*, pp. 89-96

Hirdes, W., Davis, D.W., Lüdtke, G., Konan, G. (1996) Two generations of Birimian (Paleoproterozoic) volcanic belts in northeastern Côte d'Ivoire (West Africa): consequences for the 'Birmimian controversy', *Precambrian Research 80*, pp. 173-191

Hirdes, W., and Davis, D.W. (2002) U-Pb geochronology of Paleoproterozoic rocks in the southern part of the Kedougou-Kéniéba Inlier, Senegal, West Africa: Evidence for diachronous accretionary development of the Eburnean Province, *Precambrian Research 118*, pp. 83-99

Hodgson, C.J. (1987) The structure of shear-related, vein-type gold deposits: A review, *Ore Geology Reviews*, Vol. 4, pp. 231-273

Holcombe, R. (2007) Structural Framework, Siguiri Gold Mine, Guinea, *Company Report,* pp. 1-33

Jamison, W.R., (1991) Kinematics of compressional fold development in convergent wrench terranes: Tectonophysics 190, pp. 209–232

Kerrich, R., and Cassidy, K.F. (1994) Temporal relationships of lode gold mineralization to accretion, magmatism, metamorphism and deformation – Archean to present: A review*, Ore Geology Reviews*, Vol. 8, pp. 263-310

Kouamelan A.N., Delor, C., Peucat, J.J. (1997) Geochronological evidence for reworking of Archean terrains during the Early Proterozoic (2.1 Ga) in the western Côte d'Ivoire (Man Rise-West African Craton), *Precambrian Research 86*, pp. 177-199

Kuiper, Y.D., Jiang, D. (2010) Kinematics of deformation constructed from deformed planar and linear elements: the method and its application, T*ectonophysics 492*, pp. 175-191

Lahondère, D., Thiéblemont, D., Tegyey, M., Guerrot, C. and Diabate, B. (2002) First evidence of early Birimian (2.21 Ga) volcanic activity in Upper Guinea: the volcanics and associated rocks of the Niani suite, *Journal of African Earth Sciences 35*, pp. 417-431

Ledru, P., Pons, J., Milési, J.P., Feybesse, J.L., Johan, V. (1991) Transcurrent tectonics and polycyclic evolution in the Lower Proterozoic of Senegal-Mali, *Precambrian Research 50*, pp. 337-354

Ledru, P., Johan, V., Milési, J.P., and Tegyey, M. (1994) Markers of the last stages of the Palaeoproterozoic collision: evidence for a 2 Ga continent involving circum-South Atlantic provinces, *Precambrian Research 69*, pp. 169–191

Lompo, M. (2010) Paleoproterozoic structural evolution of the Man-Leo Shield (West Africa). Key structures for vertical to transcurrent tectonics, *Journal of African Earth Sciences 58*, pp. 19-36

Merle, O., Gapais, D. (1997) Strains within thrust-wrench zones, *Journal of Structural Geology*, Vol 19, pp. 1011-1014

Milési, J.P., Ledru, P., Ankrah, P., Johan, V., Marcoux, E., Vichhon, C. (1991) Gold deposits of the Lower Proterozoic succession of Ghana, *Mineralium Deposita, Vol. 25*, pp. 271-286

Milési, J.P., Ledru, P., Feybesse, J.L., Dommanget, A., Marcoux, E. (1992) Early Proterozoic ore deposits and tectonics of the Birimian orogenic belt, West Africa, *Precambrian Research 58*, pp. 305-344

Oliver, N.H.S. (1996) Review and classification of structural controls on fluid flow during regional metamorphism, *Journal of Metamorphic Geology*, Vol. 14, pp. 477-492

Oliver, N.H.S. (2001) Linking of regional and local hydrothermal systems in the mid-crust by shearing and faulting, *Tectonophysics 335*, pp. 147-161

Ollier, C.D. and Galloway, R.W. (1990) The laterite profile, ferricrete and unconformity, *CATENA,* Vol. 17, pp. 97-109

Paranhos, C. (2008) Siguiri Gold Mine - State of knowledge of the main geological controls of gold mineralization, *Company Report,* pp. 1-40

Ramsay, J.G., and Huber, M.I. (1983) The Techniques of Modern Structural Geology, Vol. 1: Strain Analysis, *Academic Press*, London

Ridley, J. (1992) The relations between mean rock stress and fluid flow in the crust: With reference to vein- and lode-style gold deposits, *Ore Geology Reviews*, Vol. 8, pp. 23-37

Ridley, J.R. and Diamond, L.W. (2000) Fluid chemistry of orogenic lode gold deposits and implications for genetic models, *Society of Economic Geologist Reviews*, Vol. 13, pp. 141-162

Robert, F. and Poulsen, K.H. (2001) Vein formation and deformation in greenstone gold deposits, *Society of Economic Geologist Reviews*, Vol. 14, pp. 111-155

Sanderson, D.J., Marchini, W.R.D. (1984) Transpression, *Journal of Structural Geology,* Vol. 6, pp. 449-458

Sibson, R.H., Robert, F., Poulsen, K.H. (1988) High-angle reverse faults, fluid-pressure cycling, and mesothermal gold-quartz deposits, Geology, Vol. 16, pp. 551-555

Sibson, R.H. (1996) Structural Permeability of fluid-driven fault-fracture meshes, *Journal of Structural Geology*, Vol. 18, pp. 1031-1042

Sibson, R.H. and Scott, J. (1998) Stress/fault controls on the containment and release of overpressured fluids: Examples from gold-quartz vein systems in Juneau, Alaska; Victoria, Australia and Otago, New Zealand, *Ore Geology Reviews 13***,** pp. 293–306

Taylor, P.N., Moorbath, S., Leube, A., Hirdes, W. Early (1992) Preoterozoic crustal evolution in the Birimian of Ghana: constraints from geochronology and isotopes, *Precambrian Research 56*, pp. 97-111

Theron, S.J., Coetzee, L.L. (2010) Explomin^{tm} lithotyping and mineralogical characterization of 114 diamond drill core samples from the Siguiri deposit, Guinea, *Minerological Report*, pp. 1-179

Tikoff, B. and Fossen, H. (1993) Simultaneous pure and simple shear: the unified deformation matrix. *Tectonophysics*, 217, pp. 267-283.

Tikoff, B., Peterson, K. (1998) Physical experiments of transpressional folding, *Journal of Structural Geology 20*, pp.661-672

Viola, G., Odonne, F., Mancktelow, N.S. (2004) Analogue modelling of reverse fault reactivation in strike-slip and transpressive regimes: application to the Giudicarie fault system, Italian Eastern Alps, Journal of Structural Geology 36, pp. 401-418

Vearncombe, J.R. (1993) Quartz vein morphology and implications for formation depth and classification of Archaean gold-vein deposits, *Ore Geology Reviews*, Vol. 8, pp. 407-424